

**The Response Dynamics of Indium Telluride
Quantum Dots Impedimetric Genosensor for
Telomerase Cancer Biomarker**



By

Samantha Fiona Douman

BSc Honours (*Cum Laude*)

UNIVERSITY of the
WESTERN CAPE

A thesis submitted in fulfilment of the requirements for the degree of

Magister Scientiae in Chemistry

Faculty of Science

University of the Western Cape

Cape Town, South Africa

Supervisor: Prof Emmanuel I. Iwuoha

November 2013

KEYWORDS

Cancer

DNA

Quantum dots

3-mercaptopropionic acid

Indium telluride

Biomarker

Telomerase

Biosensors

Genosensor

Electrochemical impedance spectroscopy



ABSTRACT

Cancer, the second most common cause of death after heart disease, is a complex and multifactorial disease that up to date is still under extensive research. To achieve early detection of cancer disease the discovery of specific, sensitive and reliable biomarkers is required. Telomerase is a ribonucleo-protein complex that has been identified as an important target for cancer diagnostics and cancer therapy, because 85% of more than 950 primary tumours express telomerase activity. The standard method for the detection and quantification of telomerase activity is the polymerase chain reaction (PCR)-based assay known as the telomeric repeat amplification protocol (TRAP) assay. TRAP and other methods developed for telomerase detection have limitations for example its time consuming, requires complicated machinery, expensive equipment and reagents thus there is a need for a more sensitive, reliable and high-throughput method. Electrochemical biosensors are quickly emerging as an alternative for early detection of cancer because they can be designed to detect developing cancer biomarkers and to allow improved monitoring of cancer growth and patient therapy. This research study reported for the first time the successful fabrication and implementation of highly sensitive 3-mercaptopropionic acid indium telluride quantum dots (3MPA-In₂Te₃ QDs) based genosensor for detection of telomerase biomarker. The colloidal poly-dispersed 3MPA-In₂Te₃ QDs introduced into the genosensor system were successfully synthesized by a simple, inexpensive and reproducible aqueous method. The as prepared 3MPA-In₂Te₃ QDs was characterized by Ultraviolet Visible (UV-VIS) spectroscopy, Fluorescence (FL) spectroscopy, X-ray Diffraction (XRD), Fourier Transform Infrared (FT-IR) spectroscopy and High Resolution Transmission/Scanning Electron Microscopy (HR-TEM/SEM). Electro-analysis of 3MPA-In₂Te₃ QDs was done by Cyclic Voltammetry (CV) and Electrochemical Impedance Spectroscopy (EIS). HR-TEM studies revealed formation of small sized QDs about 6 nm in diameter while UV-VIS studies showed presence of

absorption peaks in the ultraviolet region (100-400 nm) which confirmed the formation of these small sized QDs. The good electrochemical, optical, physical and chemical properties of the 3MPA-In₂Te₃ QDs allowed them to be used as a mediating platform between deoxyribonucleic acid (DNA) and gold electrode (AuE). The successful detection of telomerase was achieved by hybridization process between the probe single stranded deoxyribonucleic acid (ssDNA) drop coated on the 3MPA-In₂Te₃ QDs/AuE surface and its complementary ssDNA in biological buffer solution (0.10 M tris-ethylenediamine tetraacetic acid (TE) buffer solution, pH 8.00). The response of the 3MPA-In₂Te₃ QDs based genosensor towards different concentration of complementary ssDNA was studied by CV, square wave voltammetry (SWV) and EIS. It was observed that all three analytical techniques exhibited good linearity since their linear correlation coefficients (R^2) corresponded to 0.99. However, it was observed that EIS was the best technique for the detection of telomerase compared to both CV and SWV since it showed a higher sensitivity (2.44 Ω /nM) towards detecting telomerase with a detection limit as low as 0.00014 ng/mL. Control experiments were also carried out by monitoring the hybridization process in the presence and absence of complementary ssDNA and it was determined that the QDs based genosensor was highly selective towards complementary ssDNA. In view of the attractive analytical characteristics and advantages, the ultimate goal of the developed QDs based genosensor is to apply it in real clinical samples of cancer cells or bodily fluids of cancer patients for the detection of telomerase cancer biomarker.

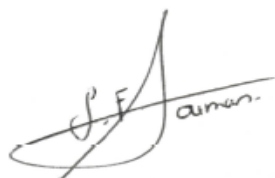
DECLARATION

I declare that *The response dynamics of indium telluride quantum dots impedimetric genosensor for telomerase cancer biomarker* is my own work and has not been submitted before for any degree or examination in any other university, and that all sources I have used or quoted have been indicated and acknowledged as complete references.



Samantha Douman

Year: 2013

A handwritten signature in black ink, appearing to read "S.F. Douman".

Signed.....

ACKNOWLEDGEMENT

Firstly, I want to thank my Heavenly Father the God Almighty for giving me the strength, wisdom, courage, patience and perseverance to complete this dissertation to the best of my ability.

My dear parents who are the centre of my being I honestly do not have words to describe how thankful I am. I can never repay you but I want to take this opportunity to thank both of you for your love, support and motivation. Thank you for all the sacrifices that you both have made I owe all my success to you.

To my Supervisor: Prof. Emmanuel Iwuoha, thank you for giving me a chance to showcase what I am capable of achieving in life. I am very grateful for your support, encouragement and guidance. I am truly honoured to be taught by you.

My thanks also go to Dr. Rachel Fanelwa Ajayi, thank you my Doctor for your support, advice and mentorship. I truly admire your love and compassion as a lecturer towards your students.

To the Department of Chemistry staff and all the SensorLab members especially Ms Wilhelmina Jackson, Prof. Priscilla Baker, Dr. Tesfaye Waryo, Dr. Paul Mushonga, Dr. Chinwe Ikpo, Dr. Stephen Mailu, Dr. Masikini Milua, Oluwakemi Tovide, Godfrey Fuku, Lindsay Wilson, Ezo Nxusani, Usisipho Feleni, Unathi Sidwaba and Bulelwa Mpushe thank you for your encouragement and input.

To all my friends not mentioned thank you for your loving friendship and support during my stay at UWC and just making me happy everytime we see each other.

I would also like to extend my acknowledgement to the National Research Foundation (NRF) for awarding me a Masters Innovation Scholarship.

Lastly I would also like to acknowledge the Electron Microscope Unit (EMU) at the Physics Department (University of the Western Cape), for assistance with the HRTEM/SEM.



DEDICATION

This dissertation is dedicated to my late aunt Janet Douman who lost the battle against cancer may your soul rest in peace and my aunt Angeline Josephs who survived cancer, may there be many more years of good health.

Last but not least to my loving father, Frederick Douman; mother, Gadija Douman and brother, Sebastiaan Douman.



LIST OF PUBLICATIONS

1. **Samantha Dومان**, Unathi Sidwaba, Rachel F. Ajayi, Nicolette Hendricks, Usisipho Feleni, Priscilla G.L Baker, Emmanuel I Iwuoha. Gallium selenide quantum-dots genosensors for the determination of telomerase – a breast cancer biomarker. (Nano Hybrids, 2014, Accepted).
2. Rachel F. Ajayi, Unathi Sidwaba, Usisipho Feleni, **Samantha Dومان**, Subelia Botha, Priscilla G.L. Baker, Emmanuel I. Iwuoha (2013) Chemically amplified cytochrome P450-2E1 drug metabolism nanobiosensor for rifampicin antituberculosis drug (Electrochimica Acta, Accepted).
3. Usisipho Feleni, Unathi Sidwaba, **Samantha Dومان**, Ezo Nxusani, Rachel F. Ajayi, Priscilla G.L Baker and Emmanuel I Iwuoha. Selenide quantum dots electrochemical biotransducer for the determination of indinavir-a protease inhibitor anti-retroviral drug. (International Journal of Electrochemical Sciences, 2014, Submitted).
4. Unathi Sidwaba, Rachel F. Ajayi, Nicolette Hendricks, **Samantha Dومان**, Usisipho Feleni, Priscilla G.L Baker, Emmanuel I Iwuoha. Electrosynthetic carbon nanotubes and CYP 2E1-derivatized polyanilino nanobiosensor for the detection of anti-TB drugs. (IET Nanotechnology, 2014, Submitted).

LIST OF ABBREVIATIONS AND ACRONYMS

3MPA	3-Mercaptopropionic acid
QDs	Quantum dots
In ₂ Te ₃	Indium Telluride
DNA	Deoxyribonucleic Acid
ssDNA	Single Stranded Deoxyribonucleic Acid
dsDNA	Double Stranded Deoxyribonucleic Acid
PBS	Phosphate Buffer Solution
TE buffer	Tris-ethylenediamine tetraacetic acid buffer
EDC	1-Ethyl-3-(3-Dimethylaminopropyl) Carbodiimide Hydrochloride
NHS	N-Hydroxysuccinimide
AuE	Gold Electrode
UV-VIS	Ultraviolet – Visible Spectrophotometry
FL	Fluorescence Spectroscopy
FT-IR	Fourier Transformation Infrared spectroscopy
XRD	X-ray diffraction
HR-SEM	High Resolution Scanning Electron Microscopy
HR-TEM	High Resolution Transmission Electron Microscopy
CV	Cyclic Voltammetry

SWV	Square Wave Voltammetry
EIS	Electrochemical Impedance Spectroscopy
EDX	Energy Dispersive X-ray Spectrometry
PCR	Polymerase Chain Reaction
TRAP	Telomeric Repeat Amplification Protocol
ELISA	Enzyme Linked Immunoabsorbant Essay
E_{pa}	Anodic Peak Potential
E_{pc}	Cathodic Peak Potential
I_{pa}	Anodic Peak Current
R_{ct}	Charge Transfer Resistance
LOD	Limit of detection



TABLE OF CONTENTS

TITLE PAGE.....	i
KEYWORDS	ii
ABSTRACT	iii
DECLARATION.....	v
ACKNOWLEDGEMENT	vi
DEDICATION.....	viii
LIST OF PUBLICATIONS.....	ix
LIST OF ABBREVIATIONS AND ACRONYMS	x
TABLE OF CONTENTS.....	xii
LIST OF FIGURES	xvii
LIST OF SCHEMES.....	xx
LIST OF TABLES	xxi
CHAPTER 1	1
Chapter overview	1
1.0 INTRODUCTION	1
1.1 Background	1
1.2 Problem identification, research aims, approach and objectives.....	3
CHAPTER 2	7
Chapter overview	7
2.0 LITERATURE REVIEW	7

2.1 Quantum dots	7
2.1.1 Capping agents.....	9
2.1.1.1 3-Mercapto propionic acid	10
2.2 Deoxyribonucleic acid (DNA)	11
2.2.1 Electrochemistry of DNA	13
2.3 Cancer biomarkers	14
2.3.1 Telomerase	16
2.3.1.1 The traditional TRAP assay	18
2.4 Biosensors	19
2.4.1 Affinity biosensor-Genosensor (DNA biosensor)	20
CHAPTER 3	23
Chapter overview	23
3.0 EXPERIMENTAL SECTION	23
3.1 Chemicals	23
3.2 Safety Note	24
3.3 Materials and Instrumentation	25
3.4 Procedure	26
3.4.1 Synthesis of 3MPA capped In ₂ Te ₃ QDs	26
3.4.1.1 Preparation of sodium hydrogen telluride (NaHTe) solution.....	27
3.4.1.2 Preparation of 3MPA-InCl ₃ ion solution.....	28
3.4.2 Sample preparation	29
3.4.2.1 Preparation of electrolyte buffer solution.....	29
3.4.2.2 Preparation of stock and working solutions	30



3.4.3 Preparation of 3MPA-In ₂ Te ₃ QDs AuE	30
3.4.4 Probe adsorption, target hybridization and electrochemical detection	31
3.5 Characterization techniques.....	33
3.5.1 Electrochemical techniques	33
3.5.1.1 Cyclic Voltammetry (CV).....	33
3.5.1.2 Square Wave voltammetry (SWV)	37
3.5.1.3 Electrochemical Impedance Spectroscopy (EIS)	39
3.5.2 Spectroscopic techniques	43
3.5.2.1 Ultraviolet-visible spectroscopy (UV-VIS)	43
3.5.2.2 Fluorescence spectroscopy (FL).....	44
3.5.2.3 X-Ray diffraction (XRD)	46
3.5.2.4 Fourier transform infrared spectroscopy (FT-IR)	47
3.5.3 Microscopic techniques	48
3.5.3.1 High resolution transmission electron microscopy (HR-TEM)	48
3.5.3.2 High resolution scanning electron microscopy (HR-SEM)	49
CHAPTER 4	51
Chapter overview	51
4.0 RESULTS AND DISCUSSION.....	51
4.1 Spectroscopic techniques	51
4.1.1 Ultraviolet-visible spectroscopy studies (UV-VIS).....	51
4.1.2 Fluorescence spectroscopy (FL)	54
4.1.3 X-ray diffraction (XRD)	56
4.1.4 Fourier transform infrared spectroscopy (FT-IR)	57
4.2 Microscopic techniques	59

4.2.1 High resolution transmission electron microscopy (HR-TEM).....	59
4.2.2 High resolution scanning electron microscopy (HR-SEM).....	62
4.3 Electrochemical techniques	66
4.3.1 Cyclic Voltammetry (CV).....	66
4.3.2 Electrochemical Impedance spectroscopy (EIS)	73
4.4 Characterization of 3MPA-In₂Te₃ QDs based genosensor	76
4.4.1 Cyclic Voltammetry (CV).....	76
4.4.2 Electrochemical Impedance Spectroscopy (EIS).....	77
4.5 Genosensor measurements.....	80
4.5.1 Response dynamic of 3MPA-In ₂ Te ₃ QDs based genosensor to complementary ssDNA (target) using voltammetric techniques (CV and SWV).....	80
4.5.2 Response dynamic of 3MPA-In ₂ Te ₃ QDs based genosensor to complementary ssDNA (target) using EIS	84
4.6 Comparison of the analytical performance of the QDs based genosensor using CV, SWV and EIS	86
4.7 Sensor control experiments.....	88
4.7.1 Sensor control experiments using SWV	88
4.7.2 Sensor control experiments using EIS	89
CHAPTER 5	92
Chapter overview	92
5.0 CONCLUSION AND RECOMMENDATIONS.....	92
5.1 Conclusion	92
5.2 Recommendations for future study.....	93

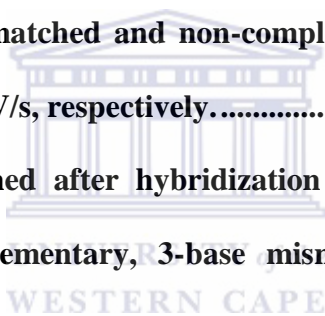


LIST OF FIGURES

Figure 1: Mercapto acids.....	10
Figure 2: The chemical formulas of the four nucleotide bases.	12
Figure 3: Digital image of the three electrodes WE, RE and CE, respectively (left) and a typical three electrode system set up (right).	26
Figure 4: The NaHTe solution (purple) after 40 min.....	27
Figure 5: The milky white 3MPA-InCl ₃ solution.	28
Figure 6: 3MPA-In ₂ Te ₃ QDs solution at 0 min.....	29
Figure 7: 3MPA-In ₂ Te ₃ QDs solution at 30 min.....	29
Figure 8: A cyclic voltammogram for a reversible redox system.	35
Figure 9: Potential waveform (a) and its respective current response (b) for SWV.....	38
Figure 10: Sinusoidal Current Response in a Linear System.	40
Figure 11: A typical Nyquist plot (a) and the corresponding equivalent circuit with RC parallel element (b).....	41
Figure 12: A typical Bode plot.	42
Figure 13: UV-VIS spectrum of 3MPA-InCl ₃ (black line) and NaHTe (purple line).	52
Figure 14: UV-VIS spectrum of 3MPA-In ₂ Te ₃ QDs.	53
Figure 15: Fluorescence (emission and excitation) spectra of 3MPA-In ₂ Te ₃ QDs.	55
Figure 16: XRD pattern of 3MPA-In ₂ Te ₃ QDs.....	56
Figure 17: FT-IR spectrum of 3MPA and 3MPA-In ₂ Te ₃ QDs.....	57
Figure 18: HR-TEM micrographs of 3MPA-In ₂ Te ₃ QDs 20 nm (A) 2 nm (B) and 50 nm (C) scale view.	60
Figure 19: HR-TEM Energy-dispersive X-ray (EDX) spectrum of 3MPA-In ₂ Te ₃ QDs..	61
Figure 20: HR-SEM micrographs of 3MPA-In ₂ Te ₃ QDs (A) and probe DNA/3MPA-In ₂ Te ₃ QDs (B) at 200 nm scale view.....	64

Figure 21: HR-SEM Energy-dispersive X-ray (EDX) spectrum of 3MPA-In₂Te₃ QDs..	65
Figure 22: Cyclic voltammograms of InCl₃ versus bare AuE (A) and NaHTe versus bare AuE (B) in 0.10 M PBS, pH 7.4 at 10 mV/s.....	67
Figure 23: Cyclic voltammograms of bare AuE (a) and 3MPA-In₂Te₃ QDs/AuE (b) in 0.10 M PBS, pH 7.4 at 10 mV/s.	69
Figure 24: Multi-scan voltammograms of 3MPA-In₂Te₃ QDs in 0.10 M PBS, pH 7.4 at (4-300 mV/s).....	70
Figure 25: Anodic (peak A₂) plot of peak current (I_{p,a}) versus scan rate (v).....	71
Figure 26: Anodic (peak A₂) plot of log peak current (I_{p,a}) versus log scan rate (v).	72
Figure 27: Nyquist plots corresponding to Randles equivalent circuit of bare AuE and 3MPA-In₂Te₃ QDs/AuE in 0.10 M PBS, pH 7.4.	74
Figure 28: Randles equivalent circuit used to model impedance data of bare AuE and 3MPA-In₂Te₃ QDs/AuE in 0.10 M PBS, pH 7.4.	74
Figure 29: Bode plots of bare AuE and 3MPA-In₂Te₃ QDs/AuE in 0.10 M PBS, pH 7.4.	75
Figure 30: Cyclic voltammograms of bare AuE, 3MPA-In₂Te₃ QDs/AuE and probe ssDNA/3MPA-In₂Te₃ QDs/AuE in 0.10 M PBS, pH 7.4 at 10 mV/s.....	77
Figure 31: Nyquist (A) and Bode (B) plots of bare AuE, 3MPA-In₂Te₃ QDs/AuE and probe ssDNA/3MPA-In₂Te₃ QDs/AuE in 0.10 M PBS, pH 7.4, respectively.....	79
Figure 32: CV response of probe ssDNA/3MPA-In₂Te₃ QDs/AuE to different concentrations of complementary ssDNA (target) in 0.10 M TE buffer solution, pH 8.00 at 10mV/s.....	81
Figure 33: SWV response of probe ssDNA/3MPA-In₂Te₃ QDs/AuE to different concentrations of complementary ssDNA (target) in 0.10 M TE buffer solution, pH 8.00 at 10mV/s.....	82

Figure 34: Calibration curve of 3MPA-In₂Te₃ QDs based genosensor showing CV responses to different concentration of complementary ssDNA (target).	83
Figure 35: Calibration curve of 3MPA-In₂Te₃ QDs based genosensor showing SWV responses to different concentration of complementary ssDNA (target).	84
Figure 36: Impedimetric response of probe ssDNA/3MPA-In₂Te₃ QDs/AuE to different concentrations of the complementary ssDNA (target) in 0.10 M TE buffer solution, pH 8.00.	85
Figure 37: Calibration curve of 3MPA-In₂Te₃ QDs based genosensor showing EIS response to different concentration of complementary ssDNA (target).	86
Figure 38: Anodic SWV response of the probe ssDNA/3MPA-In₂Te₃ QDs/AuE to 10 nM of complementary, 3 base mismatched and non-complementary ssDNA in 0.10 M TE buffer solution, pH 8.00 at 10mV/s, respectively.	89
Figure 39: Δ_{Ratio} values obtained after hybridization of probe ssDNA/3MPA-In₂Te₃ QDs/AuE with 10 nM complementary, 3-base mismatch and non-complementary ssDNA, respectively.	91



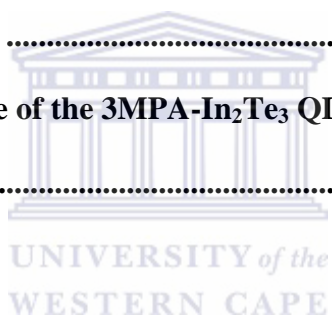
LIST OF SCHEMES

Scheme 1: Schematic representation of DNA double helix.	13
Scheme 2: Schematic diagram of the elongation process.	17
Scheme 3: Schematic diagram illustrating the main components of a biosensor.....	19
Scheme 4: Fabrication of the electrochemical 3MPA-In₂Te₃ QDs-based genosensor.....	32
Scheme 5: Jablonski's electronic transition energy level diagram.	45
Scheme 6: Schematic of XRD illustrating the conditions required for Bragg diffraction to occur.	46



LIST OF TABLES

Table 1: Different types of cancer biomarkers (Gouvea et al., 2011).	15
Table 2: Different types of genosensors for telomerase detection.	22
Table 3: DNA sequences used in this study	24
Table 4: Properties of the chemicals used in this experiment.	24
Table 5: Cyclic voltammogram diagnostics for an electrode reaction at an electrode surface involving chemically stable and soluble redox couples	35
Table 6: Charge transfer resistance (R_{ct}) values of bare AuE, 3MPA-In₂Te₃ QDs/AuE and probe ssDNA/3MPA-In₂Te₃ QDs/Au.	78
Table 7: Change in phase angle values of bare AuE, 3MPA-In₂Te₃ QDs/AuE and probe ssDNA/3MPA-In₂Te₃ QDs/AuE.	78
Table 8: Analytical performance of the 3MPA-In₂Te₃ QDs based genosensor for CV, SWV and EIS techniques used	87



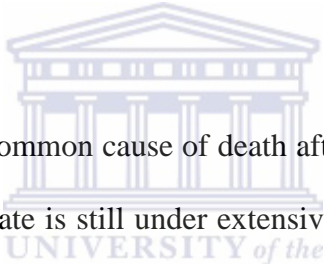
CHAPTER 1

Chapter overview

This chapter gives a brief overview on the background of cancer disease, with special attention focused on telomerase cancer biomarker and its existing detection methods. In addition other important aspects such as biosensors and nanomaterials were also discussed. This chapter also includes the problem statement, motivation, aim and objectives of the present study.

1.0 INTRODUCTION

1.1 Background



Cancer, the second most common cause of death after heart disease, is a complex and multifactorial disease that up to date is still under extensive research. This melanoma illness can be defined as group of diseases characterized by cell invasion, uncontrollable growth, and metastatic behaviour into surrounding tissues or distant organs (*Kulla and Katz, 2008*). It is said that cancer can be preventable since only 5-10 % of all cancers are caused by inheritance whereas the remaining 90-95% results from various environment factors and individual lifestyle (*Anand et al., 2008*). Despite the implementation of numerous populations screening programmes characterized by better detection of the specific types of cancers (breast, prostate, cervical, and colorectal), improvement in the survival rates is still relatively low. This is mainly due to the fact that most patients are diagnosed when the cancer has reached an advanced stage. To achieve early detection of any cancer disease, the discovery of specific, sensitive and reliable biomarkers are required (*Whelan et al., 2009*). Many reports indicate telomerase, a ribonucleo-protein complex (*Schmidt et al., 2002*) as an interesting and important target for cancer diagnostics and cancer therapy, because its activity has been

demonstrated in 75% of oral carcinomas, 84% of prostate cancers, 85% of liver cancers, 93% of breast cancers, 95% of colorectal cancers, and 98% of bladder cancers (*Belair et al., 1997*). However obtaining telomerase samples from most tumours is invasive and not amenable to serial analyses (*Hess and Highsmith, 2002*). Thus several studies have been done and investigators found measurable levels of telomerase activity in body fluids such as (urine, cervical smears, or sputum) of cancer patients hence allowing the detection of the telomerase biomarker to be carried out non-invasively. The standard method for the detection and quantification of telomerase activity is the polymerase chain reaction (PCR)-based assay known as the telomeric repeat amplification protocol (TRAP) assay (*Hess and Highsmith 2002*). But, TRAP and other methods developed for telomerase detection have limitations thus require a more sensitive, reliable and high-throughput method that will be able to statistically verify the presence of telomerase within cancer cells or body fluids of cancer patients (*Jakupciak et al., 2004*). Electrochemical biosensors are quickly emerging as an alternative for early detection of cancer because they can be designed to detect developing cancer biomarkers and to allow improved monitoring of cancer growth and patient therapy. Bio-affinity based biosensors such as genosensors that involve nucleic acids are the most crucial when it comes to cancer diagnostics since they are able to identify specific target sequence and validate their existence by hybridization. The main principle of electrochemical genosensors is based on the detection of hybridization that occurs between a surface-confined single stranded deoxyribonucleic acid (ssDNA) probe and its complementary ssDNA sequence. To meet the need of a more sensitive genosensor towards detection of target analyte, nanomaterials can be incorporated to improve the response. Quantum dots (QDs), gold nanoparticles, magnetic nanoparticles, carbon nanotubes, gold nanowires and many other nanomaterials (*Choi et al., 2010*) have shown great potential in biomedical applications. One of the main factors which make QDs particularly interesting and desirable to biomedical

science is the size of the materials (*Madani et al., 2013*). The properties of QDs differ greatly between bulk semiconductor and nanocrystals of the same material as a result of the quantum confinement effect (*Yun et al., 2007*). QDs are semiconductors that are a few nanometers in diameter and due to their high surface area, favourable electronic properties, electro-catalytic activity, good biocompatibility and specific physicochemical characteristics (*Sadik et al., 2009*) they can be incorporated into electrochemical biosensors for the detection of ultralow levels of cancer biomarkers. The use of QDs for electrochemical bio-sensing has been growing rapidly over the last few years. Dozens of research articles that deals with the use of QDs for electrochemical detection of cancer biomarkers have since been published. For instance, Yang and co-workers reported sensitive immunoelectrochemical detection of prostate specific antigen (PSA) a cancer biomarker using quantum dot functionalized graphene sheets as labels (*Yang et al., 2011*).

The present research study focused on the synthesis of 3-mercaptopropionic acid indium telluride quantum dots (3-MPA In₂Te₃ QDs) which were used as a mediating platform in the fabrication of a genosensor system for the quantitative determination of telomerase, a cancer biomarker.

1.2 Problem identification, research aims, approach and objectives

In 2005 The Cancer Association of South Africa (CANSA) in partnership with the National Cancer Registry (NCR) reported that more than 100 000 South Africans are diagnosed with cancer every year. On the other hand, the International Agency for Research in Cancer (IARC) reported that there were 681 000 new cancer cases and 512 400 cancer deaths in Africa in 2008. It is believed that by the year 2030 these numbers will double due to ageing and growth in the population. This is a major problem for the human population as a whole because even though significant amount of research regarding early detection of cancer has been carried out over the last decade, not much improvement in the survival of cancer

patients was achieved. There are different factors that contribute to this problem. Firstly, lack of access to health care facilities and appropriate treatment. Secondly, lack of manpower to deal with scarcity of training supports in oncology and lastly traditional diagnostic methods that are not very powerful when it comes to early detection of cancer. However of all the above mentioned factors the diagnostic methods are of significance in this study. The following are some current traditional methods used for the detection of various cancers: (i) Papanicolau test for cervical cancer, (ii) mammography for breast cancer, (iii) prostate-specific antigen (PSA) level detection in blood for prostate cancer, (iv) occult blood detection for colon cancer, and (v) endoscopy, CT scans, X-ray, ultrasound imaging and MRI.

Some of these screening methods are limited and expensive, and even after treatment options whether surgical removal, chemotherapy or radiation therapy some tumours can return after a period of time. These screening methods can also lead to false positive results and subsequent invasive procedures. The survival of cancer patients depends greatly on early detection because it will provide a higher chance of successful treatment. Cancer biomarkers are also of utmost importance however low sensitivity and low specificity of some cancer biomarkers makes it unreliable for early cancer detection. Telomerase is regarded as a useful biomarker for early detection of cancer, but methods that were developed for telomerase detection have disadvantages of their own such as being time consuming, gives false-positive results, it requires complicated machinery, expensive equipment and reagents.

Hence this research study aimed to develop a fast, simple, sensitive and cost effective 3-MPA In_2Te_3 QDs based genosensor for determination of telomerase biomarker. The intension of such a device is to eliminate the lengthy waiting periods patients have to endure for their results pertaining to cancer detection when using available techniques; as mentioned above. This genosensor device will offer a highly sensitive and easy to use method thus create a friendly and comfortable environment for patients to be tested. This device will also

allow health care practitioners to receive results promptly and at point-of-care thus allowing adequate treatment to commence and therefore allowing individualization of treatment regimes.

In this research study a quantitative research approach was applied and the aim was achieved through the following objectives:

- i. Synthesis of 3MPA-In₂Te₃ QDs.
- ii. Spectro-electrochemical characterization of 3MPA-In₂Te₃ QDs by Ultraviolet-Visible (UV-VIS) absorption and Fluorescence (FL) spectroscopy.
- iii. Spectroscopic and microscopic characterization of 3MPA-In₂Te₃ QDs by X-ray Diffraction (XRD), Fourier Transform Infra-red (FT-IR) spectroscopy and High Resolution Scanning/Transmission Electron Microscopy (HR-SEM/TEM).
- iv. Modification of a bare gold electrode (AuE) with 3MPA-In₂Te₃ QDs.
- v. Electroanalysis of the 3MPA-In₂Te₃ QDs-modified AuE using Cyclic Voltammetry (CV), Osteryoung Square Wave (OSW) voltammetry and Electrochemical Impedance Spectroscopy (EIS).
- vi. Fabrication of the novel 3MPA-In₂Te₃ QDs based genosensor with an amine terminated 23 bases ssDNA, whose sequence is 5'- NH₂-GGGATTGGGATTGGGATTGGGTT-3'.
- vii. Response dynamics of the novel 3MPA-In₂Te₃ QDs genosensor with standard telomerase solutions containing complementary (5'- AACCCAATCCCAATCCCAATCCC-3', non-complementary (5' - TATCGGAATGCGTATGGCTTAGG-3') and 3-base mismatch (5' -

AACCTAATCCCGATCCCAAATCC-3') ssDNA sequences using electrochemical techniques.



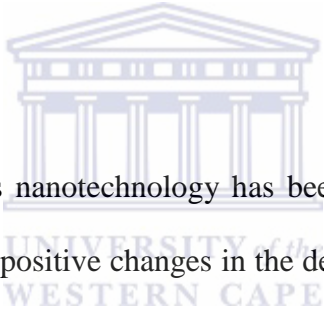
CHAPTER 2

Chapter overview

This chapter gives a brief outline of various aspects and their contribution towards the success of the present study. It discusses the background and uses of QDs as supporting materials in biosensors systems and it gives a brief introduction on the importance and electrochemistry of DNA. This chapter also gives an overview on the importance of cancer biomarkers and it outlines the theory and types of biosensors systems with the main focus on the approach and design of the proposed genosensor system for telomerase detection.

2.0 LITERATURE REVIEW

2.1 Quantum dots



Over the last two decades nanotechnology has been one of the most popular fields since it showed potential to make positive changes in the detection, treatment, and prevention of certain diseases (*Peng and Li, 2010*). At the present-day nanomaterials such as QDs are of great interest since they can be used as supporting materials in different applications due to their remarkable properties. Some of these applications include amplifiers, biosensors, high-resolution cellular imaging, tumour targeting, and diagnostics. QDs are also known as colloidal semiconductor nanocrystals that range from 2 – 10 nanometers in diameter and can contain roughly hundreds to thousands of atoms (*Peng and Li, 2010*). QDs can be arranged in binary (*e.g.* GaAs) as well as ternary compounds (*e.g.* InGaAs) and can be produced from group II–VI (*e.g.* CdTe, CdSe), III–V (*e.g.* InAs, InP) or IV–VI (*e.g.* PbS, PbSe) elements of the periodic table (*Wagner et al., 2010*). Additional shells can also be used to cover the core materials of QDs therefore forming core-shell structures (*e.g.* CdSe QD with ZnS shell). These shells can either help to increase the QDs stability or improve their luminescence

properties. The properties of QDs are different to those of the bulk material of the same sample, due to the high surface area to volume ratio. QDs also have a tuneable bandgap making them more favourable to be used in applications ranging from biology to photovoltaic devices. Another advantage of QDs is that they can be shaped into a variety of different forms such as sheets or three-dimensional arrays whereas conventional semiconductor materials are rigid. Other properties of QDs include narrow emission spectra, which make them feasible to perform 'multiplexing'; high quantum yield, which causes QDs to have extremely high brightness when excited; low photobleaching, which is crucial for long-term real-time image tracking; broad absorption spectra and high photochemical stability (*Zhang et al., 2008*). The properties of the QDs show size and shape dependences which are due to quantum confinement of the exciton (electron-hole pair) (*Ning et al., 2011; Frasco and Chaniotakis, 2009*). When the size of the QDs are decreased or increased this can either cause a confinement of a higher or lower degree thereby producing an exciton of higher or lower energy hence increasing or decreasing the bandgap energy (*Gao and Dave, 2007*). The bandgap energy is equivalent to the minimum energy required to move an electron from valence to conduction band (*Frasco and Chaniotakis, 2009*). Therefore due to altering of QD size the larger particles will emit toward the infrared region (red-shift) while smaller particles will emit toward the ultraviolet region (blue-shift). This phenomenon is called "quantum confinement" and applies to particles that are smaller than the Bohr exciton radius (*Michalet et al., 2005*).

There are different synthesis routes when it comes to producing QDs. For instance methods like atomic deposition on solid-phases, colloidal synthesis in aqueous solution or in non-polar solvents (*Gao and Dave, 2007; Crouch et al., 2003*). The aqueous synthesis results in water-soluble QDs making this type of procedure simpler, inexpensive, and more reproducible than organic synthesis (*Weng and Ren, 2006*). Synthesis in non-polar solvents

results in hydrophobic QDs with high degrees of monodispersity (<5%) (*Murray et al., 1993*). However, the best quality QDs are prepared at higher temperature ranging from 25 °C to about 400 °C in organic solvents, such as tri-n-octylphosphine oxide (TOPO) and hexadecylamine (*Gao and Dave, 2007*).

2.1.1 Capping agents

Capping agents are molecules such as dendrimers, polymers and surfactants which coat the QDs in order to avoid grouping of the QDs in solution and also help to control the shape and size (*Quintanilla et al., 2010*). The amount of capping agent introduced to the system plays an important role since it can affect the interfacial diffusion and later the solubility of the QDs (*Koç et al., 2012*). Thus it is necessary to determine accurately the amount of capping agent for any synthesis route followed, so that the bonding between the capping agent and the growing QDs should neither be too strong nor too weak.

QDs are hydrophobic by nature therefore when using them in biological studies the QDs needs to be made water soluble before application by surface modification with bio-functional molecules (*Peng and Li, 2010*). In order to make QDs biocompatible with various affinity reagents such as antibodies, aptamers, specific DNA sequences, and peptides, (*Wagner et al., 2010*) the surface of the QDs needs to be modified. At this stage the capping agents comes in to play. Different thiolated organic surfactants like, 3- mercapto propionic acid (3-MPA), thioglycolic acid, thiolactic acid, cysteine or cysteamine are commonly used as capping agents during the synthesis of QDs. This study will make use of 3MPA which will act as a stabilising agent for the In₂Te₃ QDs. Below are a few examples of commonly used capping agents for the synthesis of QDs.

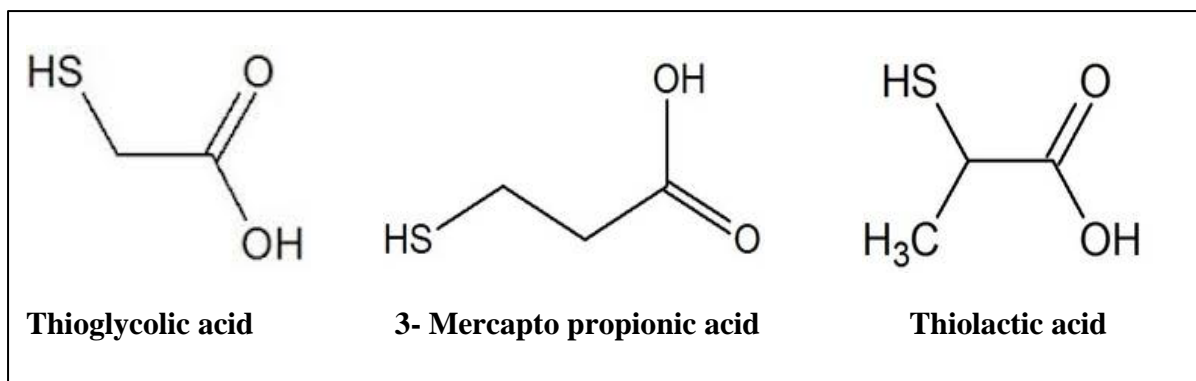


Figure 1: Mercapto acids.

2.1.1.1 3-Mercapto propionic acid (3MPA)

3MPA is an organic molecule (Wageh *et al.*, 2013) which consists of both thiol (-SH) and carboxylic acid (-CO₂H) groups. It is one of the shortest chained mercapto acids and its unique reducing properties make it ideal for use in a variety of chemical reactions. Mercapto acids are mostly used to make self-assembled monolayers (SAMs), a process created by chemisorption of hydrophilic “head groups” onto substrates from either the vapour or liquid phase followed by a slow two-dimensional organization of hydrophobic “tail groups”. The 3MPA plays an important role during synthesis of QDs in aqueous media because it acts as a stabilising agent. The two functional groups associated with the mercapto acid have advantages that makes the mercapto acid favourable for use in biological applications. The carboxylic group offers a biocompatible surface which allows it to react favourably with amino groups of enzymes etc. While the coordination of the thiol group to the QDs allows for the passivation of dangling bonds on the surface of the QDs (Ndangili *et al.*, 2011; Wageh *et al.*, 2013).

In this study, In₂Te₃ QDs were produced from elements found in groups III and VI of the periodic table. These QDs were capped with 3-MPA to make it biocompatible with biological molecules. The production of these QDs from elements found in both groups III-

VI allowed the QDs to have interesting properties as discussed in section 2.1. These properties were essential when the QDs were employed as a mediating platform in the electrochemical genosensor system that was fabricated for telomerase detection in this study.

2.2 Deoxyribonucleic acid (DNA)

DNA is a nucleic acid that carries genetic information in the cells of humans and all other living organisms for growth and functioning which is important for their existence. DNA is made up of nucleotide bases known as adenine (A), guanine (G), thymine (T), and cytosine (C) with a backbone as support. The DNA backbone consists of alternating pentose sugars and phosphate groups. A ssDNA consist of these nucleotide bases linked together in a chain whereas a double stranded DNA (dsDNA) consist of two spiral chains that are complementary in their nucleotide bases. The two spiral chains of the dsDNA are held together by hydrogen bonds that arise between a purine (adenine, guanine) - and a pyrimidine (thymine, cytosine)-derived nucleic bases, shown in **Figure 2** (*Guerra et al., 1999*). Adenine always pairs up with thymine and guanine with cytosine. The order of these four bases is very significant since it is the arrangement of these bases that makes one person prone to cancer and another to epilepsy disease.

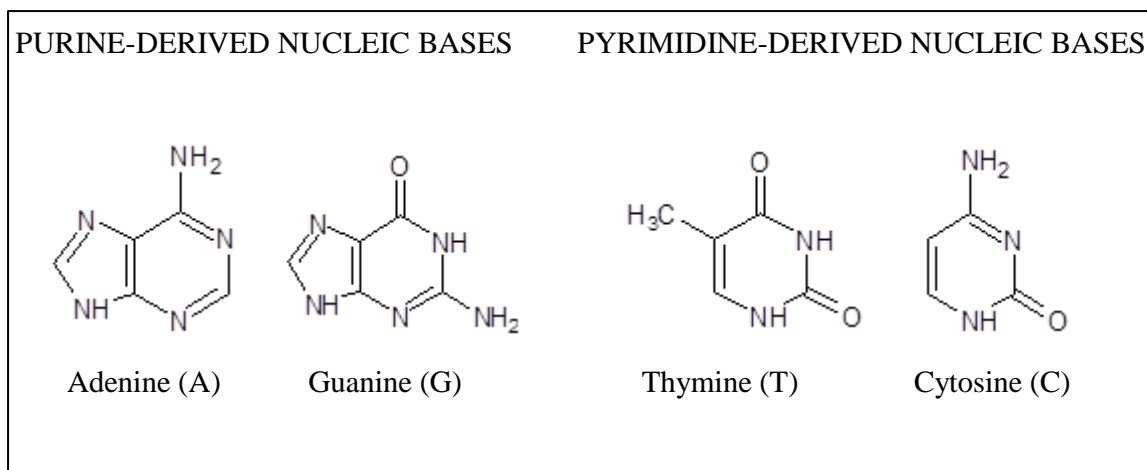
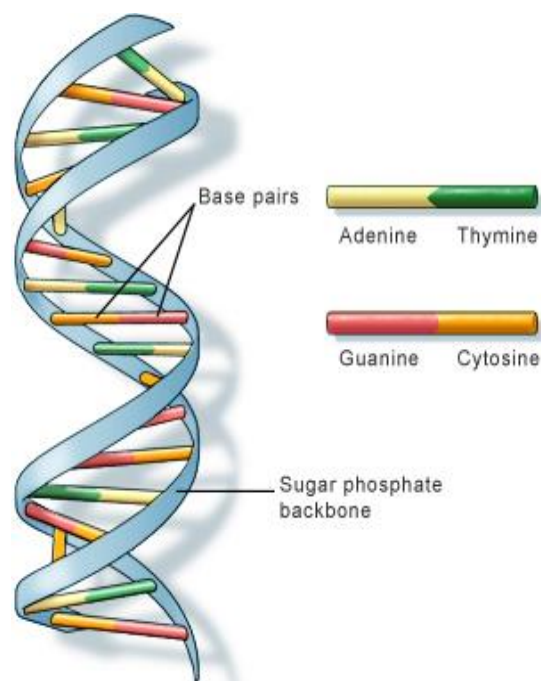


Figure 2: The chemical formulas of the four nucleotide bases.

The DNA double-helix (**Scheme 1**) was first discovered by J. Watson and F. Crick in 1953 (*Watson and Crick, 1953*). This DNA double helix structure looks like a twisted ladder and there are three different structural forms namely A-DNA, B-DNA and Z-DNA. The right-handed B-DNA is the common structural form because it is found in almost all living cells. The structural form A-DNA was discovered due to a greater electrostatic response between the phosphate groups when DNA became strongly dehydrated (*Arnott and Hukins, 1972*). The left-handed Z-DNA exists in response to certain types of biological activity and it plays a significant biological role in protection against viral illnesses (*Rich and Zhang, 2003*). Due to the different structural forms of the DNA double helix, different dynamic interactions may occur. During cell division the DNA double helix's distinctive structure allows it to copy itself by unwinding and forming two ssDNA sequences which are then used as templates to construct two new dsDNA molecules. In addition it also unwinds so that ssDNA's instructions can be used to make proteins by a process called gene expression. This gene expression process consists of two steps namely transcription and translation.



Scheme 1: Schematic representation of DNA double helix.

2.2.1 Electrochemistry of DNA

The adsorption and electrochemical conduct of DNA at the surface of different electrodes has been studied for a number of years (Wang *et al.*, 1996; Brett *et al.*, 1999; Li *et al.*, 2009a) and the ability of DNA to produce electrochemical oxidation and reduction signals was first reported by Palecek between the late 1950's and early 1960's. The first reported electrochemical analysis of DNA adsorption was with mercury and carbon electrodes and at a later stage with solid electrodes such as gold, platinum and copper. It was shown that nucleic acid (NA) adsorb at mercury electrodes giving reduction signals which were due to adenine and cytosine residues whereas guanine residues produced oxidation signals (Palecek *et al.*, 2002a). It was also found that mercury-containing electrodes (both liquid and solid) are much more optimal for studying the NA reduction whereas the latter electrodes better suited for studying the NA oxidation. When natural and denatured DNA undergoes voltammetric analysis, it is observed that the transition of electrons from the inside

of a ssDNA is much greater than for dsDNA due to the flexibility of the ssDNA's structure (*Palecek, 2002b*).

The DNA double helix in solution can be physically affected by conditions such as pH and extremely high temperatures. If the pH value is between 8.11 and 12 the DNA becomes denatured or if the pH < 3 the phosphodiester backbone becomes hydrolysed. Nevertheless, for the duration of the denaturation of DNA, no covalent bonds are broken only the hydrogen bonds between base-pairs and stacking interactions between consecutive bases are broken. Thus the DNA double helix is disrupted into ssDNA. The renaturation process also known as the hybridization process is the reverse of denaturation and it is of great importance for achieving the biological functions of DNA. Therefore various kinds of NA interactions can be studied by electrochemical methods.



2.3 Cancer biomarkers

A biomarker is defined as a biological molecule found in bodily fluids (blood, serum, urine or cerebral spinal fluid) and body tissues of humans (*Gouvea, 2011; Bohunicky and Mousa, 2011*). It is a measurable and reliable indicator since it can be used to evaluate abnormal conditions or diseases (*Manne et al., 2005*). Over the past few years tumour biomarkers also known as cancer biomarkers became an attractive topic in cancer diagnosis. The reason for its growing popularity is because it can play an important role in early cancer detection; since it can monitor disease development, determine the reaction of the cancer to the treatment and observe the recurrence of cancer (*Levenson, 2007*). There are a variety of cancer biomarkers that are associated with certain types of cancers. Some of these biomarkers include DNA modifications, RNA, protein and related molecules (*Bohunicky and Mousa,*

2011). **Table 1** below shows a range of biomarkers associated with different cancers (Gouvea, 2011).

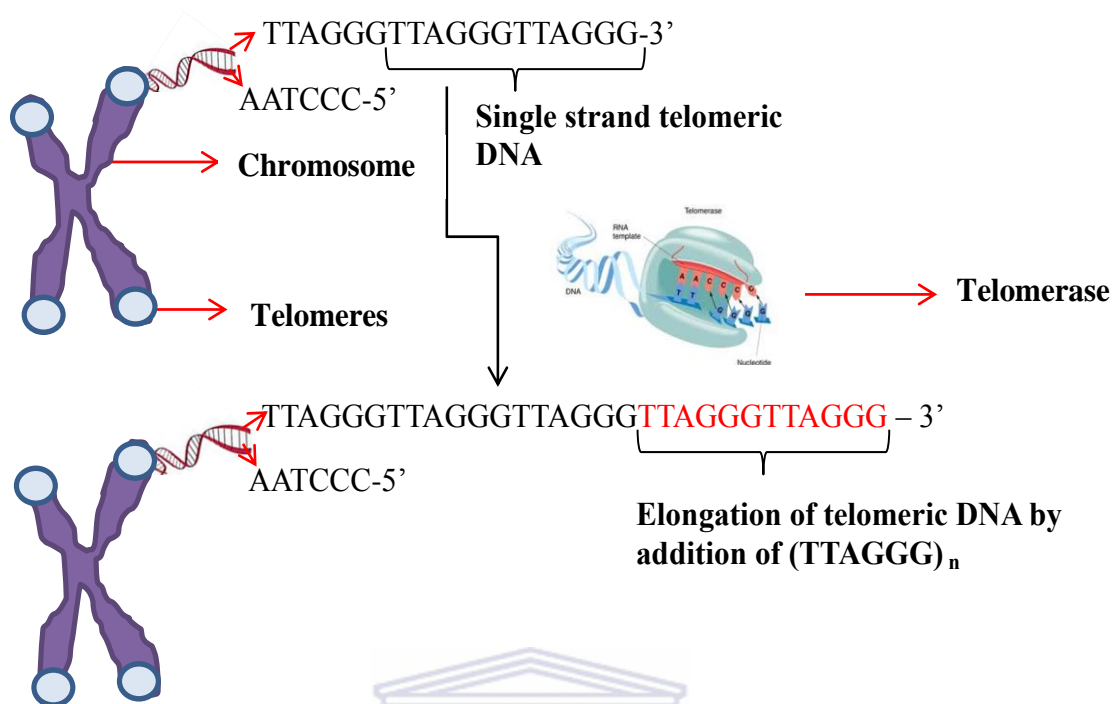
Table 1: Different types of cancer biomarkers (Gouvea et al., 2011).

Cancer	Biomarker
Breast	ER,PR, HER2, CA15.3, CA125, CA27.29, CEA BRCA1, BRCA2, MUC-1, CEA, NY-BR-1, ING-1
Bladder	BAT, FDP, NMP22, HA-Hase, BLCA-4, CYFRA 21-1
Cervix	P53, Bcl-2, Brn-3a, MCM, SCC-Ag, TPA, CYFRA 21-1, VEGF, M-CSF
Colon	HNPCC, FAP, CEA, CA19-9, CA24-2, p53
Prostate	PSA, PAP

The sensitivity and specificity of an ideal cancer biomarker needs to be 100% but none of the current cancer biomarkers achieve such a good combined sensitivity and specificity (Manne et al., 2005). For example, prostate specific antigen (PSA) a cancer biomarker for prostate cancer has a high sensitivity (>90%) but a very low specificity (<25%) while CA15.3 a serum tumour biomarker for breast cancer has a low sensitivity of 23% but a high specificity of 69% (Manne et al., 2005). By using a cancer biomarker that has more or less 100% sensitivity and specificity one is able to avoid unnecessary biopsies and under or over diagnosis. Therefore, researches need to find a more specific and sensitive cancer biomarker that would be of great use for cancer diagnosis when applied in biosensor systems (Kocevar et al., 2013). In this research study telomerase cancer biomarker was under investigation.

2.3.1 Telomerase

Human telomerase a ribonucleoprotein complex, is an enzyme that consists of two major components: a protein reverse transcriptase unit (hTERT) that provides catalytic function to replicate the ends of linear chromosomes and a RNA component (hTR) acting as a template for the synthesis of the human telomeric repeat (TTAGGG)_n (Ohshima *et al.*, 2003). The telomerase complex adds specific G-rich DNA sequence repeats (TTAGGG)_n to the 3' end of DNA strands of the telomeres, which are found at the ends of eukaryotic chromosomes (Sreenivasulu and Lakshmi, 2011). These telomeres are short G-rich nucleotide sequences (5'-TTAGGG-3') that plays an important role in the nucleus of a cell since it caps the ends of chromosomes in order to prevent it from degradation and also stop chromosomes from fusing to each other (Meyerson, 2000; Blackburn, 2005). When cell division takes place these telomeres becomes consumed losing about 50-200 base pairs per division (Maesawa *et al.*, 2003). As cell division continues and reaches the hayflick limit, the cell loses its ability to divide and enters the senescence phase. Telomerase comes into play before this stage is reached and it replenishes the telomeric nucleotide sequence by adding the G-rich sequences as shown in **Scheme 2** below.



Scheme 2: Schematic diagram of the elongation process.



Telomerase enzyme is regarded as an essential biomarker for cancer cells and malignancy because it has sensitivities of 60–90% as a tumour marker with clinical specificities for cancer of ~90% (*Hess and Highsmith, 2002*). Telomerase is responsible for the immortality and uncontrollable growth of cancer cells and it was found that 85% of more than 950 primary tumours expressed telomerase activity (*Pavlov et al., 2004; Kulla and Katz, 2008*). Some of these tumour tissues include lung cancer, rectal cancer, gastric carcinoma, carcinoma of prostate, and so on (*Zhong et al., 2005*). Telomerase are also found in reproductive organs and embryonal tissues such as stem cells and germ line cells respectively, but undetectable in normal somatic cells (*Skvortsov et al., 2011*). It was discovered that increased levels of telomerase activity within the cells is associated with early stage cancer formation (*Schmidt et al., 2002*). Therefore, a significant amount of interest has

been focused on telomerase since it is believed to play a critical role in assays for cancer diagnosis, research into cell biology and for evaluating anti-cancer therapeutics (*Maesawa et al., 2003*). There are different methods for the detection of telomerase however the telomeric repeat amplification protocol (TRAP) assay is the most common.

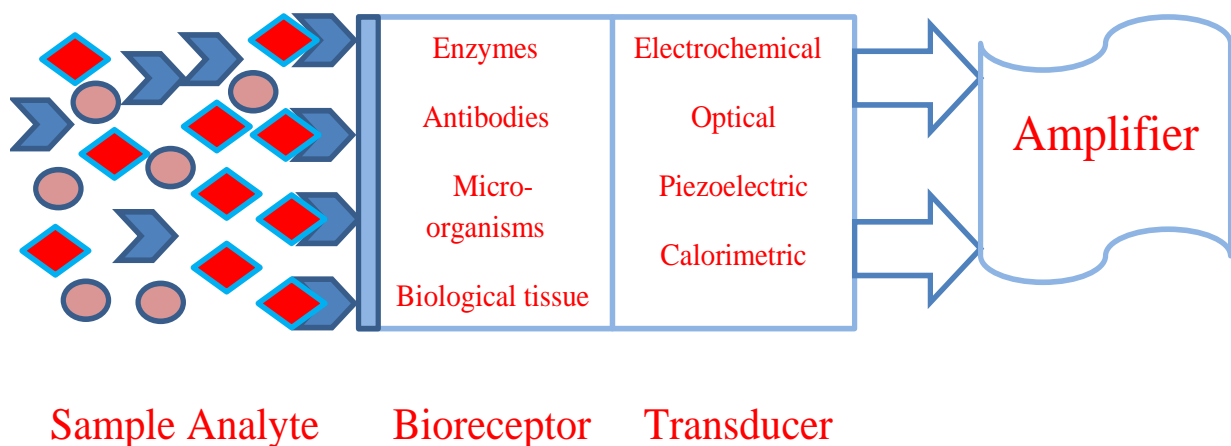
2.3.1.1 The traditional TRAP assay

The standard method for the detection of telomerase activity over the years has been the TRAP assay which is a polymerase chain reaction (PCR) based process (*Kim et al., 1994a*). This TRAP assay involves two steps: 1) elongation of the telomeric substrate (TS) that occurs in the presence of telomerase and 2) the elongated TS are amplified using a reverse primer that is complimentary only to the elongated sequence of the TS. Only the elongated part of the TS becomes amplified by PCR and can be detected by label-based methods (*Saldanha et al., 2003*). The TRAP assay does not only have a wide detection range but it is quite a sensitive method since it has the ability to detect telomerase activity in a single cell (*Saldanha et al., 2003*) however the TRAP assay has limitations. It is poorly quantifiable, its time consuming, labour-intensive and requires the use of radioactivity and polyacrylamide gel electrophoresis (*Kim, 1997b*). The traditional TRAP assay was modified in order to make it more “user-friendly” and improve the detection of telomerase activity. Although development of improved TRAP assays such as the TRAP-eze® (Intergen Discovery Products) (*Holt et al., 1996*) and TRAP ELISA (*Wu et al., 2000*) there are still drawbacks that needs to be resolved. Electrochemical biosensors are quickly emerging as an alternative for early detection of cancer because they can be designed to detect developing cancer biomarkers and to allow improved monitoring of cancer growth and patient therapy.

2.4 Biosensors

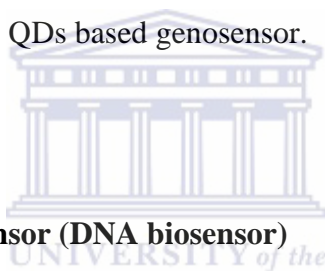
Over the current years, demand has grown for the development of simple, highly sensitive, fast and cost effective devices for medical diagnosis (*Gouvea et al., 2011*). These devices known as biosensor systems have a promising future as a detection method since they can be applied in clinical diagnosis, drug therapy, drug delivery and pharmaceutical analysis. The first research on biosensors was done by Professor Leland C Clark Jr. in 1956 (*Clark, 1956*). From then on a great number of publications on biosensor systems were done. A biosensor can be defined as a sensor that integrates biomolecules be it environmental or biological in origin (ie, within the human body) with a physiochemical transducer to produce an electronic signal which can be amplified, displayed, and analysed (*Bohunicky and Mousa, 2011*). Some of these common biomolecules are enzymes, antibodies, micro-organisms, biological tissue, and organelles (*Gouvea et al., 2011*). A typical biosensor consist of three main components, a mediator which converts a substrate to product, a transducer which recognizes the reaction and converts it into a signal and an amplifier where the signal gets organized and then sent into the microelectronics where it gets processed into the display.

Scheme 3 below shows the main components of a typical biosensor.



Scheme 3: Schematic diagram illustrating the main components of a biosensor.

A difference in biological element or transduction element such as electrochemical (*Li et al., 2010*), optical (*Schmidt et al., 2002*) or piezoelectric (*Su et al., 2013*) can allow for different types of biosensors such as catalytic/enzymatic biosensor, electrochemical biosensor, photoluminescence biosensor or affinity biosensors etc. The catalytic/enzymatic sensors were of the first generation biosensors whereas the affinity sensors that make use of different biological elements were of the second generation biosensors (*Mascini and Tombelli, 2008*). In a typical affinity biosensor the binding between the analyte and the biomolecule deposited on the transducer surface are possible through affinity interactions such as the antigen – antibody, the DNA - DNA or the protein - nucleic acid binding (*Mascini and Tombelli, 2008*). This present study also reports the use of such interactions for the determination of telomerase using QDs based genosensor.



2.4.1 Affinity biosensor-Genosensor (DNA biosensor)

More recently, in the last couple of years DNA based sensing received considerable attention because it can be useful in criminal investigations, testing for genetic or infectious diseases and the detection of food contaminants. In order to have a successful functional genosensor it needs to be highly sensitive and specific towards the target analyte. The detection of a specific ssDNA sequences is based on either direct sequencing or DNA hybridization methods (*Pividori et al., 2000*). DNA hybridization methods are the most preferred when it comes to diagnostics tests due to their simplicity (*Pividori et al., 2000*). The hybridization process occurs only between a target ssDNA sequence and its complementary probe ssDNA either in solution or on a solid support (*Gouvea et al., 2011*). When following the process whereby the probe ssDNA is adsorbed on the surface of an electrode it is always necessary to optimise the density of the probe ssDNA. The reason for this is to prevent the density of the probe ssDNA from influencing the thermodynamics of hybridization and hence

the selectivity of the genosensor (*Watterson et al., 2000*). Other experimental variables such as salt concentration, temperature, viscosity, the presence of accelerating agents, contacting time and base composition (G + C, %) can also affect the hybridization event at the transducer-solution interface (*Wang, 2002b*).

There are two main approaches that can be followed when fabricating a genosensor. The first is label-based and the second label free methods (*Bonannia and Del Vallea, 2010*). When following the label-based method the most common labels used for hybridization detection is fluorescent dyes (*Schmidt et al., 2002*) redox active enzymes (*Pavlov et al., 2004*), magnetic particles (*Weizmann et al., 2004*) and nanoparticles (*Li et al., 2010b*). Although fabrication of various detection systems for DNA analysis (e.g. optical and micro-gravimetric) are common, the electrochemical genosensors is one of the most popular detection systems due to their short assay time, low cost, simple design, portability, high sensitivity and high selectivity (*Bonanni et al., 2006; Topkayaa et al., 2012*). Therefore, these unique properties of the electrochemical genosensor will allow them to play a growing role in cancer diagnostic tests.

In this research study, nanomaterials such as QDs were incorporated into the genosensor system to create a more sensitive platform for target analyte detection. The genosensor developed in this study is novel since it is the first time a 3MPA-In₂Te₃ QDs based genosensor for the detection of telomerase is reported. It may not have been applied in real sample but the detection was in terms of concentration where a solution-phase method was followed. However, in the future this QDs based genosensor will be used to detect telomerase invasively and non-invasively. Invasive detection involves the extraction of cancerous cells from a tumour and telomerase is detected while non-invasive detection makes use of oral washes or urine samples of cancer patients. There is no base for comparison with the current study and what has been reported in literature since in literature the detection was

done by using cancerous cells while herein various concentrations of telomerase were detected. **Table 2** below discusses a few examples of the developed genosensors for the detection of telomerase in cancerous cells. These discussions are based on the detection limit, advantages and disadvantages.

Table 2: Different types of genosensors for telomerase detection.

Name of the biosensor	Detection limit (in terms of Cells)	Advantages	Additional requirements	Disadvantages	References
Traditional TRAP	100 HeLa cells			PCR	<i>Fajkus et al., 2006</i>
Bio-barcode amplification assay	10 HeLa cells	Elimination of PCR and cross reaction	S1 oligonucleotide, S3-DNA–Au NP conjugate and $[\text{Ru}(\text{NH}_3)_6]^{3+}$ required	Labels and expensive reagents required	<i>Li et al., 2010</i>
Cascade isothermal signal amplification based on three-way junction and base-stacking hybridization	3 HeLa cells	PCR free	3WJ-probes, two primers, molecular beacons, 3WJ-DNA machine and BSHBC-DNA machine required.	Complicated machinery and labels required	<i>Zhao et al., 2013</i>

CHAPTER 3

Chapter overview

This chapter firstly discuss the various chemicals and instrumentation used. Secondly it outlines the experimental procedures involving the synthesis of 3MPA-In₂Te₃ QDs; preparation of electrolyte buffer solutions, stock and working solutions; and preparation of modified AuE with 3MPA-In₂Te₃ QDs. Furthermore it gives an overview on the approach, design and application of the 3MPA-In₂Te₃ QDs based genosensor for the detection of telomerase cancer biomarker. Lastly it describes the techniques used for characterization of synthesized 3MPA-In₂Te₃ QDs as well as techniques used for characterization and application of the 3MPA-In₂Te₃ QDs based genosensor.



3.0 EXPERIMENTAL SECTION

3.1 Chemicals

Chemicals used in this study are analytical grade sodium hydroxide (NaOH), granular 98 % sodium borohydrate (NaBH₄), anhydrous $\geq 99.999\%$ trace metals basis indium(III) chloride (InCl₃) powder, 99.99% metal basis tellurium (Te) powder, 3-mercaptopropionic acid (3MPA), 1-ethyl-3-(3-dimethylaminopropyl) carbodiimide hydrochloride (EDC), N-hydroxysuccinimide (NHS), ethanol, disodium hydrogen phosphate (Na₂HPO₄), sodium dihydrogen phosphate (NaH₂PO₄) and tris-ethylenediamine tetraacetic acid buffer (TE buffer) solution comprised of 10 mM Tris-Hydrochloric acid and 1.00 mM disodium EDTA (molecular grade), pH 8.00 were all purchased from Sigma-Aldrich (Cape Town, South Africa). The 3MPA-In₂Te₃ QDs were synthesized at the University of the Western Cape, department of Chemistry Laboratories. Probe ssDNA no.1, complementary ssDNA no.2, non-

complementary ssDNA no.3 and 3 base mix mismatch ssDNA no.4 were all purchased from Inqaba Biotechnical Industries (Pty) Ltd., Hatfield, South Africa. The sequences of each oligonucleotide are listed in **Table 3** below. The distilled water used for preparing solutions and cleaning of electrodes was purified using a Milli-Q Water System (Millipore Corp., Bedford, MA, USA).

Table 3: DNA sequences used in this study.

Name	Sequence
Probe ssDNA No.1	5'- NH ₂ -GGGATTGGGATTGGGATTGGGTT-3'
Complementary ssDNA No.2	5'- AACCCAATCCCAATCCCAATCCC-3'
Non-complementary ssDNA No.3	5'- TATCGGAATGCGTATGGCTTAGG-3'
3 Base mix mismatch ssDNA No.4	5'- AACCTAATCCCGATCCCAAATCC-3'

3.2 Safety Note

Table 4: Properties of the chemicals used in this experiment.

Chemical name	Inhaled	Swallowed	Absorbed	Other
InCl ₃		Harmful	Harmful	Corrosive, irritant
Te powder		Toxic		
NaBH ₄	Harmful	Toxic	Toxic	Corrosive, highly flammable
3MPA	Harmful	Toxic	Harmful	Corrosive, irritant
NaOH				Corrosive, irritant
EDC	Harmful	Harmful	Harmful	Irritant

3.3 Materials and Instrumentation

All electrochemical experiments were carried using a BAS 100W integrated and automated electrochemical work station from Bio Analytical Systems (BAS), Lafayette, USA. All voltammograms; both cyclic and osteryoung square wave, were recorded with a computer interfaced to the BAS 100W electrochemical workstation.

A conventional three electrode set up was used as shown in **Figure 3**. This three electrode set up consisted of an electrochemical cell that bathes mainly three electrodes in an electrolyte solution.

- (1) Gold working electrode (WE), ($A = 0.0201 \text{ cm}^2$), from BAS
- (2) Platinum wire, from Sigma Aldrich, acted as a counter electrode (CE), and
- (3) Ag/AgCl (3 M KCl) from BAS was the reference electrode (RE).

Analytical grade argon and nitrogen gases used for degassing the cell solutions were purchased from Afrox Company, South Africa. Alumina polishing pads and powder (0.05, 0.3 and 1.0 μm) used to clean electrode surface were purchased from Buehler, Illinois, USA.

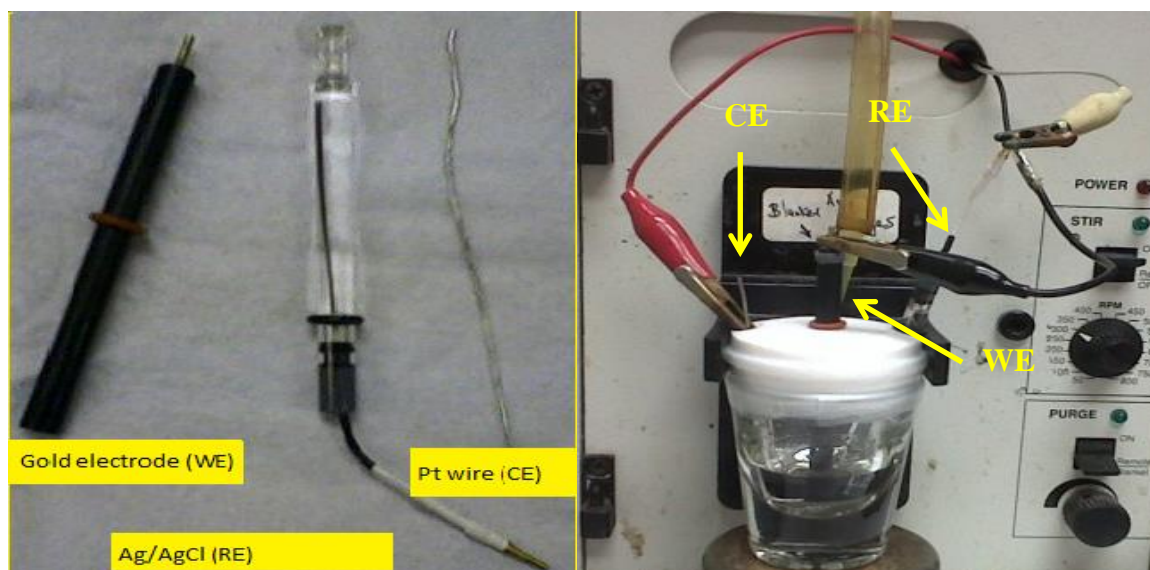


Figure 3: Digital image of the three electrodes WE, RE and CE, respectively (left) and a typical three electrode system set up (right).

EIS measurements were recorded with VoltaLab PGZ 402 from Radiometer Analytical (Lyon, France). UV-VIS absorption measurements were made on a Nicolet Evolution 100 Ultraviolet–visible spectrometer (Thermo Electron Corporation, UK). FL spectra were recorded using Horiba NanoLog™ 3-22-TRIAx (USA). XRD analyses were performed by using a Bruker AXS (Germany) D8 Advance diffractometer (voltage 40 kV; current 40 mA). All FT-IR spectra were recorded on PerkinElmer spectrum 100, FT-IR spectrometer. HR-TEM analyses were done using a Tecnai G2 F20X-Twin MAT 200 kV Field Emission Transmission Electron Microscope from FEI (Eindhoven, Netherlands) and HR-SEM analyses were done using Zeiss Auriga Scanning Electron Microscope.

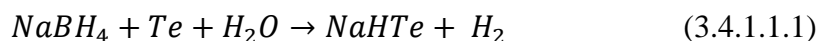
3.4 Procedure

3.4.1 Synthesis of 3MPA capped In_2Te_3 QDs

The 3MPA- In_2Te_3 QDs was prepared according to methods described by (Tian *et al.*, 2009; Swalec, 2011), with some modifications.

3.4.1.1 Preparation of sodium hydrogen telluride (NaHTe) solution

Te powder and NaBH₄ were combined in the ratio 1: 2 in a round bottom flask. The Te should always be the limiting factor. The round bottom flask was shaken and tapped to mix the powders. Te powder is a metallic black, and NaBH₄ is white. Together, they made a grainy grey mixture. 10 mL of distilled water was then added to the round bottom flask to give the powders a medium in which to react. The mixture became a dark grey or black, and quickly lightened to a very translucent grey-purple as the mixture was stirred. At this point, bubbles could be observed within the round bottom flask. This meant that hydrogen gas was forming, and that the following reaction was taking place:



The reaction occurs best in a place that is cold and dark (*Tian, et al. 2009*). The mixture was then stirred continuously at room temperature under nitrogen (N₂) saturation for 40 min after which a medium purple solution formed as shown in **Figure 4**.

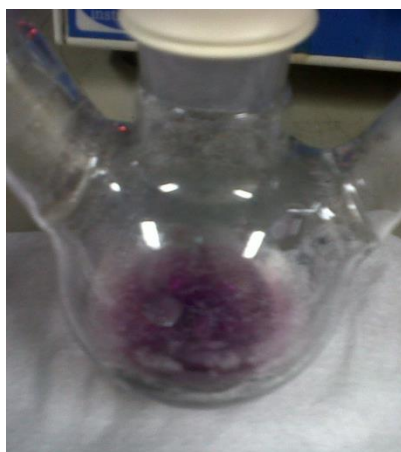


Figure 4: The NaHTe solution (purple) after 40 min.

3.4.1.2 Preparation of 3MPA-InCl₃ ion solution

While the NaHTe solution was still stirring under nitrogen gas, the second step of the synthesis was underway. InCl₃ was dissolved in 10 mL of distilled water. The In compound was a white powder, but when dissolved in water, the solution was clear. Next, 122.5 μ L of concentrated 3MPA was added to the InCl₃ solution and the pH of the solution was adjusted to 11.65 using NaOH. The solution became milky white as shown in **Figure 5**. This reaction was saturated with N₂ gas for 30 min. The ratio of InCl₃: Te: 3-MPA was 1.5:1:2, respectively.

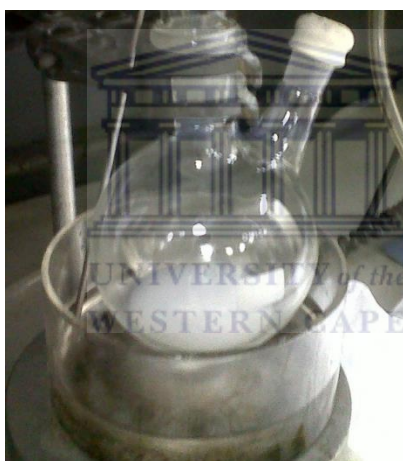


Figure 5: The milky white 3MPA-InCl₃ solution.

Freshly prepared NaHTe was added drop wise into the nitrogen saturated 3MPA-InCl₃ solution at room temperature. The mixture was then refluxed at 100 °C under N₂ gas for 30 min. When the NaHTe was added, the milky white 3MPA-InCl₃ solution immediately turned a yellow colour, shown in **Figure 6** and after 30 min under refluxing the colour changed to dark yellow-orange, shown in **Figure 7**. The reaction was quenched by immediately placing the reaction flask in a freezer at -18 °C.



Figure 6: 3MPA-In₂Te₃ QDs solution at 0 min.



Figure 7: 3MPA-In₂Te₃ QDs solution at 30 min.

3.4.2 Sample preparation

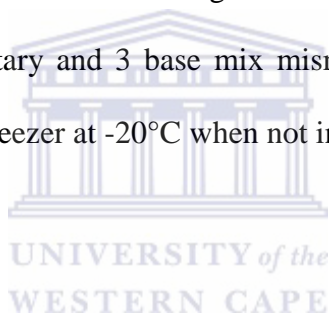
3.4.2.1 Preparation of electrolyte buffer solution

0.10 M phosphate buffer solution (PBS), pH 7.40, was prepared from Na₂HPO₄ and NaH₂PO₄ and it was used as an electrolyte solution throughout the course of this study unless where stated otherwise. Although this study made use of PBS buffer, pH 7.40 for most of the experiments, TE buffer, pH 8.00 was also used. TE buffer is a biological buffer and was best used for the hybridization processes since it protects the DNA from degradation. However both PBS, pH 7.40 and TE buffer, pH 8.00 have pH values within the optimal buffering range

pH 7.3- 9.3. The prepared PBS electrolyte solutions were kept refrigerated at -4 °C while the TE buffer electrolyte solutions were stored at room temperature when not in use.

3.4.2.2 Preparation of stock and working solutions

The eppendorf tubes that consist of the probe, complementary, non-complementary and 3 base mix mismatch ssDNA, respectively were centrifuged for 20 seconds in order to remove the sample attached to the walls of the eppendorf tubes. This was done to prevent sample loss. 100 μ M stock solutions of these four synthetic ssDNA sequences were prepared. This was done by adding 136.84, 377.92, 441.46 and 430.88 μ L of 0.10 M TE buffer solution, pH 8.00 to probe, complementary, non-complementary and 3 base mix mismatch ssDNA, respectively. Thereafter different working solutions from the stock solutions of the complementary, non-complementary and 3 base mix mismatch ssDNA were prepared. All these solutions were kept in the freezer at -20°C when not in use.



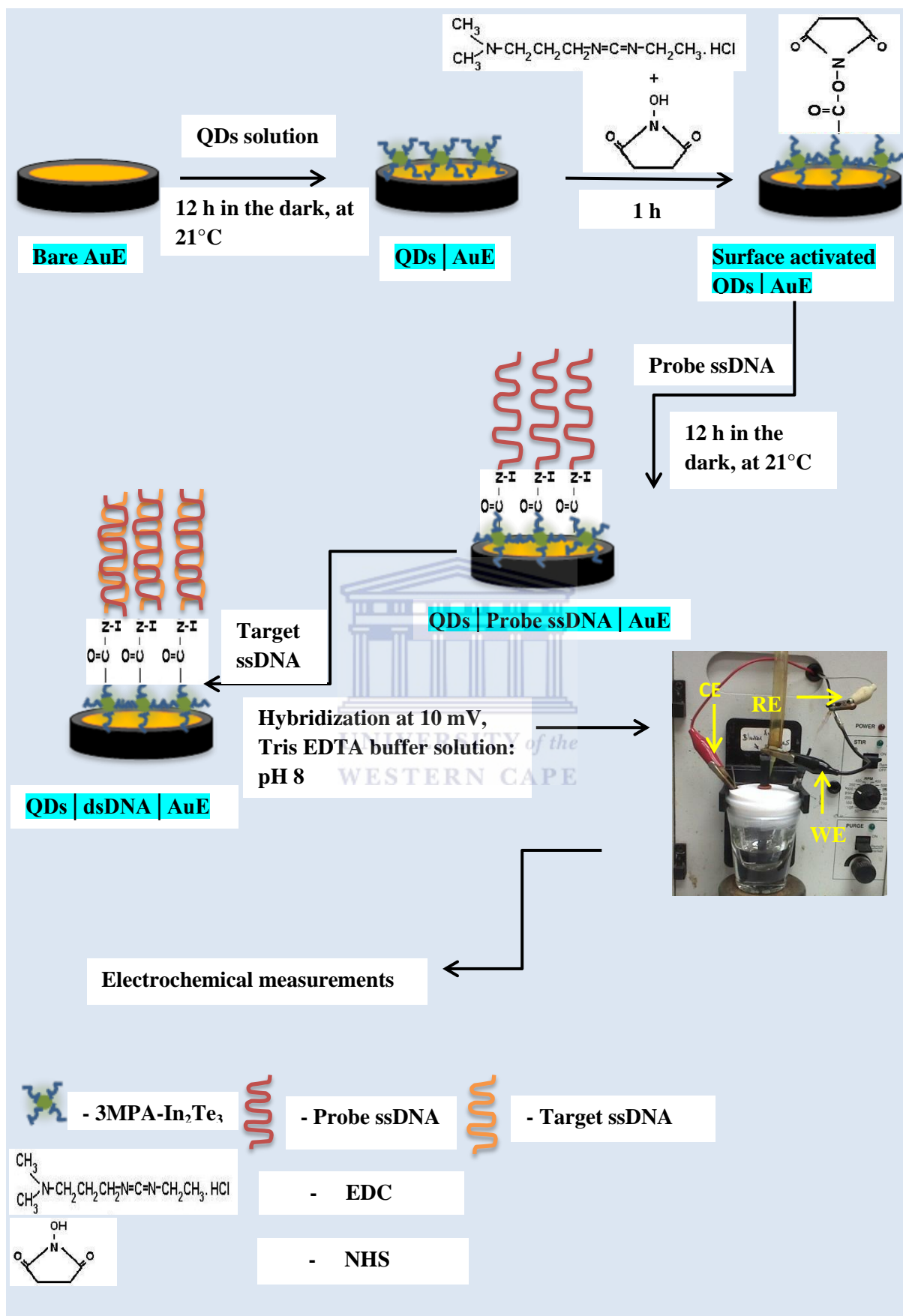
3.4.3 Preparation of 3MPA-In₂Te₃ QDs AuE

AuE was thoroughly polished and cleaned using 1.00, 0.30 and 0.05 μ M alumina slurries on separate polishing pads for 10 minutes, respectively. It was then ultrasonicated for about 10 minutes with distilled water and absolute ethanol to remove any possible absorbed alumina crystals on the AuE surface. After ultrasonication the AuE was rinsed with distilled water and ready for use. 2 μ L of 3MPA-In₂Te₃ QDs solution was then drop coated on the AuE surface and dried for 12 hours in the dark at 21°C.

3.4.4 Probe adsorption, target hybridization and electrochemical detection

The dried 3MPA-In₂Te₃ QDs modified AuE was then slightly rinsed with de-ionized water to remove physically or weakly adsorbed QDs. 2 μL of (1:1) EDC and NHS solution was drop coated on the 3MPA-In₂Te₃ QDs/AuE surface and left to dry for 1 hour at 21°C. The EDC and NHS solution served to activate the carboxyl groups on the 3MPA-In₂Te₃ QDs. 2 μL of 20 μM probe ssDNA solution was drop coated on the 3MPA-In₂Te₃ QDs/AuE surface. The adsorption was carried out for about 12 hours in the dark at 21°C. After the adsorption process the fabrication of the QDs-based genosensor was completed and ready for detection of the complementary target ssDNA. Hybridization was carried out by immersing the probe ssDNA/3MPA-In₂Te₃ QDs/AuE in a stirred solution (0.10 M TE buffer solution, pH 8.00) containing different concentrations (1-15 nM) of the complementary ssDNA for 5 minutes. Electrochemical detection was done by carrying out CV, OSW and performing EIS studies of the probe ssDNA/3MPA-In₂Te₃ QDs/AuE in the absence and presence of the complementary ssDNA with 0.10 M TE buffer solution, pH 8.00 as the redox indicator. Control reactions were also done by studying the response dynamics of the 3MPA-In₂Te₃ QDs-based genosensor with different concentrations of non-complementary and 3-base mismatch ssDNA sequences in a stirred solution (0.10 M TE buffer solution, pH 8.00).

Scheme 4 below shows a schematic representation of the construction of the electrochemical 3MPA-In₂Te₃ QDs-based genosensor.



Scheme 4: Fabrication of the electrochemical 3MPA- In_2Te_3 QDs-based genosensor.

3.5 Characterization techniques

A fast, simple and cost-effective 3MPA-In₂Te₃ QDs-based genosensor for the determination of telomerase biomarker was successfully fabricated. A variety of electrochemical techniques such as CV, SWV and EIS have been used for characterization as well as application of the electrochemical DNA biosensor. UV-VIS, FL, XRD, FT-IR and HR-TEM/SEM have been used to study the materials associated with the electrochemical genosensor system. The following is just a brief overview of the principles of these techniques as well their application in the present research study.

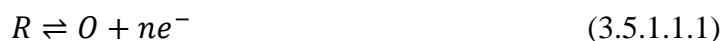
3.5.1 Electrochemical techniques

The electrochemical methods that will be discussed here have a central feature. They make use of an electrode that provides a surface or interface where charge-transfer processes can take place. This happens when an electric potential is applied and current passes. Therefore in this study, electrochemistry is used to derive thermodynamic information concerning charge transfer processes in the samples under study.

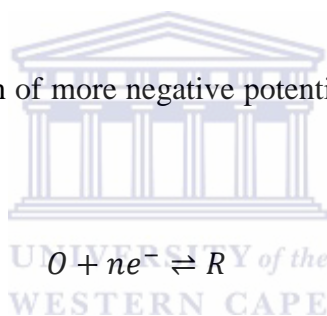
3.5.1.1 Cyclic Voltammetry (CV)

CV is a set of linear sweep voltammetry (LSV) experiments and has become a very important electroanalytical technique in electrochemical studies of new systems. It is usually the first experiment performed in an electroanalytical study (*Hayyana et al., 2013*). Its main principle is to investigate electron transfer mechanisms and potentials of electrode reactions (oxidation–reduction processes) under various conditions. Advantages of this technique include its broad availability of low cost instrumentation and the accessibility to extensive theory for electrochemist as well as other field of specialists. However this technique has

shortcomings such as difficulty to determine the mechanism of the second of two or more closely spaced charge transfer reactions (*Helfrick and Bottomley, 2009*). There is also a concentration limit (10 μM) that must be met in order to accomplish reliable mechanistic information (except when the analyte is confined to the electrode surface) (*Helfrick and Bottomley, 2009*). CV is based on monitoring the current when the applied potential at the working electrode is varied in both forward and reverse directions at a certain scan rate. In other words CV can complete a scan in both directions. For instance when scanning in the direction of more positive potentials (forward scan), an oxidation reaction for species R occurs and produces species O as illustrated below,



Whereas scanning in the direction of more negative potentials (reverse scan) the species O is reduced back to species R .



Different redox systems can be obtained such as reversible, irreversible and quasi reversible depending on the outcome of diagnostic test. Some of these diagnostic tests are tabulated below.

Table 5: Cyclic voltammogram diagnostics for an electrode reaction at an electrode surface involving chemically stable and soluble redox couples.

CV parameter	Reversible	Quasi-reversible	Irreversible
E_p	Independent of v	Shift with v	Cathodic shift by $0.03/\alpha n$ V for 10-fold increase in v
$E_{p,a} - E_{p,c}$	$\sim 0.059/n$ V at 25°C	May approach $60/n$ at low v but increases as v increases	No return peak or > 200 mV
$I_{p,a}/I_{p,c}$	1 and independent of v	1 only if $\alpha = 0.5$	No current on the reverse scan
$I_p/v^{1/2}$	Constant	Constant	Constant

Figure 8 below shows the response of a typical cyclic voltammogram for a reversible redox system and the different parameters such as peak potentials (E_{pc} , E_{pa}) and peak currents (I_{pc} , I_{pa}) of the cathodic and anodic peaks, respectively.

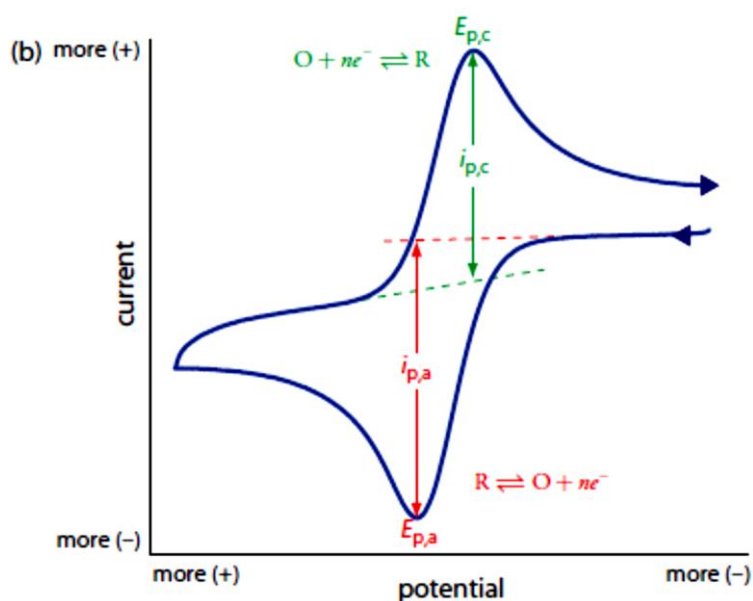


Figure 8: A cyclic voltammogram for a reversible redox system.

The degree of independence or dependence of E_p values on scan rates, and the magnitude of ΔE_p can give a hint on reversibility. In this case the reaction is reversible and n (no of electrons) can be obtained from average peak separation

$$\Delta E_p = |E_{p,a} - E_{p,c}| = 2.303 RT/nF \quad (3.5.1.1.3)$$

The formal potential (E^0) is usually estimated as the average of $E_{p,a}$ and $E_{p,c}$ where,

$$E^0 = \frac{E_{p,a} + E_{p,c}}{2} \quad (3.5.1.1.4)$$

For a reversible reaction, the concentration is related to peak current and thus the initial sweep peak for a reversible electron transfer is given by the Randles–Sevcik equation below,

$$i_p = 0.4463nFA \left[\frac{nF^{1/2}}{RT^{1/2}} \right] C^* D^{1/2} \nu^{1/2} \quad (3.5.1.1.5)$$

Where i_p = Peak Current in A, $n = 1$ number of electrons, $F = 96485$ C mol⁻¹, Faradays Constant, $A = 0.0201$ cm² geometric area of the electrode, $R = 8.314$ J mol⁻¹ K⁻¹, Gas Constant, $T = 298.15$ K absolute Temperature and ν = Scan Rate in V s⁻¹ and D is the diffusion coefficient (cm² s⁻¹),

And at 25°C

$$i_p = 2.686 \times 10^5 n^{3/2} A c^0 D^{1/2} \nu^{1/2} \quad (3.5.1.1.6)$$

Where i_p is the peak current in amps, A is the electrode area (cm²), D is the diffusion coefficient (cm² s⁻¹), c^0 is the concentration in mol cm⁻³, and ν is the scan rate in V s⁻¹. Scanning the potential in both directions provides us with the opportunity to explore the electrochemical behaviour of species generated at the electrode.

In this research study CV was performed using the instrument described in section 3.3. The electrochemical characterization of the QDs was carried out in 6 mL of (0.10 M

PBS, pH 7.4) electrolyte solution. 3MPA-In₂Te₃ QDs/AuE was cathodically scanned from -900 (initial potential, E_i) to +1100 mV (switch potential, E_s) at different scan rates (2 -350 mV/s). For comparison reasons the Bare AuE, 3MPA-In₂Te₃ QDs/AuE and probe ssDNA/3MPA-In₂Te₃ QDs/AuE (genosensor) were all cathodically scanned from -900 to +1100 mV in 6 mL of 0.10 M PBS, pH 7.4 at a fixed scan rate of 10 mV/s. Reader should bear in mind that the materials (3MPA-In₂Te₃ and probe ssDNA) are surface-confined to the AuE. Application of the probe ssDNA/3MPA-In₂Te₃ QDs/AuE towards different concentrations of analyte was carried out in 3mL of 0.10 M TE buffer solution, pH 8.00 over a potential range - 900 to +1100 mV at 10 mV/s. The reason why a fixed scan rate of 10 mV/s was used for most CV and SWV analysis is because it's an appropriate scan rate that ensured a maximum response as well as a reasonable stability of the QDs based genosensor. The probe ssDNA/3MPA-In₂Te₃ QDs/AuE was allowed to stay for 5 minutes in the electrolyte solution that contained different concentrations of complementary ssDNA, respectively. This was done so that hybridization could occur before any CV analysis was carried out. All CV measurements were done at room temperature. The electrolyte solutions (0.10 M PBS, pH 7.4 and 0.10 M TE buffer solution, pH 8.00) were degassed with nitrogen for at least 30 minutes prior to an electrochemical experiment.

3.5.1.2 Square Wave voltammetry (SWV)

SWV forms part of pulse voltammetry techniques and it is a powerful electroanalytical method that can be applied in both eletrokinetic and quantitative determination of redox couples that is strongly surface-confined (*Mirceski and Gulaboski, 2001*). In comparison to both LS and CV, it has a much broader dynamic range and lower detection limit because of its efficient discrimination of capacitance current (*Helfrick and Bottomley, 2009*). SWV is also more regularly employed than normal pulse voltammetry

(NPV) and differential pulse voltammetry (DPV) techniques due to its short scan rate time. It is among the most sensitive means because it can analytically determine concentrations as low as 10 nM (Helfrick and Bottomley, 2009). Compared to the DPV response, SWV is 4 and 3 times higher for reversible and irreversible systems, respectively (Dogan-Topal et al., 2010). The high sensitivity and rapidity of SWV make this technique useful for drug analysis in their dosage forms and biological samples (Dogan-Topal et al., 2010). A typical SW voltammogram and its excitation signal response is shown in **Figure 9** below.

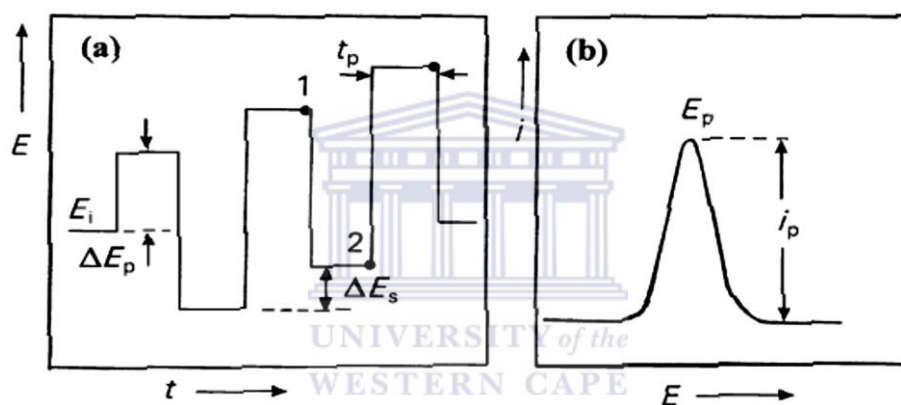


Figure 9: Potential waveform (a) and its respective current response (b) for SWV.

The excitation signal in SWV denoted by curve (a) consists of a symmetrical square-wave pulse of amplitude E_{sw} superimposed on a staircase waveform of step height ΔE , where the forward pulse of the square wave coincides with the staircase step. The net current, i_{net} , is obtained by taking the difference between the forward and reverse currents ($i_{forward} - i_{reverse}$) and is centred on the redox potential. The peak height is directly proportional to the concentration of the electroactive species.

Just as CV, SWV was performed using the instrument described in section 3.3. Application of the probe DNA/3MPA-In₂Te₃ QDs/AuE (genosensor) towards different

concentrations of complementary ssDNA was carried out in 3 mL of 0.10 M TE buffer solution, pH 8.00. The SWV was scanned in one direction cathodically from $E_{p,a} = -900$ to $E_{p,a} = +1100$ mV. SWV amplitude of 25 mV was used with a step potential of 2 mV and a frequency of 5 Hz. The probe DNA/3MPA-In₂Te₃ QDs/AuE was allowed to stay for 5 minutes in the electrolyte solution that contained different concentrations of complementary ssDNA, respectively. This was done so that hybridization could occur before any SWV analysis was carried out. All SWV measurements were done at room temperature. The electrolyte solutions (0.1 M TE buffer solution, pH 8.00) were degassed with nitrogen for at least 30 minutes prior to an electrochemical experiment.

3.5.1.3 Electrochemical Impedance Spectroscopy (EIS)

Initially EIS was applied to determine the double-layer capacitance (*Mohilner, 1966*) and ac polarography (*Smith, 1966*) but in recent years its application became more popular in characterization of electrode processes and complex interfaces. EIS is a powerful, rapid and accurate non-destructive method for studying the mechanisms of electrochemical reactions and evaluating the properties of wide range of materials (*Hamdy et al., 2006; Sluyters-Rehbach and Sluyters, 1970*). EIS is a method in which the electrochemical system under investigation (typically in the equilibrium state) is excited by a small amplitude ac sinusoidal signal of potential or current in a wide range of frequencies and the response of the current or voltage is measured. The data obtained can be plotted in a Nyquist plot or a Bode plot. The electrochemical process on an electrode can be simulated to an equivalent circuit consisting of resistors and capacitor (*Lee et al., 2005*). EIS is a linear technique and hence the results are readily interpreted in terms of Linear Systems Theory (*Macdonald, 2006*). In order to obtain a linear (or pseudo-linear) system the electrochemical impedance is measured using a small

excitation signal. In this condition, a sinusoidal potential input to the system leads to a sinusoidal current output at the same frequency but shifted in phase, shown in **Figure 10**.

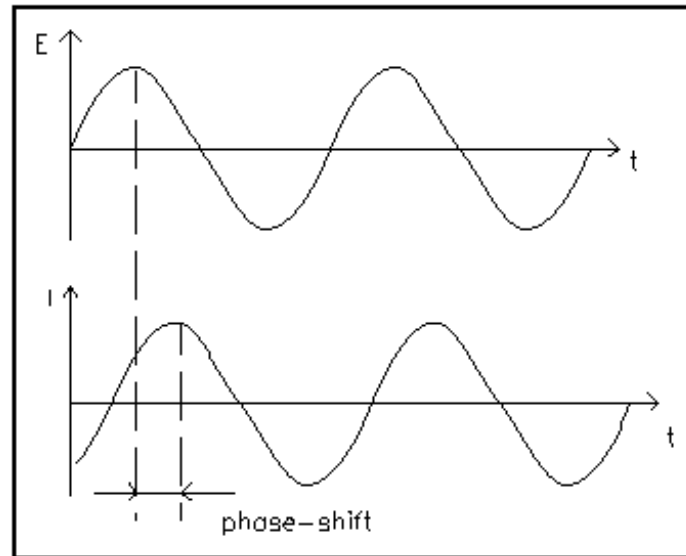


Figure 10: Sinusoidal Current Response in a Linear System.

The excitation signal, expressed as a function of time, has the form

$$E(t) = E_0 \sin(\omega t) \quad (3.5.1.3.1)$$

Where $E(t)$ is the applied potential at time t , E_0 is the potential amplitude, and ω is the angular frequency that is defined as the number of vibrations per unit time, where Frequency in Hz is multiplied by 2π and expressed in rad s^{-1} and it is given by

$$\omega = 2\pi f \quad (3.5.1.3.2)$$

In a linear system, the response signal, I_t , is shifted in phase (Φ) and has a different amplitude than I_0 . This is expressed as

$$I_t = I_0 \sin(\omega t + \phi) \quad (3.5.1.3.3)$$

Then, the impedance of the system Z_t is calculated from Ohm's law:

$$Z_t = \frac{E_t}{I_t} = Z_0 \frac{\sin(\omega t)}{\sin(\omega + \phi)} \quad (3.5.1.3.4)$$

Based on Ohm's law, we get the expression for the impedance as a complex number,

$$Z(\omega) = \frac{E}{I} = Z_0(\cos\phi + j\sin\phi) \quad (3.5.1.3.5)$$

When the real part of the impedance is plotted on the axis of the abscissa and the imaginary part is plotted on the axis of the ordinate, we get a Nyquist plot. In the Nyquist plot, a vector of length $|Z|$ is the impedance and the angle between this vector and the real-axis is the phase angle (deg). A typical Nyquist plot denoted by (a) with its corresponding equivalent circuit (b) is shown in **Figure 11** below.

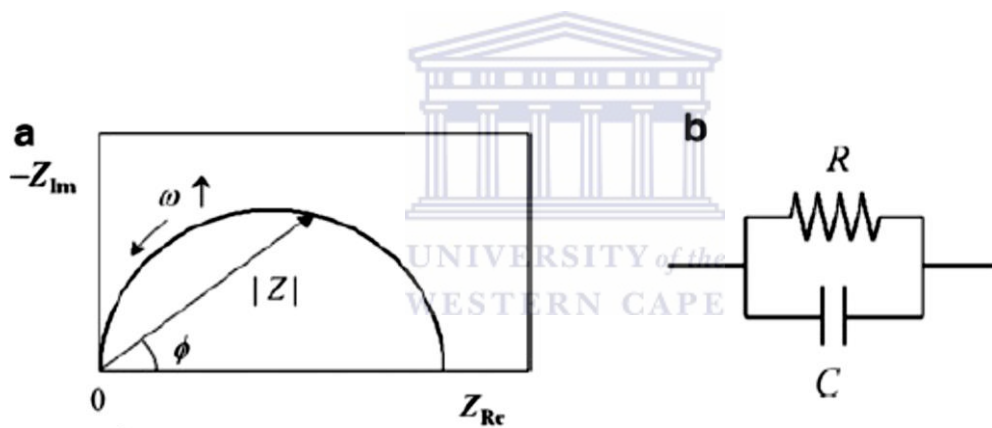


Figure 11: A typical Nyquist plot (a) and the corresponding equivalent circuit with RC parallel element (b).

One short coming of this widely used Nyquist plot is that it is unable to show at what frequency the specific impedance point is recorded. Bode plots might be useful because the frequency information is given. In bode plots the axis of the abscissa is the logarithmic frequency and the axis of the ordinate is both the absolute value of the logarithmic impedance ($\log |Z|$) and phase angle (deg). **Figure 12** shows a typical Bode plot for an electrochemical system.

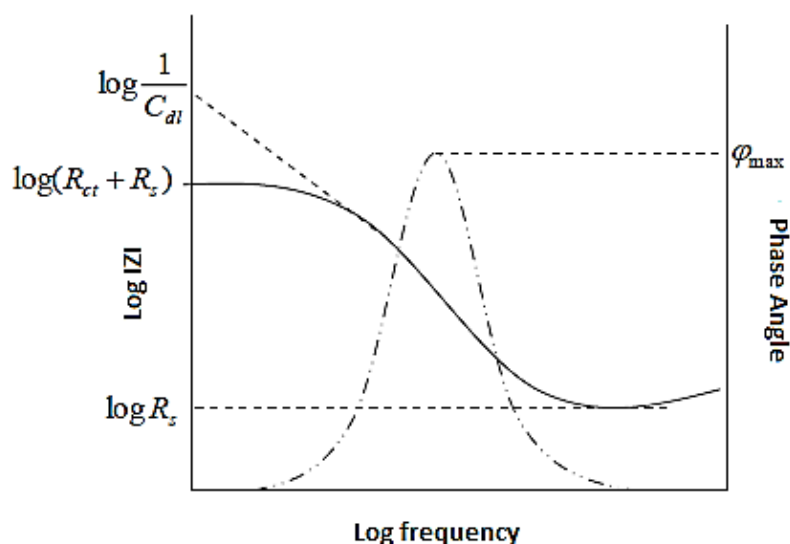


Figure 12: A typical Bode plot.

In this study EIS was used to investigate the electrochemical behaviours of the modified and unmodified surface of AuE. EIS was performed using the instrument described in section 3.3. The conductivity of bare AuE, 3MPA-In₂Te₃ QDs/AuE and probe DNA/3MPA-In₂Te₃ QDs/AuE (genosensor) was investigated by EIS in 6 mL of 0.10 M PBS, pH 7.4. The EIS measurements was carried out by applying a potential of 190 mV to an electrochemical cell and then measuring the current through the cell ranging from an initial frequency of 100 kHz to a final frequency of 15 mHz. Excitation amplitude of 10 mV was used throughout EIS measurements. By the use of very small excitation amplitude minimal perturbation of the electrochemical test system was caused. EIS was also used to investigate the application of the probe DNA/3MPA-In₂Te₃ QDs/AuE towards different concentrations of complementary ssDNA in 3 mL of 0.10 M TE buffer solution, pH 8.00 at a fixed potential 190 mV within the frequency range of 100 kHz to 50 mHz. The probe DNA/3MPA-In₂Te₃ QDs/AuE was allowed to stay for 5 minutes in the electrolyte solution that contained different concentrations of complementary ssDNA, respectively. This was done so that hybridization could occur before any EIS analysis was carried out. All EIS measurements

were done at room temperature. The electrolyte solutions (0.1 M PBS, pH 7.4 and 0.1 M TE buffer solution, pH 8.00) were degassed with nitrogen for at least 30 minutes prior to an electrochemical experiment.

3.5.2 Spectroscopic techniques

3.5.2.1 Ultraviolet-visible spectroscopy (UV-VIS)

UV-VIS is a simple, versatile, fast, and accurate technique that studies the sample's reaction to light. It measures the absorption of radiation by a material, as a function of the wavelength. Although it provides a limited amount of qualitative information it is almost entirely used for quantitative analysis. For qualitative analysis this technique can provide information on the identity of certain compounds. However for quantitative analysis this technique is able to estimate the amount of a compound known to be present in the sample. The sample under analysis is usually examined in solution. The Lambert's (or Bouguer's) Law states that each layer of equal thickness of an absorbing medium absorbs an equal fraction of the radiant energy that traverses it. For instance when a beam of light passes through a substance or a solution, some of the light may be absorbed and the remainder transmitted through the sample. The ratio of the intensity of the light entering the sample (I_0) to that exiting the sample (I) at a particular wavelength is defined as the transmittance (T) given by

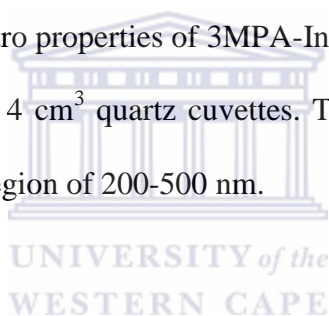
$$T = \frac{I}{I_0} \quad (3.5.2.1.1)$$

The absorbance (A) is directly proportional to the concentration (c , g.L⁻¹) of the absorbing species and to the path length (b , cm) of the absorbing medium. Therefore the above equation can be transformed into a linear expression by taking the logarithm and is expressed by:

$$A = -\log T = -\log \frac{I}{I_0} = \log \frac{I_0}{I} = \epsilon bc \quad (3.5.2.1.2)$$

where ϵ is the molar extinction coefficient (ϵ , L.mol⁻¹cm⁻¹). The expression above is known as the Lambert-Beer's law and it states that there is a linear relationship between absorbance and path length at a fixed concentration (*Muda et al., 2009*). However the linearity of the Beer-Lambert law is limited by chemical and instrumental factors.

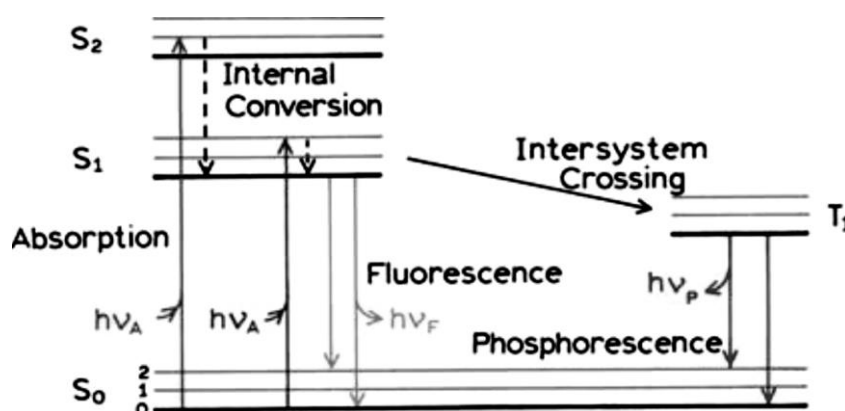
Numerous research studies on semiconductor nanocrystals with UV-VIS as the characterization technique was done. UV-VIS has the ability to study the interband electronic transition in semiconductor nanocrystals and therefore is able to understand their behaviour. In this study UV-VIS was performed using the instrument described in section 3.3. UV-VIS was used to study the spectroelectro properties of 3MPA-In₂Te₃ QDs. 3MPA-In₂Te₃ QDs was dissolved in water and placed in 4 cm³ quartz cuvettes. The UV-VIS absorption spectra of these QDs were recorded in the region of 200-500 nm.



3.5.2.2 Fluorescence spectroscopy (FL)

FL is a spectrochemical method of analysis where the molecules of the analyte are excited by irradiation at a certain wavelength and emit radiation of a different wavelength. In simpler words it is an excitation and emission process. There are several factors that can affect the ability of a compound to fluoresce for instance the compound's structure, including its rigidity, temperature of surroundings, pH of the solution, and the concentration. Fluorescence spectral data are generally presented as emission spectra. The emission spectrum provides information for both quantitative as well as qualitative analysis. Although fluorescence measurements do not provide detailed structural information, the technique is popular for its important sensitivity to changes in the structural and dynamic properties of compounds. Fluorescence results from a process in the electron shell of fluorophores or

fluorescent dyes. This process can be described by studying one of Jablonski diagrams shown in **Scheme 5** below.



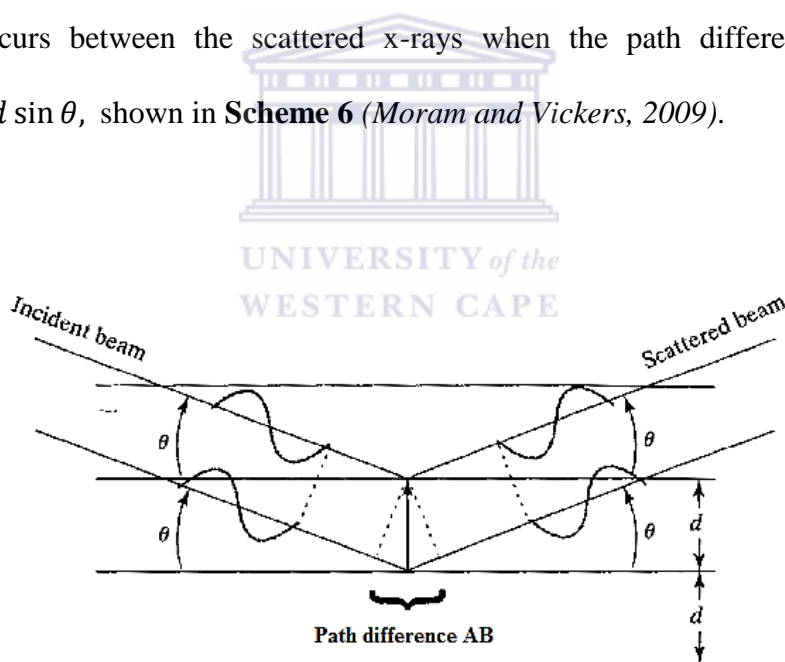
Scheme 5: Jablonski's electronic transition energy level diagram.

When light of an appropriate wavelength is absorbed by a molecule (i.e., excitation), the electronic state of the molecule changes from the ground state to one of many vibrational levels in one of the excited electronic states. The excited electronic state is usually the first excited singlet state, S_1 as shown in **Scheme 5**. The moving of electrons from the ground to excited state causes a hole in the ground state. The photo-generated electron-hole pair is known as an exciton, which, upon recombination, gives rise to the fluorescence emission of certain molecules (*Galian and de la Guardia, 2009*).

In this research study FL was performed using the instrument described in section 3.3. This technique was used to investigate if 3MPA- In_2Te_3 QDs have the ability to fluoresce. The sample was placed in a 400 μL quartz cuvette and FL was recorded with double grating excitation and emission monochromators at a slit width of 5 nm. The spectra were measured on 3MPA- In_2Te_3 colloidal solutions which were taken from the refluxing reaction mixture and diluted with water to provide the optical densities appropriate for FL measurements.

3.5.2.3 X-Ray diffraction (XRD)

XRD is a popular, non-destructive technique for the characterization of crystalline material structures. It provides detailed information on the crystalline phases, texture, orientation pattern, crystal size, crystallinity and imperfection of natural and synthetic compounds (*Tadano and Giri, 2011*). Powder XRD is the most widely used XRD technique for characterizing materials but it can also be used to study particles in liquid suspensions or polycrystalline solids. In XRD all electromagnetic radiation is treated as waves. However x-rays can also behave as particles. XRD is based on constructive interference of monochromatic x-rays and a crystalline sample. Monochromatic beam of x-ray photons are scattered by the electron cloud that surrounds each atom in the crystal. Constructive interference occurs between the scattered x-rays when the path difference AB ($n\lambda$) is equivalent to $2d \sin \theta$, shown in **Scheme 6** (*Moram and Vickers, 2009*).



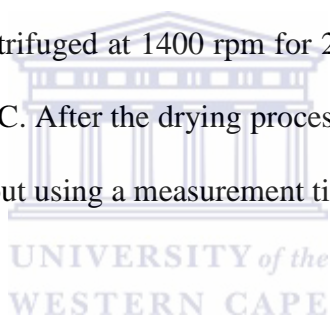
Scheme 6: Schematic of XRD illustrating the conditions required for Bragg diffraction to occur.

Therefore the diffraction of x-rays from a crystal is described by the Bragg's law:

$$2d \sin \theta = n\lambda \quad (3.5.2.3.1)$$

Here λ is the wavelength of x-ray, n is an integer denoting the order of the reflection, θ is one-half the angle between the incident and scattered x-ray beams and d is the inter-planar spacing.

In this study XRD was performed using the instrument described in section 3.3. This technique was used to find information about the crystallinity of the 3MPA-In₂Te₃ QDs. Seeing that the sample was in solution form it had to be precipitated out by a certain organic solvent known as 2-propanol. The ratio between the sample and 2-propanol was (1:2). The two solutions was mixed and centrifuged at 1400 rpm for 20 minutes. A pellet was collected and left to dry for 12 hours at 21°C. After the drying process the pellet was grind into powder form. XRD analysis was carried out using a measurement time of 0.5 at room temperature.



3.5.2.4 Fourier transform infrared spectroscopy (FT-IR)

FT-IR spectroscopy is a vibrational spectroscopic technique that offers quantitative and qualitative analysis for organic and inorganic solid, liquid or gas samples. This technique uses infrared radiation to vibrate molecular bonds within the sample that absorbs it (*Baker et al. 2008*). FT-IR is an effective analytical instrument that is able to detect functional groups and characterize covalent bonding information. It is a rapid and relatively inexpensive technique that can be used to analyse solids that are crystalline, microcrystalline, amorphous, or films. FT-IR spectroscopy is more advantageous over conventional dispersive IR spectroscopy because of its characteristic ability to self-calibrate, its rapidness, sensitivity and mechanical simplicity. It also has a higher signal to noise ratio than dispersive IR

spectroscopy. To obtain the best possible FT-IR spectra of samples it is necessary to choose the appropriate FT-IR source, detection method and accessories. In FT-IR spectroscopy absorption occurs when the energy of the beam of light (photons) are transferred to the molecule. The molecule gets excited and moves to a higher energy state. The energy transfer takes place in the form of electron ring shifts, molecular bond vibrations, rotations, and translations. FT-IR is concerned with vibrations and stretching frequencies.

In this study FT-IR spectroscopy was performed using the instrument describe in section 3.3. This technique was used to investigate if the In_2Te_3 QDs was capped with the surfactant 3MPA. The FT-IR analysis was done on liquid samples of 3MPA- In_2Te_3 QDs which were directly dropped onto the crystal (window) of the device. The FT-IR spectra were recorded from a frequency range of $4000\text{-}400\text{ cm}^{-1}$.



3.5.3 Microscopic techniques

3.5.3.1 High resolution transmission electron microscopy (HR-TEM)

HR-TEM is a popular analytical tool for studying interfaces, layer systems and lattice imperfections of specimens in the realms of microspace ($1\text{ micron}/1\mu\text{m} = 10^{-6}\text{m}$) to nanospace ($1\text{ nanometer}/\text{nm} = 10^{-9}\text{m}$). This powerful technique can provide detailed topographical, morphological and crystalline information through its high-resolution and high magnification imaging. It is widely used technique for studying of semiconductor nanocrystals. HR-TEM does not only provide atomic-resolution lattice images but also chemical information at a spatial resolution of 1 nm or better. The chemical information obtained allows for direct identification of the chemistry of a single nanocrystal (*Wang, 2000*). The structural characteristics of a single nanocrystal can be fully characterized by the finely focused electron probe of the HR-TEM tool. The structural characteristics of these

nanocrystals include surface morphology, size, strain fields and density. There are three main contrast mechanisms contributing to the formation of HR-TEM images: absorption, diffraction and phase contrast. HR-TEM produces images from a sample by illuminating the sample with electrons (i.e. the electron beam) within a high vacuum, and detecting the electrons that are transmitted through the sample.

In this study HR-TEM was performed using the instrument describe in section 3.3. This technique was used to study the shape, size and structure of the 3MPA-In₂Te₃ QDs. It was also used to determine the elemental composition of these QDs. A copper grid was used as platform for sample preparation and was allowed to dry by leaving it for 10 minutes under an infra-red lamp before performing HR-TEM analysis.



3.5.3.2 High resolution scanning electron microscopy (HR-SEM)

HR-SEM is a cutting edge imaging system that is capable of providing information on the surface topography, crystallinity and electrical behaviour of a sample. Coupled to an energy dispersive x-ray spectrometer it is also able to offer information on qualitative and quantitative chemical analysis. Much higher magnifications for HR-SEM can be achieved (up to 1,000,000 x), with an ultimate resolution of 1 nm. When compared to the image quality of optical microscopy, HR-SEM benefits from a large depth of field enabling them to capture well-focused images of complex three-dimensional objects. In comparison to HR-TEM, it permits non-destructive evaluation of the sample and its sample preparation time is much shorter depending on the material under study. To create a HR-SEM image, the incident electron beam is scanned in a raster pattern across the sample's surface. An interaction occurs between the incident electron beam and sample atoms as the beam penetrates into the sample. The depth of penetration is determined by the accelerating voltage of the beam and the

density of the sample, and ranges from a few nanometers to a few micrometers. Different interactions yield signals (secondary electrons, backscattered electrons and x-rays), each with different characteristics.

In this study HR-SEM was performed using the instrument describe in section 3.3. This technique was used to study the surface morphology of 3MPA-In₂Te₃ QDs and probe DNA/3MPA-In₂Te₃ QDs. It was also used to determine the elemental composition of the 3MPA-In₂Te₃ QDs. Carbon tape mounted onto aluminium stubs was used as platform for sample preparation and the sample was allowed to dry for 12 hours before performing HR-SEM analysis.



CHAPTER 4

Chapter overview

This chapter discusses the characterization of the 3MPA-In₂Te₃ QDs by methods like UV-VIS, FL, XRD, FT-IR and HR TEM/SEM. It discusses the electro-analysis of 3MPA-In₂Te₃ QDs and 3MPA-In₂Te₃ QDs based genosensor by analytical methods such as CV and EIS in 0.10 M PBS, pH 7.4. This chapter also gives a brief overview on the voltammetric and impedimetric responses of the 3MPA-In₂Te₃ QDs based genosensor towards different concentrations of the complementary ssDNA in biological buffer solution (0.10 M TE buffer solution, pH 8.00).

4.0 RESULTS AND DISCUSSION

4.1 Spectroscopic techniques



4.1.1 Ultraviolet-visible spectroscopy studies (UV-VIS)

UV-VIS spectroscopy provided information on the lowest energy absorption feature (the first exciton), band gap energy, particle size, and distribution of the 3MPA-In₂Te₃ QDs. The conditions for performing UV-VIS analysis were discussed in Chapter 3 section 3.5.2.1. **Figure 13** below shows the UV-VIS absorption spectra of the 3MPA-In₂Te₃ QDs precursor's 3MPA-InCl₃ and NaHTe. Three absorption peaks at 220, 280, 380 nm were observed for NaHTe while 3MPA-InCl₃ displayed only one absorption peak at 240 nm. The InCl₃ compound cannot absorb light since its d orbital are fully filled. However due to the presence of 3MPA absorption was able to occur in the UV region.

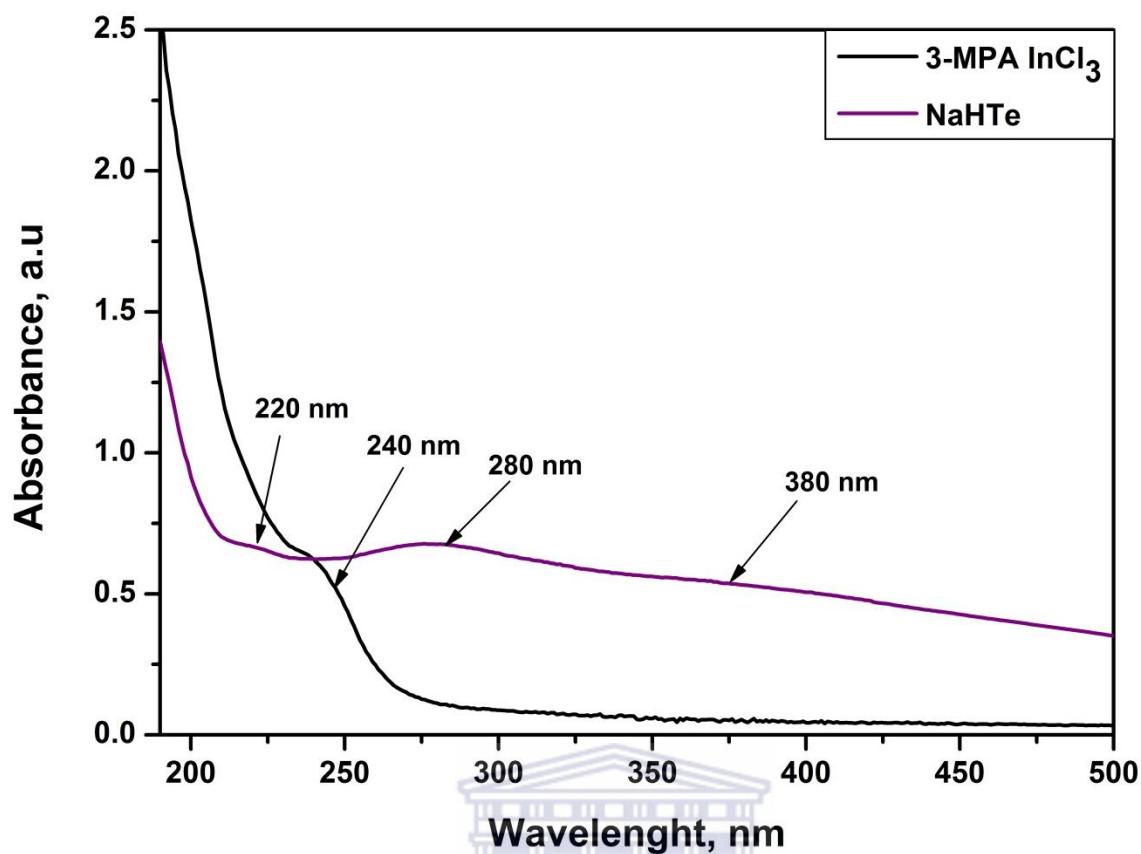


Figure 13: UV-VIS spectrum of 3MPA-InCl₃ (black line) and NaHTe (purple line).

UNIVERSITY of the
WESTERN CAPE

When NaHTe precursor was introduced to 3MPA-InCl₃ precursor, 3MPA-In₂Te₃ QDs formed. This phenomenon was observed when the UV-VIS absorption spectrum of 3MPA-In₂Te₃ QDs was studied. The absorption spectra of these QDs revealed combination of the two precursors with a first exciton at 373 nm which is attributed to the sample under investigation, shown in **Figure 14**.

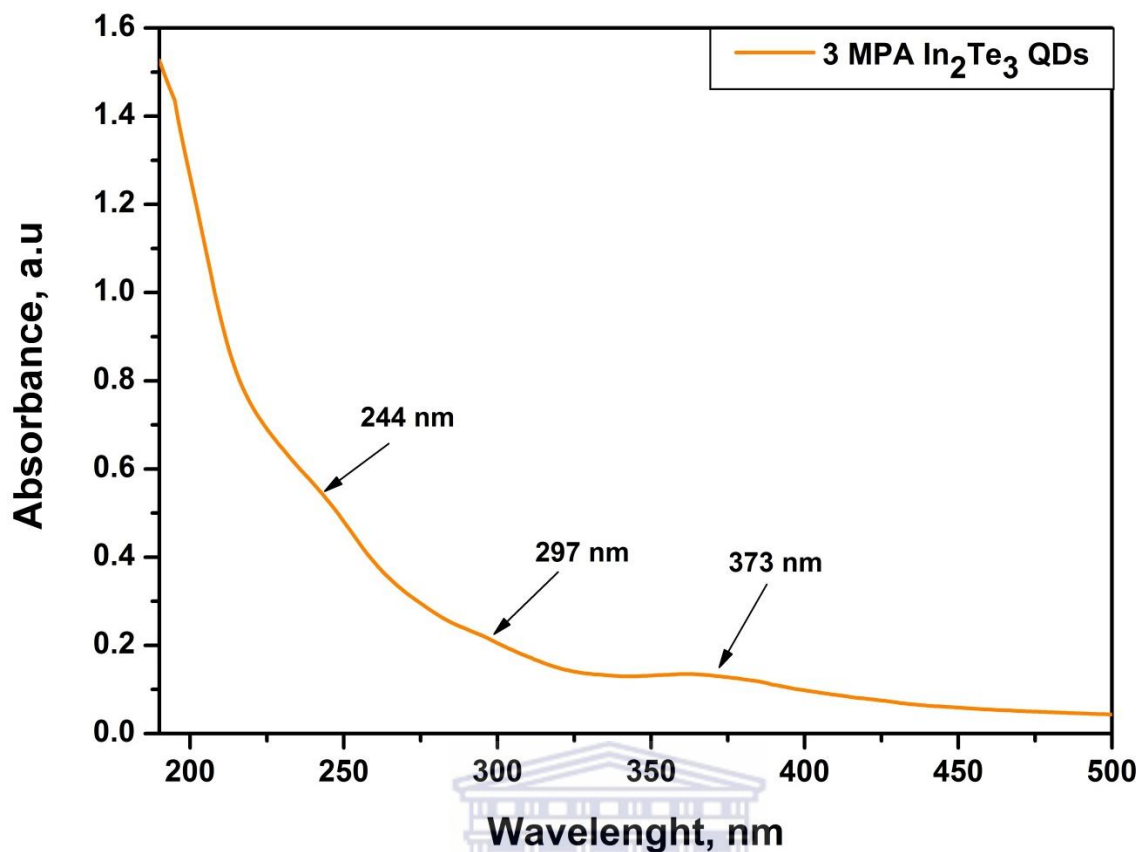


Figure 14: UV-VIS spectrum of 3MPA-In₂Te₃ QDs.

The lowest energy absorption feature (first exciton peak) at 373 nm is very weak therefore one can suggest that the 3MPA-In₂Te₃ QDs have a very broad size distribution. Due to the broad size distribution, the differences in band gap between different sized particles will be very large and hence most of the electrons will get excited over a greater range of wavelengths (*Gullapalli and Barron, 2010*). In addition, due to the broad size distribution the higher exciton peaks at 244 nm and 297 nm cannot be seen clearly. The peaks at 244, 297 and 373 nm are attributed to $n \rightarrow \sigma^*$ transitions of sulphur groups on the 3MPA and are indicative that this surfactant does in fact cap the In₂Te₃ QDs. The minimum energy associated with the electronic transition from valence to conduction band was estimated to be 5.33×10^{-19} J, by using Plank's Law, given by:

$$\Delta E = h\nu = h\left(\frac{c}{\lambda_{max}}\right) \quad (4.1.1.1)$$

Where E is the band gap energy, h is Planck's constant, c is the speed of light, and λ is the experimental optical absorption wavelength. The bandgap energy of the QDs was found to be 3.33 eV; this confirms the nanophase of material since the band gap energy of bulk In_2Te_3 is 1.1 eV (*Strehlow and Cook, 1973; Matheswaran et al., 2010*). Hence it is in accordance with effective mass approximation (EMA), as the size of semiconductor materials decreases their band gap energy increases.

4.1.2 Fluorescence spectroscopy (FL)

Figure 15 below shows the room temperature Fluorescence emission (black line) and excitation (red line) spectra of 3MPA- In_2Te_3 QDs. The conditions for performing FL analysis were discussed in Chapter 3 section 3.5.2.2. The 3MPA- In_2Te_3 QDs were excited at 373 nm which gave an emission maximum at 427 nm as shown in **Figure 15**. However, two very weak emission bands at 575 and 640 nm were also observed and can be attributed to defect-related emissions. The emission at 427 nm is the exciton emission (band edge emission) resulting from direct electron-hole recombination transitions in the QDs as explained in Chapter 3 section 3.5.2.2. The somewhat broad emission peak indicates that the 3MPA- In_2Te_3 QDs have broad dispersity which is in accordance with the information obtained from the absorption spectra of these QDs. However a low intensity for the emission peak is observed which may be attributed to some aggregation. In excitation spectra, emission wavelength was fixed at 427 nm and gave a band in the region 300-400 nm, peaking at 376 nm. Both excitation and emission spectra displays electronic transitions at higher energies.

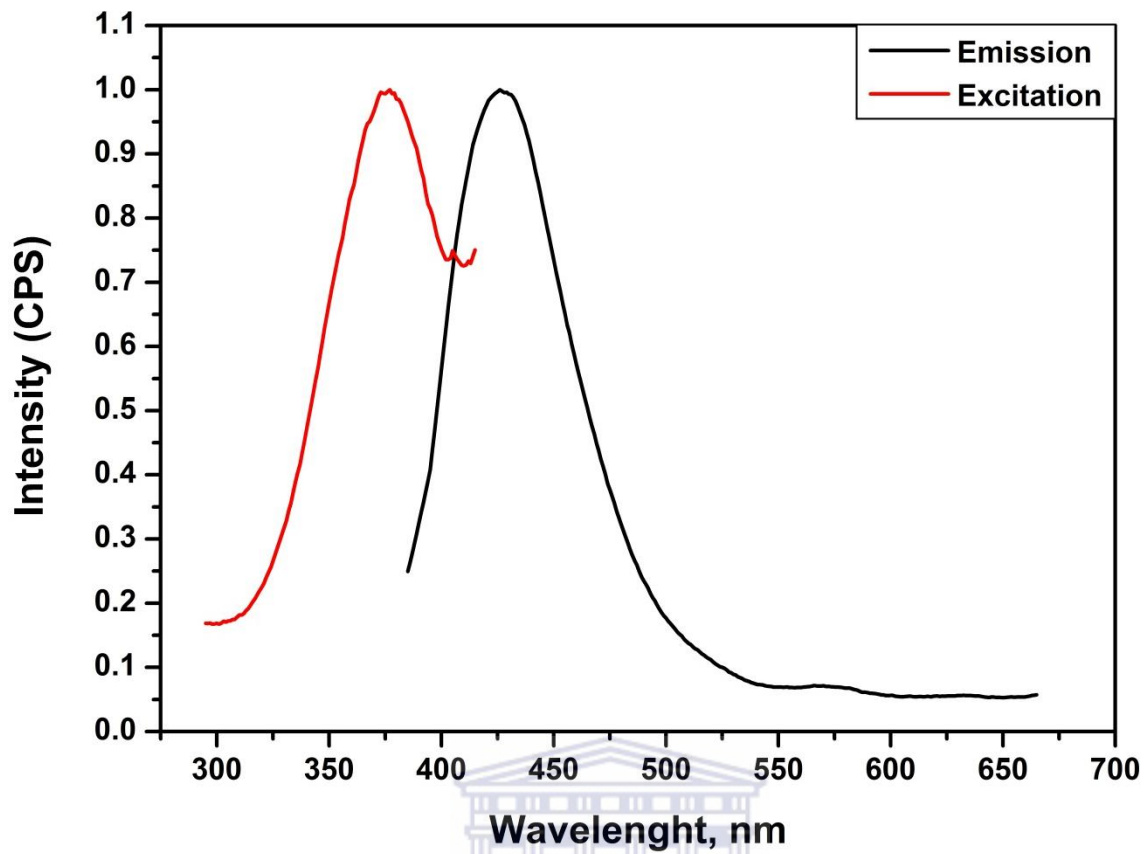


Figure 15: Fluorescence (emission and excitation) spectra of 3MPA-In₂Te₃ QDs.

4.1.3 X-ray diffraction (XRD)

XRD was used to determine the crystal structure and chemical composition of 3MPA-In₂Te₃ QDs. The conditions for performing XRD analysis were discussed in Chapter 3 section 3.5.2.3. The scanning angle range, 2θ of diffractometer, was from 20° to 80° . **Figure 16** below shows the XRD pattern of the QDs which exhibited four peaks at $2\theta = 25.02^\circ$, 41.40° , 49.02° and 75.46° which corresponds to diffractions of the (511), (822), (933) and (1266) planes, respectively (*Tai et al., 2011*). An amorphous hump around 27° in 2θ was also visible and it is the signature of the glass substrate used to put the sample on. The Miller indices correspond to bulk cubic In₂Te₃ crystals. However there was an unstable phase of In₃Te₄ and traces of pure tellurium and indium chloride also detected.

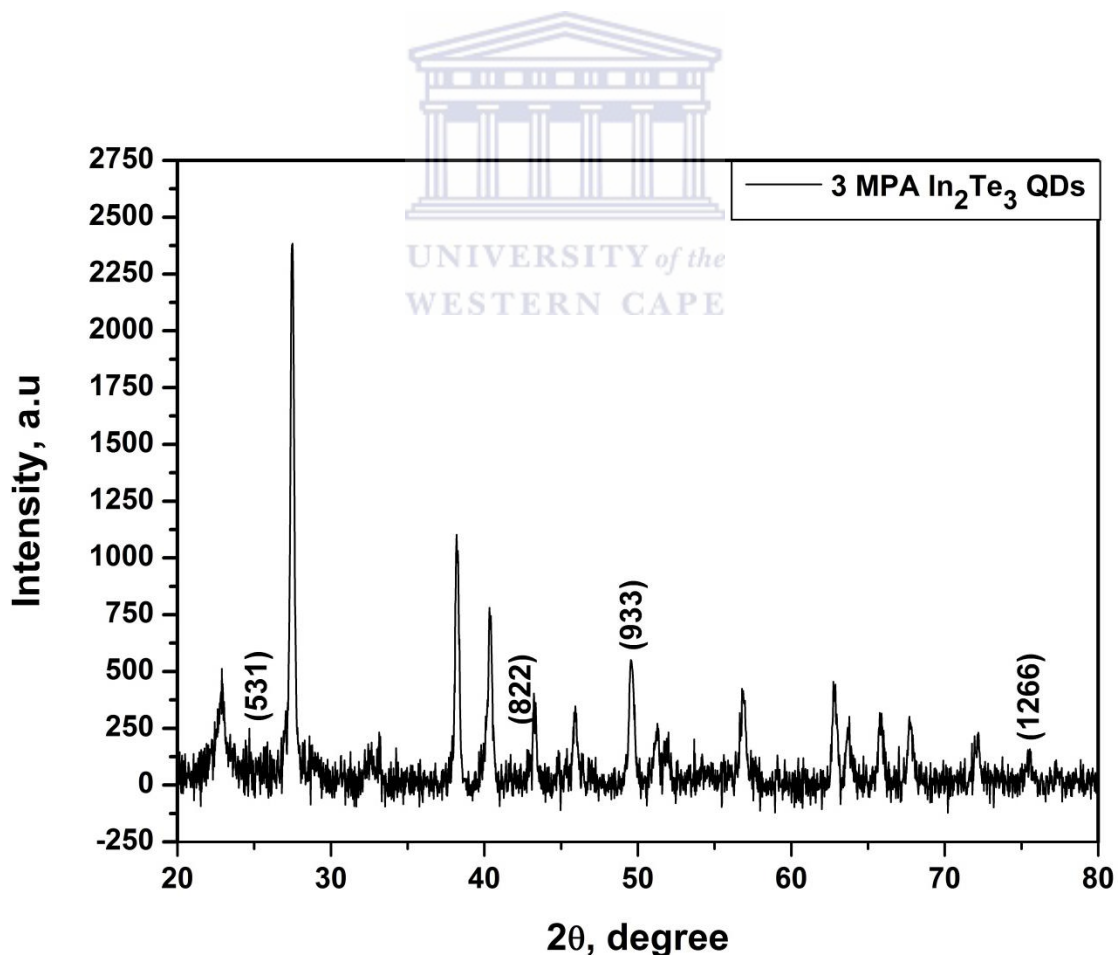


Figure 16: XRD pattern of 3MPA-In₂Te₃ QDs.

4.1.4 Fourier transform infrared spectroscopy (FT-IR)

FT-IR is an important tool in gathering information about the structure and the purity of a compound. The conditions for performing the FT-IR analysis were discussed in Chapter 3 section 3.5.2.4. **Figure 17** below represents the FT-IR spectra of 3MPA (black line) and 3MPA-In₂Te₃ QDs (red line). The FT-IR spectra of 3-MPA capped In₂Te₃ QDs exhibits well defined main peaks: four visible peaks consisting of two stretching frequencies at 3300 cm⁻¹ and 1650 cm⁻¹ in the functional group region while a medium stretching frequency at 1213 cm⁻¹ and a bending frequency at 1402 cm⁻¹ in the finger print region cm⁻¹ is observed.

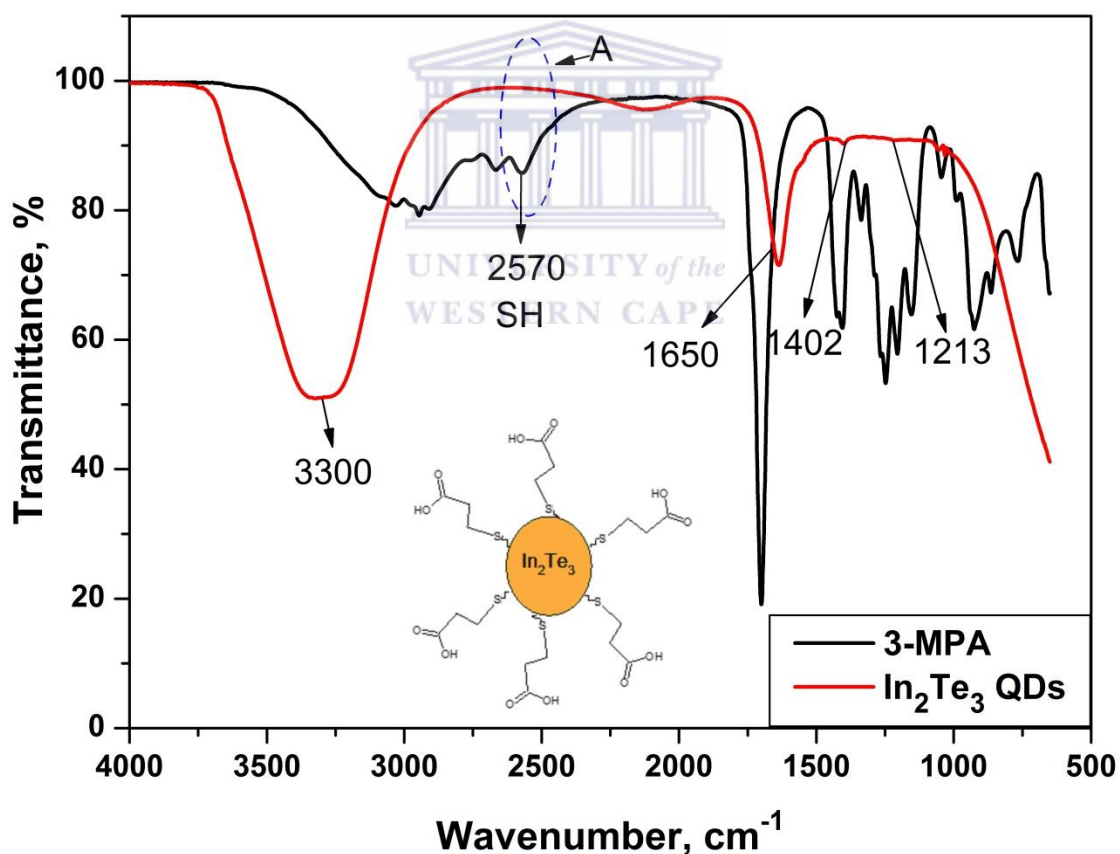
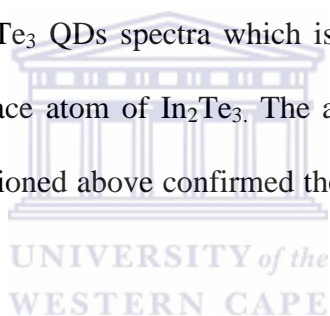


Figure 17: FT-IR spectrum of 3MPA and 3MPA-In₂Te₃ QDs.

Looking at the 3MPA-In₂Te₃ QDs spectra a broad absorption at 3300 cm⁻¹ accounts for the -OH stretching of the -COOH group from the 3MPA capping agent. The broad absorption in the 3400-2400 cm⁻¹ range is due to hydrogen binding that occurs and it often overlaps with the C-H stretching absorption that is why a C-H stretching frequency in the 3000-2850 cm⁻¹ range is not visible. A medium absorption band at 1650 cm⁻¹ indicates the presence of C=O stretch and due to conjugation the absorption band moves to a lower frequency. A weak absorption band at 1402 cm⁻¹ indicates the presence of C-O-H bend and another very weak absorption band at 1213 cm⁻¹ arises from the medium stretching vibrations of C-O bond in -COOH group from the 3-MPA capping agent. In addition an adsorption band at 2570 cm⁻¹ on the 3MPA indicates the presence of an S-H bond. It was observed that this bond is absent in the 3MPA-In₂Te₃ QDs spectra which is an indication that the S-H bond from 3MPA were bound to surface atom of In₂Te₃. The absence of this S-H bond and the presence of the other bonds mentioned above confirmed the successful capping of the In₂Te₃ QDs by the surfactant 3MPA.



4.2 Microscopic techniques

4.2.1 High resolution transmission electron microscopy (HR-TEM)

More convincing evidence of shape, size and structure of the 3MPA-In₂Te₃ QDs were observed with HR-TEM micrographs shown in **Figure 18 (A)** 20 nm, **(B)** 2nm and **(C)** 50 nm scale view. The conditions for performing HR-TEM studies were discussed in Chapter 3 section 3.5.3.1. In **Figure 18(A)** it was observed that the QDs are poly-dispersed. This is in good accordance with the QDs UV-VIS absorption spectra which showed three absorption peaks and could be attributed to refluxing process which allowed the growth of different sized QDs. Careful study of **Figure 18(B)** revealed lattice fringes that confirmed good crystallinity and the average diameter of the QDs was estimated to be 6 nm in diameter. The QDs also appeared to be spherical in shape with a broad distribution as shown in **Figure 18(C)**. The elemental composition of the 3MPA-In₂Te₃ QDs was studied using energy dispersive x-ray (EDX) spectroscopy and it revealed that the most abundant elements are In and Te, shown in **Figure 19**. The EDX spectra showed the presence of copper (Cu) which is a result of the copper grid used to put the sample on. While the presence of carbon (C), oxygen (O), and sulphur (S) is a result of the capping agent 3MPA. Furthermore, the presence of Na, results from the NaBH₄ used to reduce Te and the presence of Cl is a result of the starting material InCl₃.

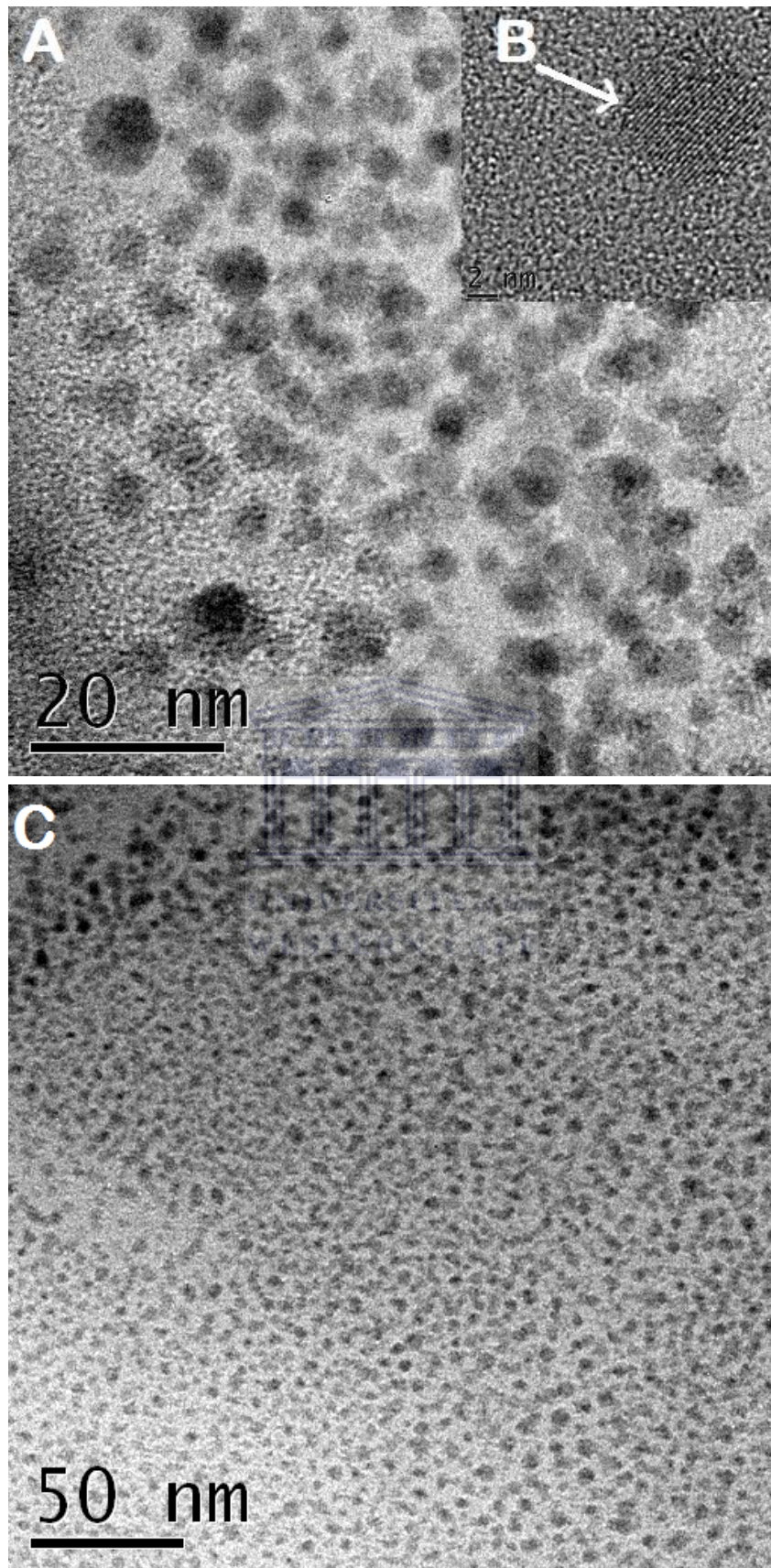


Figure 18: HR-TEM micrographs of 3MPA-In₂Te₃ QDs 20 nm (A) 2 nm (B) and 50 nm (C) scale view.

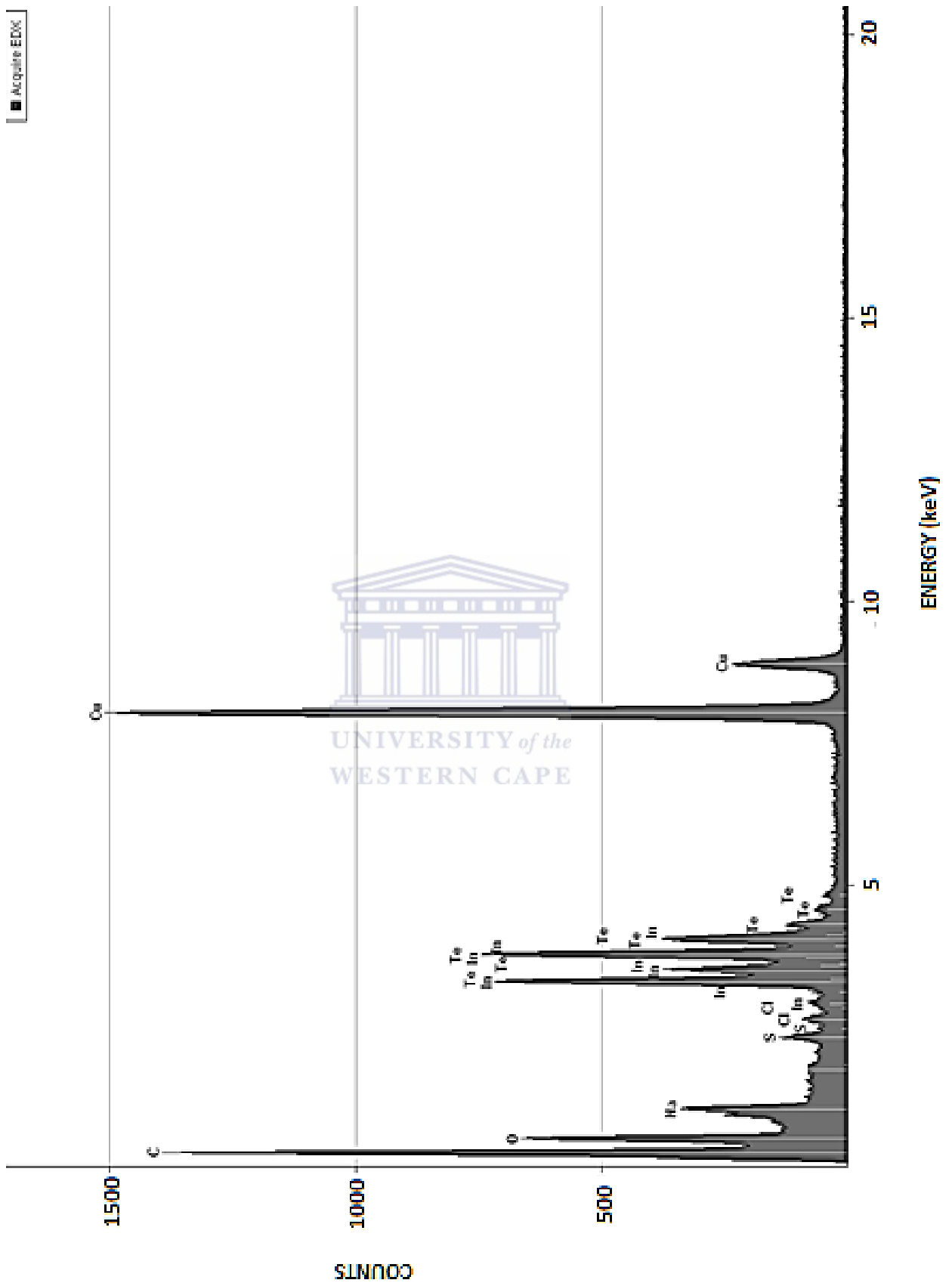


Figure 19: HR-TEM Energy-dispersive X-ray (EDX) spectrum of 3MPA-In₂Te₃ QDs.

4.2.2 High resolution scanning electron microscopy (HR-SEM)

The HR-SEM micrographs shown in **Figure 20 (A and B)** provided morphological and compositional information of the 3MPA-In₂Te₃ QDs and probe ssDNA/3MPA-In₂Te₃ QDs, respectively. The conditions for performing the HR-SEM studies were discussed in Chapter 3 section 3.5.3.2. In **Figure 20(A)** it was observed that the 3MPA-In₂Te₃ QDs appeared to be sphere-shaped nanocrystals aggregated together. This aggregation may be explained by the use of too little 3MPA capping agent. The insufficient amount of 3MPA capping agent causes an increase in the surface area to volume ratio and hence increases the attractive force between the nanocrystals thereby causing them to agglomerate. Another reason for aggregation is the fact that the capping agent might not have been fully charged at a high pH therefore was not able to maintain the colloidal stability of the QDs (*Li et al., 2007*). The QDs continued to exhibit aggregated morphology however noticeable morphology changes could be observed when the probe ssDNA were added as shown in **Figure 20(B)**. The QDs started to self-assemble into a certain configurations when attached to single strands of DNA. The same phenomenon was observed by Argonne researcher Byeongdu Lee and his colleagues (*Jone et al., 2010*). In their study it was said that ssDNA acts as a “Velcro” for nanoparticles. This “Velcro effect” is caused by the “sticky ends” of the ssDNA molecules. These “sticky ends” are regions of unpaired nucleotides. According to Lee, when they attached ssDNA to spherical gold nanoparticles the nanoparticles arranged themselves into one of two separate types of cubic crystals (face-centred or body-centred cubes). In this research study when ssDNA came in contact with the spherical QDs, the QDs then self-assembled into cubic lattice configurations denoted by (i) as shown in **Figure 20(B)**. The elemental composition of the 3MPA-In₂Te₃ QDs was studied using EDX spectroscopy, shown in **Figure 21**. The EDX spectra of HR-SEM correlate with the EDX spectra of HR-

TEM. However, for HR-SEM analysis carbon-tape was used to put sample on instead of a copper grid therefore copper (Cu) is not observed in EDX spectra.



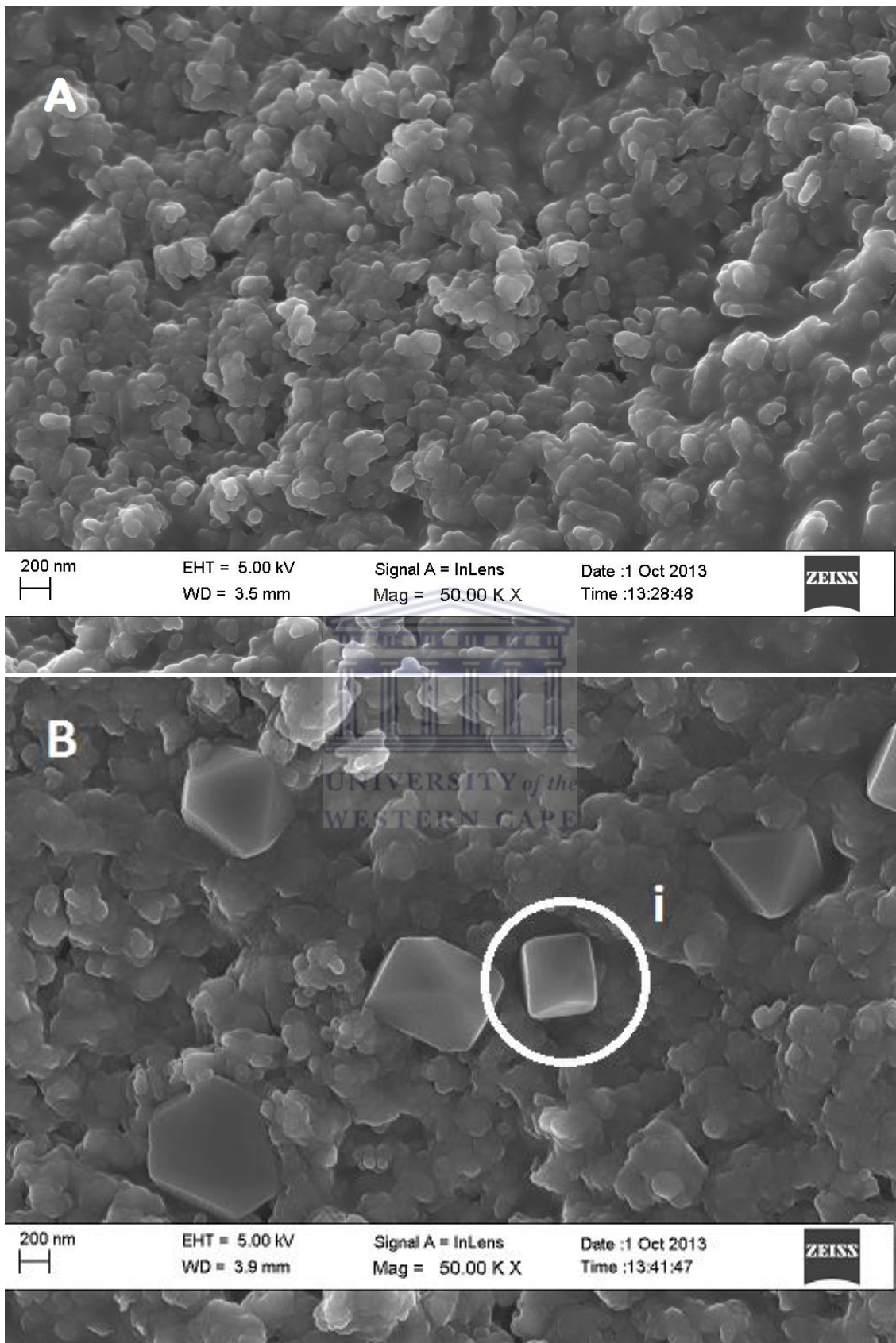


Figure 20: HR-SEM micrographs of 3MPA-In₂Te₃ QDs (A) and probe DNA/3MPA-In₂Te₃ QDs (B) at 200 nm scale view.

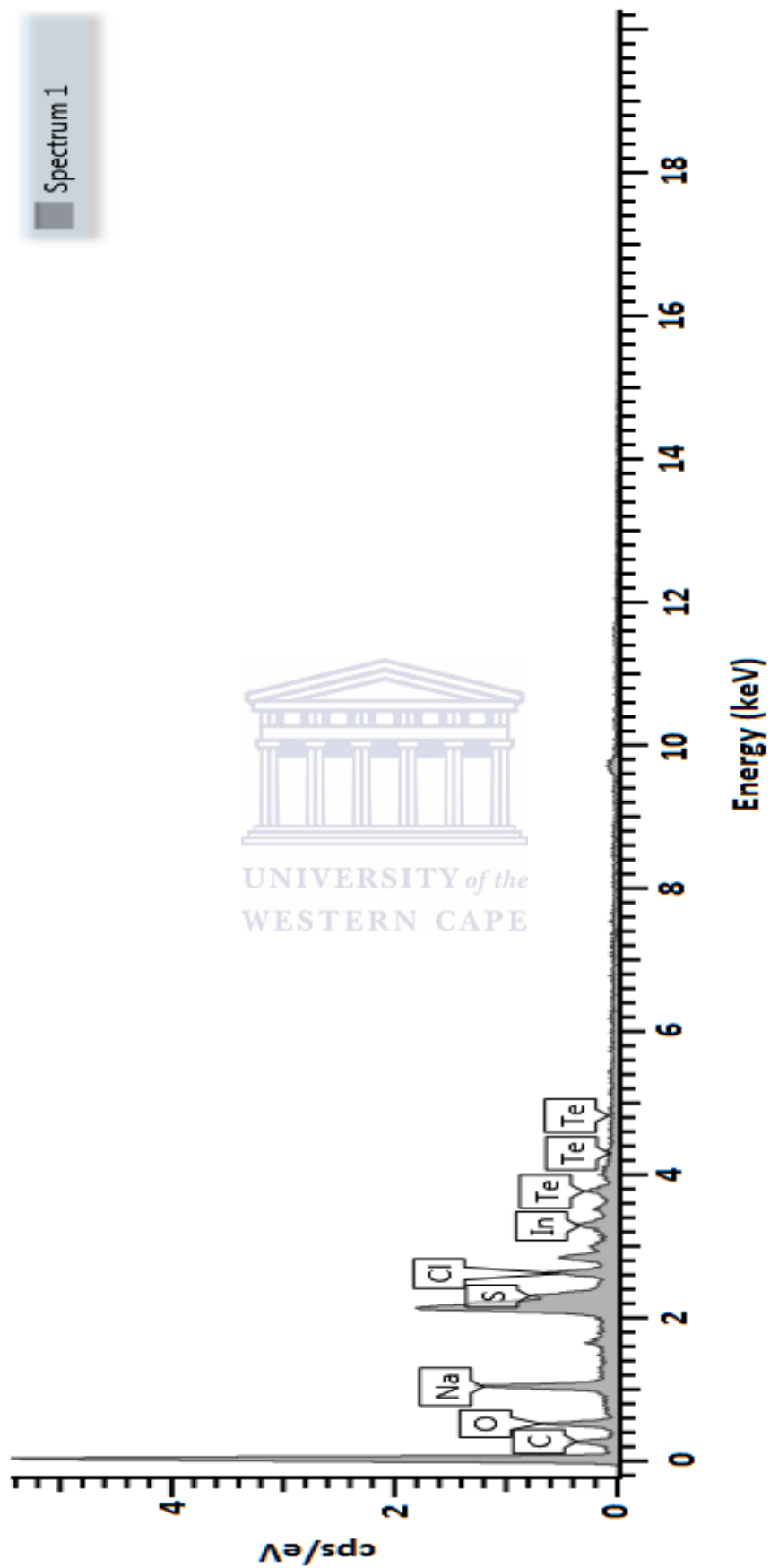


Figure 21: HR-SEM Energy-dispersive X-ray (EDX) spectrum of 3MPA-In₂Te₃ QDs.

4.3 Electrochemical techniques

4.3.1 Cyclic Voltammetry (CV)

Before studying the electrochemistry of 3MPA-In₂Te₃ QDs on AuE, the precursors of 3MPA-In₂Te₃ QDs were first investigated. This electrochemical study was done in order to determine if the observed “new peaks” were due to the reduction or oxidation of the adsorbed QDs. The conditions for performing these electrochemical processes were discussed in Chapter 3 section 3.5.1.1. **Figure 22 (A)** and **(B)** shows the cyclic voltammograms of InCl₃/AuE versus bare AuE and NaHTe/AuE versus bare AuE. The peaks on the two cyclic voltammograms are labeled by letters “A” and “C” which denotes anodic and cathodic processes, respectively. Study of peak C₁ in **Figure 22(A)** revealed the possible cathodic reduction of In³⁺ to In⁰ at $E_{p,c} = -610$ mV. The reduction of indium ions on the electrode surface has been previously reported (*Chung and Lee, 2012*). In **Figure 22(B)** the appearance of peak A₂ at $E_{p,a} = 240$ mV may be due to oxidation of QDs which in turn generates Te⁴⁺. While peak A₁ at $E_{p,a} = 370$ mV can be associated with the oxidation of Te⁴⁺ to Te⁶⁺. When the potential is swept in the negative direction two peaks C₁ at $E_{p,c} = -43$ mV and C₂ at $E_{p,c} = -610$ mV are observed. Peak C₁ may be due to the reduction of Te⁴⁺ to Te⁰ whereas peak C₂ may be due to the reduction of Te⁰ to Te²⁻. This assignment of peaks is consistent with previous reports (*Martin-Gonzalez et al., 2002; Khene et al., 2011*). However there might be shifts in some peaks depending on how acidic or basic the electrolyte solution is for a particular study. The electrochemical behaviour of Te is more complicated both because the formal oxidation state of the element can vary from Te⁶⁺ to Te²⁻ and because adsorption can play a big role due to the strong interactions between Te species and In metal (*Martin-Gonzalez et al., 2002*).

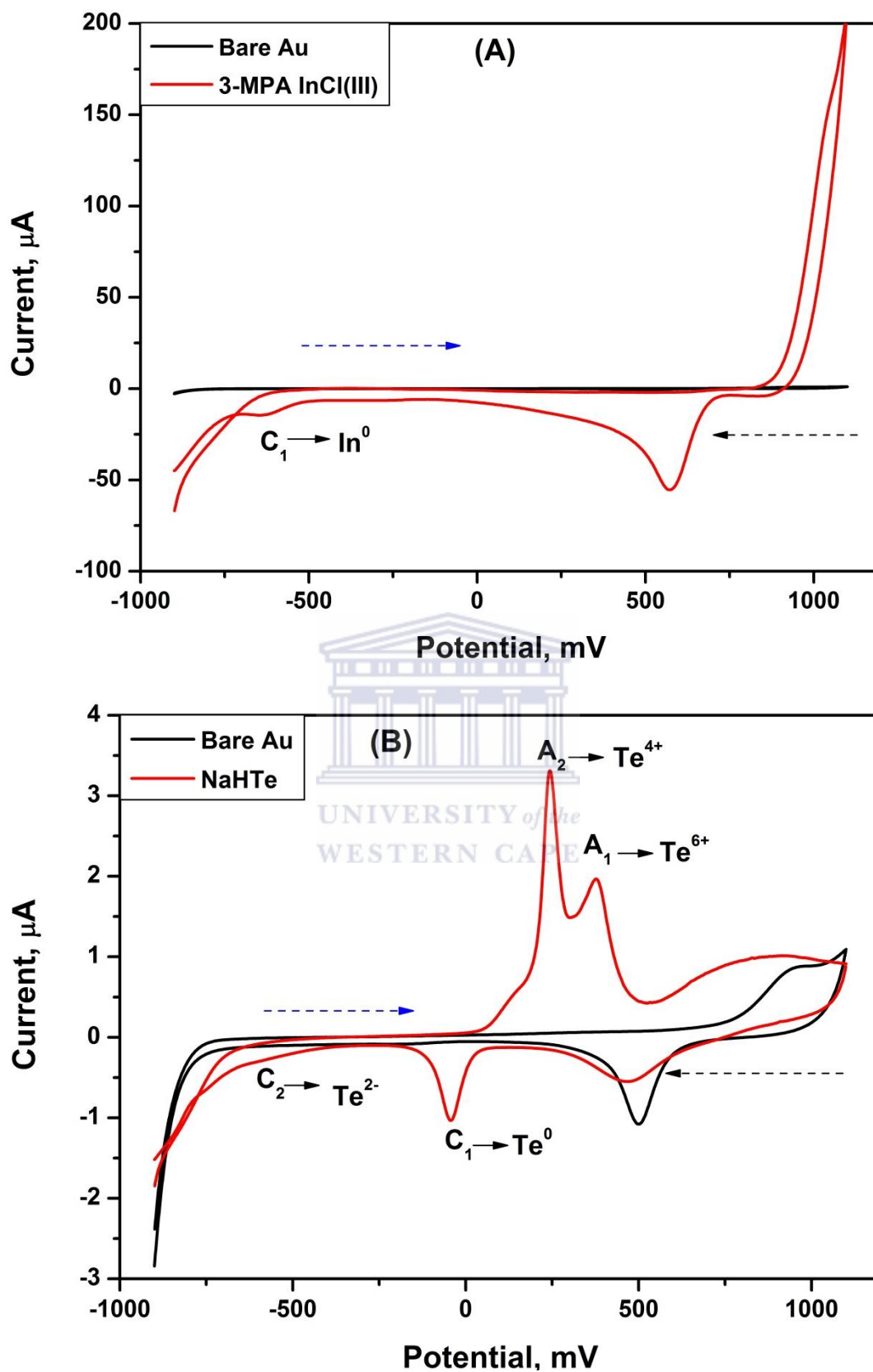


Figure 22: Cyclic voltammograms of InCl_3 versus bare AuE (A) and NaHTe versus bare AuE (B) in 0.10 M PBS, pH 7.4 at 10 mV/s.

Using CV the electrochemical properties of 3MPA-In₂Te₃ QDs was studied. **Figure 23 (a)** and **(b)** shows cyclic voltammograms of bare AuE and 3MPA-In₂Te₃ QDs modified AuE. Scanning cathodically (blue arrow) from -900 to +1100 mV, three anodic peaks were observed at $E_{p,a} = 160$ mV (peak A₃), $E_{p,a} = 440$ mV (peak A₂) and $E_{p,a} = 850$ mV (peak A₁), respectively as shown in **Figure 23 (b)**. While scanning in the opposite (negative) direction (black arrow) from +1100 to -900 mV, four cathodic peaks were observed at $E_{p,c} = 475$ mV (peak C₁), $E_{p,c} = -40$ mV (peak C₂), $E_{p,c} = -420$ mV (peak C₃) and $E_{p,c} = -610$ mV (peak C₄), respectively as shown in **Figure 23 (a)**. Peak A₁ may be attributed to 3MPA-In₂Te₃ QDs/AuE oxidation hence the enhancement in peak broadness when compared to the peak ($E_{p,a} = 950$ mV) of bare AuE denoted by (a). Peak A₃ has a small shoulder that is labelled A₂ and as previously discussed formation of peak A₃ is due to oxidation of QDs which in turn generates Te⁴⁺. However compared to the NaHTe precursor, peak A₃ of the QDs shifts to more negative potentials ($E_{p,a} = 160$ mV). The shifting to more negative potentials may be a consequence of the QD size. The QDs size along with the nature of the surfactant and pH of the electrolyte solution can influence the electrochemistry of the 3MPA-In₂Te₃ QDs (*Poznyak et al., 2005*). The cathodic scan for 3MPA-In₂Te₃ QDs/AuE shows peak C₁ which is shifted to negative potentials compared to the peak ($E_{p,a} = 500$ mV) of bare AuE. Peak C₁ is also less enhanced compared to the peak of bare AuE. This observation suggests that the oxidation products of the QDs block the AuE surface. As previously discussed, peak C₂ is due to the reduction of Te⁴⁺ to Te⁰ and peak C₃ is due to the reduction of Te⁰ to Te²⁻. Another peak labelled as C₄ is located at more negative potentials $E_{p,c} = -600$ mV and may be attributed to onset of hydrogen evolution (*Martin-Gonzalez et al., 2002*). The reduction of In³⁺ to In⁰ also occurs at peak C₃ however it overlaps with the reduction of Te species. This overlapping results in In-Te interaction. Peaks C₂ and C₃ of the QDs are shifted to more positive potentials compared

to the peaks of the individual precursors found in the same region of peak potentials. This behaviour is due to the mixture of both elements adsorbed on the surface of the AuE.

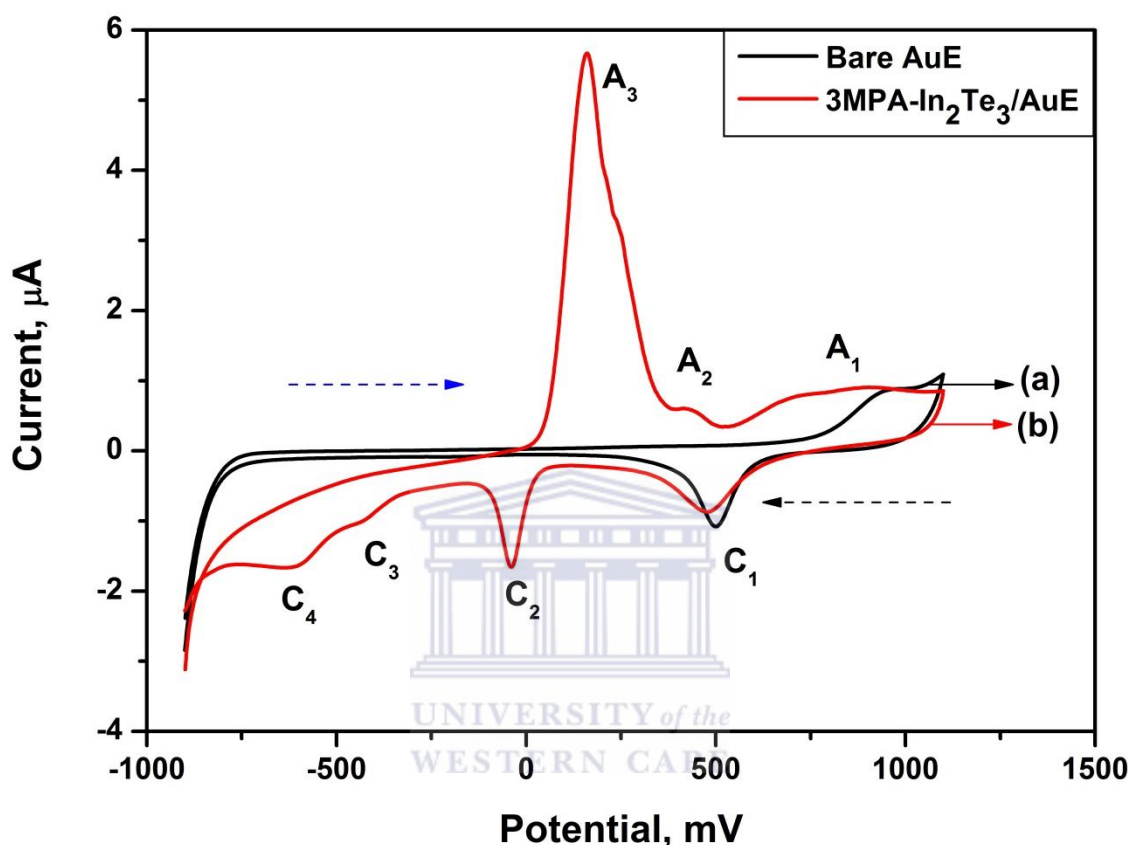


Figure 23: Cyclic voltammograms of bare AuE (a) and 3MPA-In₂Te₃ QDs/AuE (b) in 0.10 M PBS, pH 7.4 at 10 mV/s.

A multi-scan study of 3MPA-In₂Te₃ QDs on AuE was performed as shown in **Figure 24**. It was observed that with increasing scan rate the anodic peak positions are shifted to more positive potentials while the cathodic peak positions are shifted to more negative potentials. This indicates that the cathodic and anodic processes are governed by slow electron transfer processes. At lower scan rates (4-20 mV/s) all the peaks could be seen clearly however as the scan rate is increased beyond 20 mV/s some peaks becomes less

prominent such as peak C_3 . Te surface state defects are prominent in 3MPA- In_2Te_3 QDs therefore a high number of oxidizable Te defects are found in these QDs.

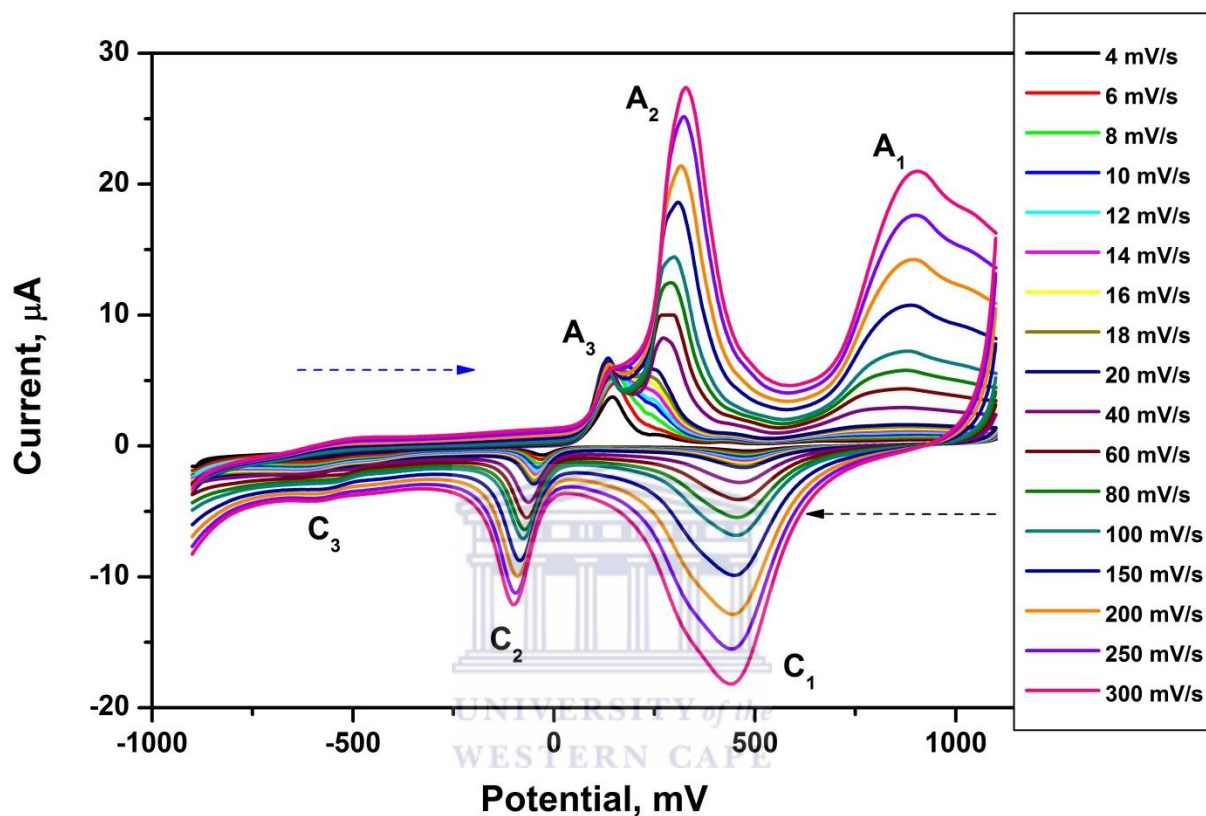


Figure 24: Multi-scan voltammograms of 3MPA- In_2Te_3 QDs in 0.10 M PBS, pH 7.4 at (4-300 mV/s).

To obtain additional information on the redox reactions involving QDs, the dependence of the peak current and the potential on the scan rate were also studied. A close study of the oxidation peak A_2 was performed by constructing a plot of peak current ($I_{p,a}$) versus scan rate (v) in the range 4- 20 mV/s as illustrated in **Figure 25**. A linear relationship between $I_{p,a}$ versus v was observed since the linear correlation coefficients (R^2) was 0.998.

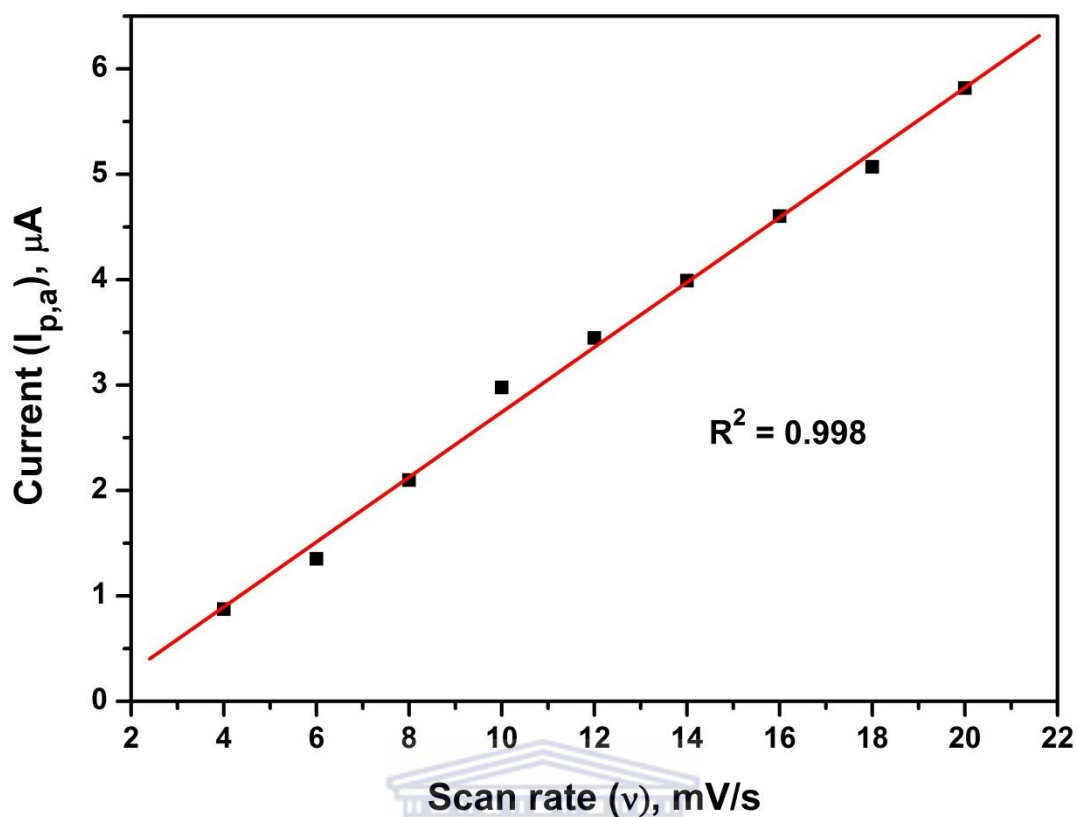


Figure 25: Anodic (peak A₂) plot of peak current ($I_{p,a}$) versus scan rate (ν).

The peaks observed in **Figure 24**, described the adsorbed electrochemistry of 3MPA-In₂Te₃ QDs. This was confirmed by plotting $\log I_{p,a}$ versus $\log \nu$, shown in **Figure 26**. A linear relationship ($R^2 = 0.996$) between $\log I_{p,a}$ versus $\log \nu$ was observed with a slope = $1.187 \mu\text{A} / \text{mV} \cdot \text{s}^{-1}$. These results indicate that the electron transfer reaction was controlled by adsorption of 3MPA-In₂Te₃ QDs on the surface of the AuE in 0.10 M PBS, pH 7.4.

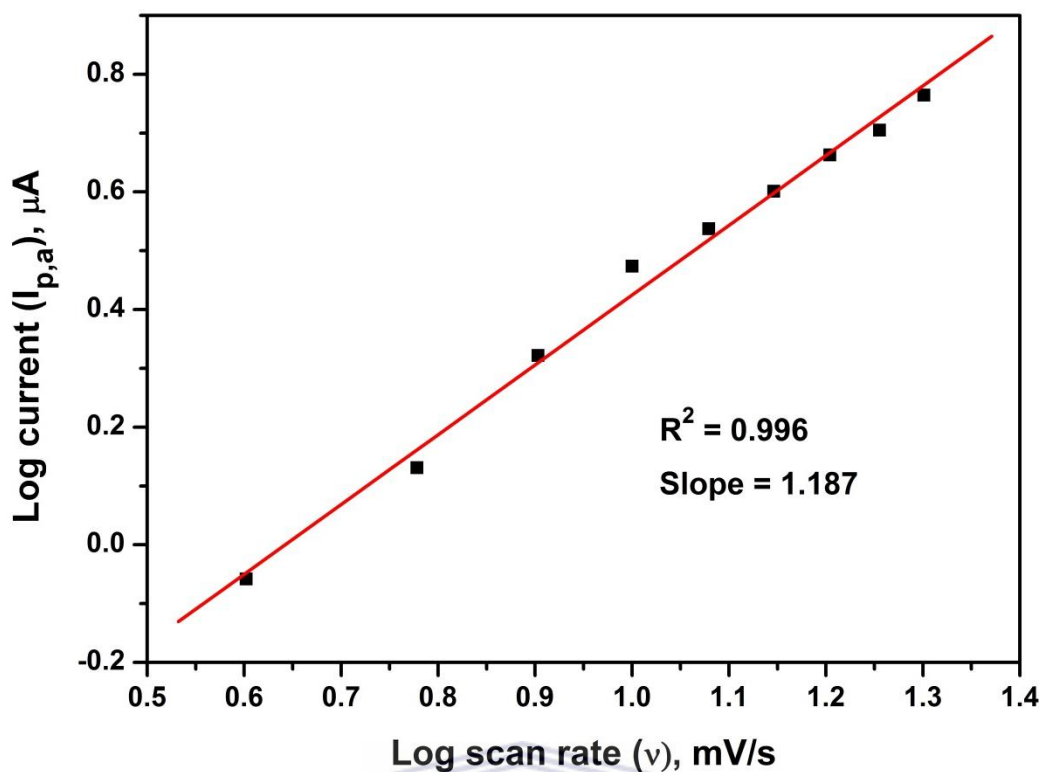


Figure 26: Anodic (peak A₂) plot of log peak current ($I_{p,a}$) versus log scan rate (v).

Since the electrochemical reaction was found to be controlled by adsorption the surface concentration of the adsorbed 3MPA-In₂Te₃ QDs on the surface of the AuE could be determined by using the Brown Anson approximation given below.

$$I_{p,a} = \frac{n^2 F^2 A \Gamma}{4RT} \nu \quad (4.3.1.1)$$

Where $I_{p,a}$ = Peak Current in A, $n = 1$ number of electrons, $F = 96485 \text{ C mol}^{-1}$ (Faradays Constant), $A = 0.0201 \text{ cm}^2$ geometric area of the electrode, $R = 8.314 \text{ J mol}^{-1} \text{ K}^{-1}$ (Gas Constant), $T = 298.15 \text{ K}$ (absolute temperature) and $\nu = \text{Scan Rate in V s}^{-1}$ and Γ is the (surface concentration coverage). Therefore the surface concentration of the surface adsorb QDs was calculated to be $\Gamma = 1.63 \times 10^{-8} \text{ mol.cm}^{-2}$

4.3.2 Electrochemical Impedance spectroscopy (EIS)

In this research study EIS was used to investigate the electrocatalytic properties of 3MPA-In₂Te₃ QDs/AuE. The data obtained was explained using Nyquist and Bode plots. The conditions for performing EIS were discussed in Chapter 3 section 3.5.1.3. **Figure 27** shows Nyquist plots of bare AuE (black line) and 3MPA-In₂Te₃ QDs /AuE (red line) in 0.10 M PBS, pH 7.4. These Nyquits plots were interpreted by the equivalent circuit model, displayed in **Figure 28** below. This circuit model consists of solution resistance of the electrolyte solution (R_s), Warburg impedance (Z_w), which is the result of the diffusion of ions to the electrode interface from the bulk of the electrolyte, constant phase element (CPE) describing double layer capacitance properties, and electron transfer resistance (R_{ct}) (*Bard et al., 2001*). From this equivalent circuit model the charge transfer resistance of bare AuE ($R_{ct} = 5.1642 \times 10^5 \Omega$) was found to be greater than the charge transfer resistance of 3MPA-In₂Te₃ QDs /AuE ($R_{ct} = 6.6886 \times 10^4 \Omega$). The greater the charge transfer resistance obtained for bare AuE indicated that the charge transfer speed was slower. Some factors that can influence the charge transfer speed are the type of reaction and temperature. The 3MPA-In₂Te₃ QDs /AuE showed less resistance to charge transfer indicating that it is a better charge conducting material.

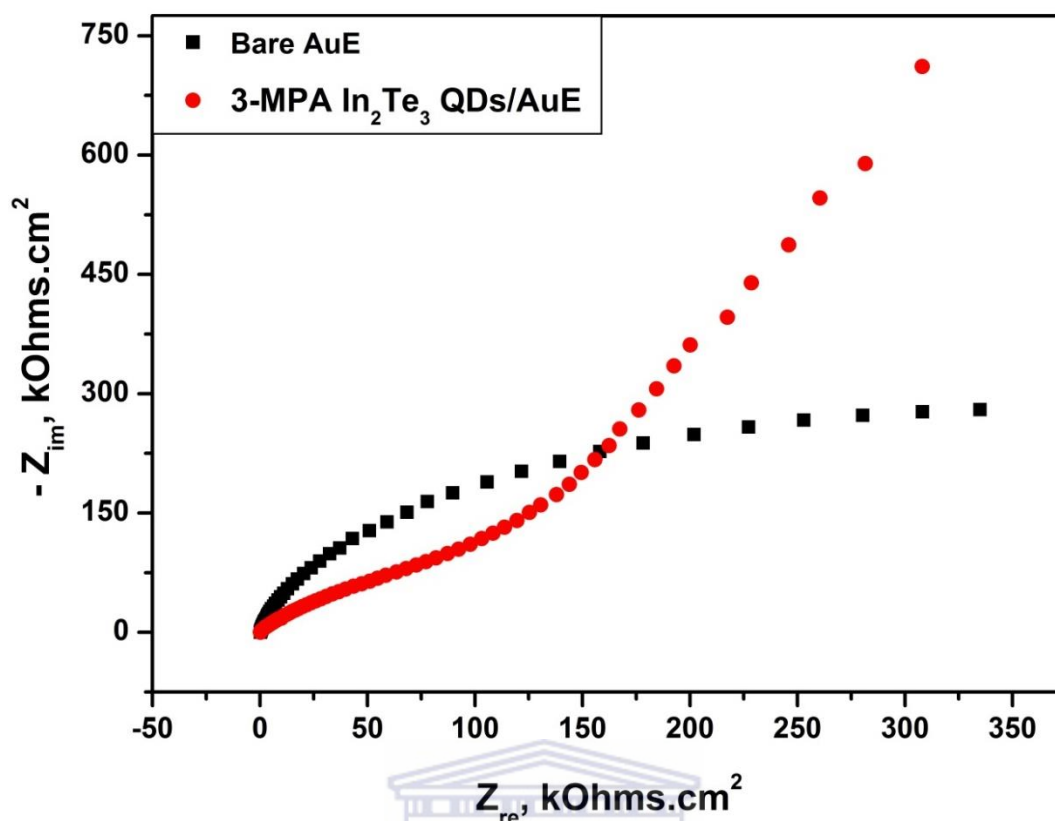


Figure 27: Nyquist plots corresponding to Randles equivalent circuit of bare AuE and 3MPA-In₂Te₃ QDs/AuE in 0.10 M PBS, pH 7.4.

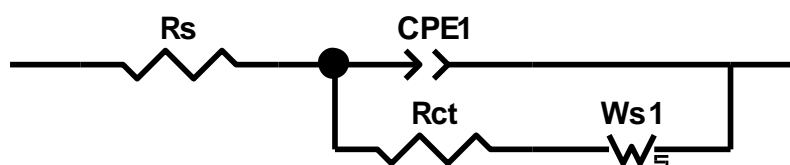


Figure 28: Randles equivalent circuit used to model impedance data of bare AuE and 3MPA-In₂Te₃ QDs/AuE in 0.10 M PBS, pH 7.4.

The frequency dependence of both the impedance and the phase angle of the bare AuE (black line) and 3MPA-In₂Te₃ QDs /AuE (red line) are represented by the Bode plots, shown in **Figure 29**. It was observed that the impedance of the bare AuE and 3MPA-In₂Te₃ QDs/AuE decreased with increasing frequency. However at lower frequencies an increase in impedance for both bare AuE and 3MPA-In₂Te₃ QDs/AuE was observed. At low frequencies

the bare AuE showed a lower phase angle of 40° compared to the 65° of 3MPA- In_2Te_3 QDs/AuE. These results indicate an increase in conductivity of 3MPA- In_2Te_3 QDs/AuE system. Even though bare AuE has a lower phase angle (40°) denoted by (a) it is still within the range of values for a typical semiconductor since Au on its own also behaves like a semiconductor. The increase in conductivity of the 3MPA- In_2Te_3 QDs makes it an ideal mediating platform in the construction of the QDs-based genosensor. The obtained results for both Nyquist and Bode analysis is in accordance with each other.

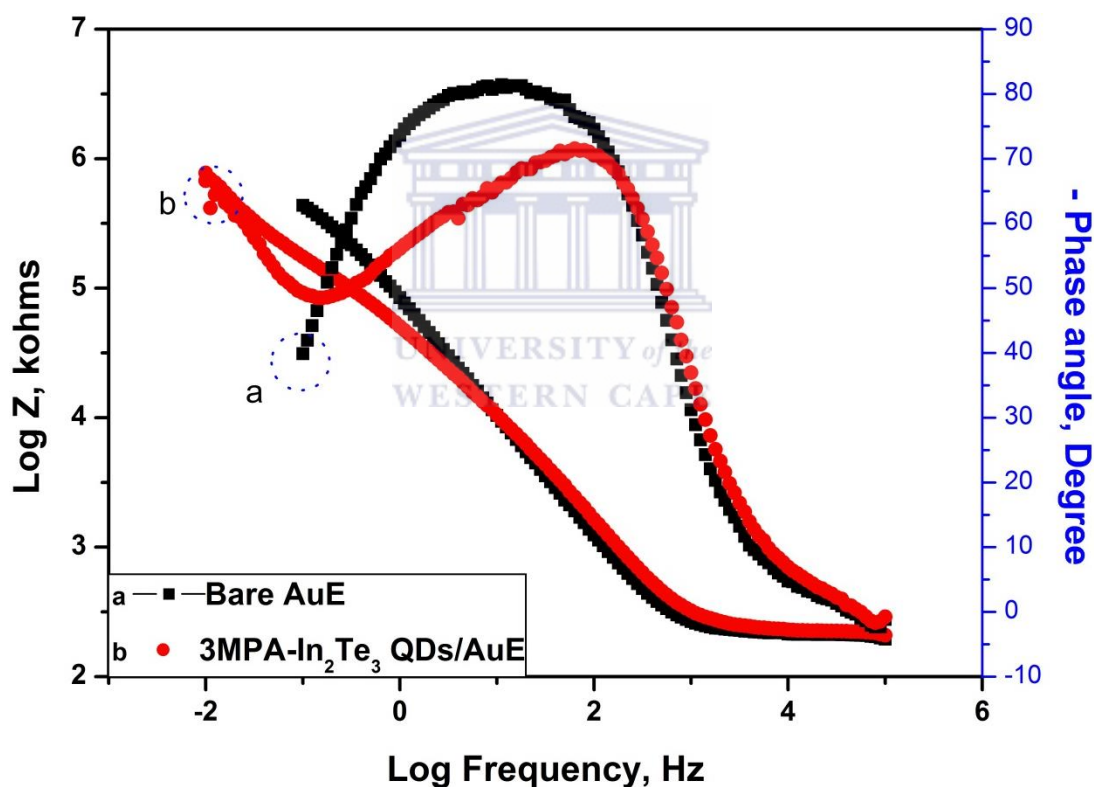


Figure 29: Bode plots of bare AuE and 3MPA- In_2Te_3 QDs/AuE in 0.10 M PBS, pH 7.4.

4.4 Characterization of 3MPA-In₂Te₃ QDs based genosensor

4.4.1 Cyclic Voltammetry (CV)

Figure 30 below shows cyclic voltammograms of bare AuE (black line), 3MPA-In₂Te₃ QDs/AuE (red line) and probe ssDNA/3MPA-In₂Te₃ QDs/AuE (green line) in 0.10 M PBS, pH 7.4. The conditions for performing these electrochemical processes were discussed in Chapter 3 section 3.5.1.1. Study of **Figure 30** revealed that there was a significant reduction in the anodic and cathodic peak currents when probe ssDNA was introduced into the 3MPA-In₂Te₃ QDs/AuE system. This can be due to slow diffusion of an equilibrium mixture of the probe ssDNA bound to the electrode surface (*Arjmand et al., 2011*). However, it is a common behaviour of ssDNA to decrease the peak currents when it is added to a particular system (*Naik and Naik, 2008; Arjmand et al., 2011*). In the case of this study the addition of probe ssDNA to 3MPA-In₂Te₃ QDs/AuE system makes the 3MPA-In₂Te₃ QDs less conductive and causing them to become more difficult to oxidize. The anodic and cathodic peaks observed in the cyclic voltammogram denoted by (c) showed shifts to more positive potentials indicating that the probe ssDNA was adsorbed to the surface of 3MPA-In₂Te₃ QDs/AuE.

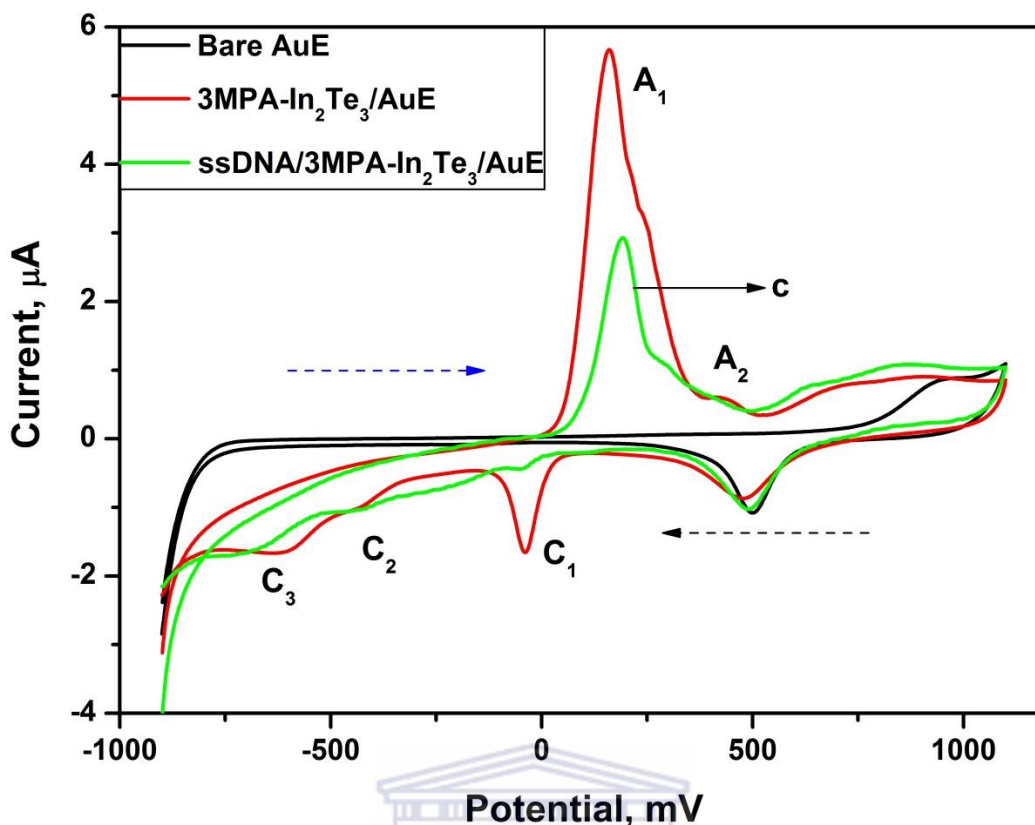


Figure 30: Cyclic voltammograms of bare AuE, 3MPA-In₂Te₃ QDs/AuE and probe ssDNA/3MPA-In₂Te₃ QDs/AuE in 0.10 M PBS, pH 7.4 at 10 mV/s.

UNIVERSITY of the
WESTERN CAPE

4.4.2 Electrochemical Impedance Spectroscopy (EIS)

Figure 31(A) and **(B)** shows the Nyquist and Bode plots of bare AuE (black line), 3MPA-In₂Te₃ QDs/AuE (red line) and probe ssDNA/3MPA-In₂Te₃ QDs/AuE (green line) respectively. The conditions for performing EIS were discussed in Chapter 3 section 3.5.1.3. By studying the Nyquist plots interpreted by the equivalent circuit model discussed in section 4.3.2, shown in **Figure 31(A)**, it was determined that probe ssDNA/3MPA-In₂Te₃ QDs/AuE has the highest charge transfer resistance ($R_{ct} = 1.5313 \times 10^6 \Omega$) compared to both bare AuE ($R_{ct} = 5.1642 \times 10^5 \Omega$) and 3MPA-In₂Te₃ QDs/AuE ($R_{ct} = 6.6886 \times 10^4 \Omega$). These results indicate that DNA is a less conductive material since the incorporation of probe ssDNA into the 3MPA-In₂Te₃ QDs/AuE system, resulted in a high resistance to charge transfer. The charge transfer resistance of the three systems are tabulated below.

Table 6: Charge transfer resistance (R_{ct}) values of bare AuE, 3MPA- In_2Te_3 QDs/AuE and probe ssDNA/3MPA- In_2Te_3 QDs/Au.

Electrode system	R_{ct} (Ω)	% Error
Bare AuE	5.1642×10^5	1.5543
3MPA- In_2Te_3 QDs/AuE	6.6886×10^4	4.4434
Probe ssDNA/3MPA- In_2Te_3 QDs/AuE	1.5313×10^6	4.2362

In **Figure 31(B)** it was observed that when probe ssDNA is added to the 3MPA- In_2Te_3 QDs/AuE system the phase angle drops from 65° to 41° , which is what one can expect because ssDNA reduces the conductivity of a material. However the probe ssDNA/3MPA- In_2Te_3 QDs/AuE system is still conductive because it is still in the region of being conductive.

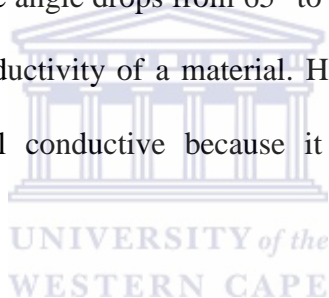


Table 7: Change in phase angle values of bare AuE, 3MPA- In_2Te_3 QDs/AuE and probe ssDNA/3MPA- In_2Te_3 QDs/AuE.

Electrode system	Phase angle (Degree)
Bare AuE	40
3MPA- In_2Te_3 QDs/AuE	65
Probe ssDNA/3MPA- In_2Te_3 QDs/AuE	41

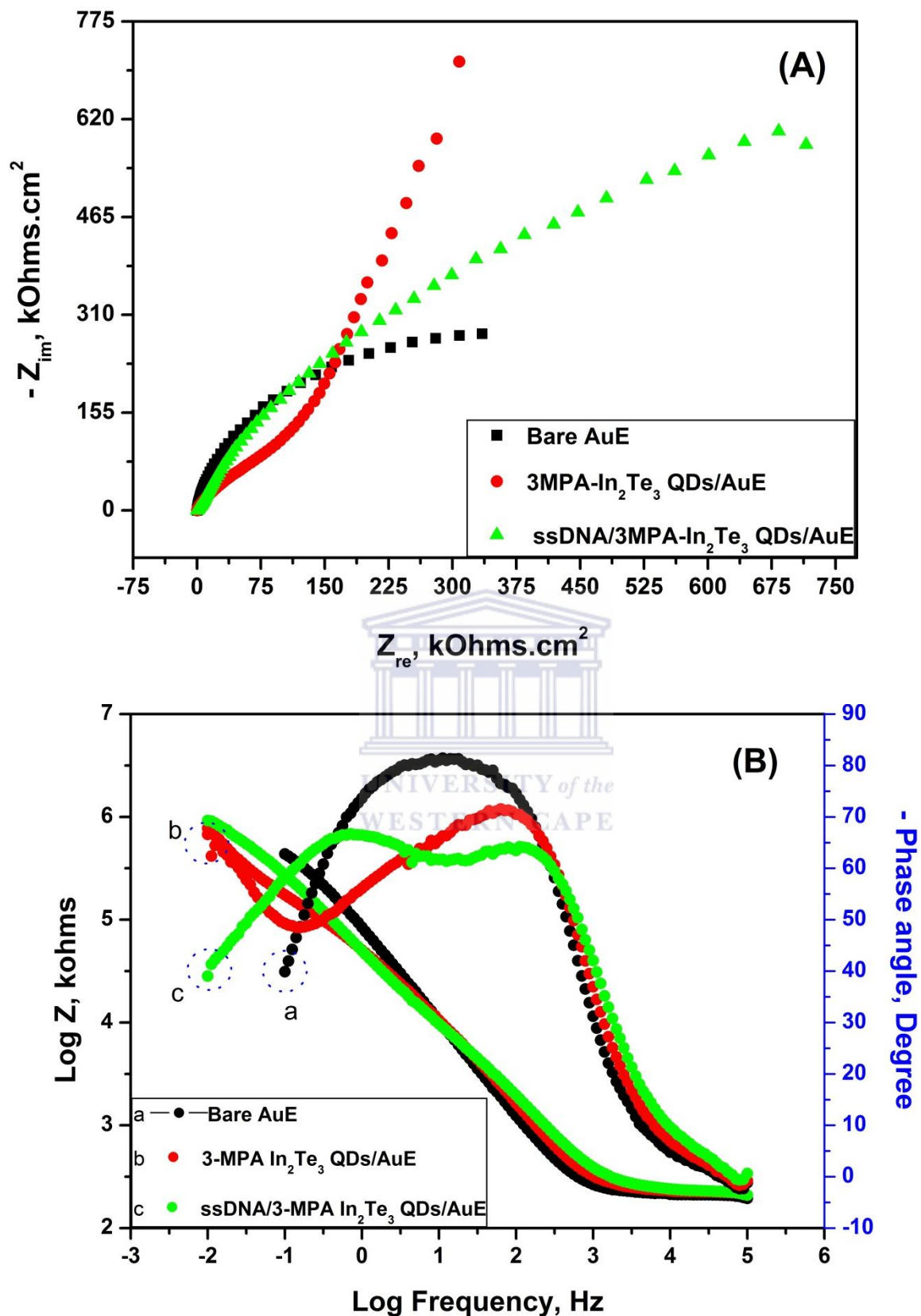


Figure 31: Nyquist (A) and Bode (B) plots of bare AuE, 3MPA- In_2Te_3 QDs/AuE and probe ssDNA/3MPA- In_2Te_3 QDs/AuE in 0.10 M PBS, pH 7.4, respectively.

4.5 Genosensor measurements

4.5.1 Response dynamic of 3MPA-In₂Te₃ QDs based genosensor to complementary ssDNA (target) using voltammetric techniques (CV and SWV)

In this study an indirect electrochemical DNA hybridization approach was followed since QDs was used as mediators. High sensitivity was achieved by one-to-one interactions between the probe ssDNA molecule and the QDs that was drop coated on the AuE surface. The probe ssDNA was covalently tethered to the surface of QDs through an amine (-NH₂) group. This amine group of the ssDNA interacted with activated carboxyl groups on the QDs/AuE surface. The incorporation of QDs is an advantage for the genosensor under study since it facilitates electron transfer between probe ssDNA and the AuE. In addition these electron mediators oxidize probe ssDNA directly and it also eliminates modification of the complementary ssDNA (Cagnin *et al.*, 2009). In order to achieve high selectivity towards specific target analyte and prevent non-specific binding, optimization of the amount of surface layer for each material used to fabricate the genosensor was done. Therefore the optimum amount used in this study was 2 μ L.

Figure 32 shows the CV response that was obtained for the probe ssDNA/3MPA-In₂Te₃/AuE to different concentrations (0-10 nM) of complementary ssDNA in 0.01 M TE buffer solution, pH 8.00. The conditions for performing these electrochemical processes were discussed in Chapter 3 section 3.5.1.1. From **Figure 32** it was observed that, after the first addition of telomerase concentration (2 nM) a decrease in peak current at $E_{p,a} = 190$ mV was observed. The peak was postulated to be due to the current response generated by the hybridization process that occurred between the probe ssDNA drop coated on the 3MPA-In₂Te₃ QDs/AuE surface and the complementary ssDNA (target analyte) in 0.10 M TE buffer solution, pH 8.00. In order to be more specific the current response is due to electrochemical

oxidation of DNA. The decrease in peak current might be due to the insulating properties of dsDNA that formed on the surface of AuE which in turn caused a decrease in the charge flow. Meaning the oxidation products of DNA became less accessible for oxidation after formation of dsDNA on AuE surface. However it is generally known that dsDNA are more conductive than ssDNA but factors such as the structural features of the dsDNA can play a major role in its conductivity (Kratochvílová *et al.*, 2008). Just like CV, SWV response was obtained for the 3MPA-In₂Te₃ QDs based genosensor to different concentrations (0-10 nM) of complementary ssDNA in 0.01 M TE buffer solution, pH 8.00 as shown in **Figure 33**.

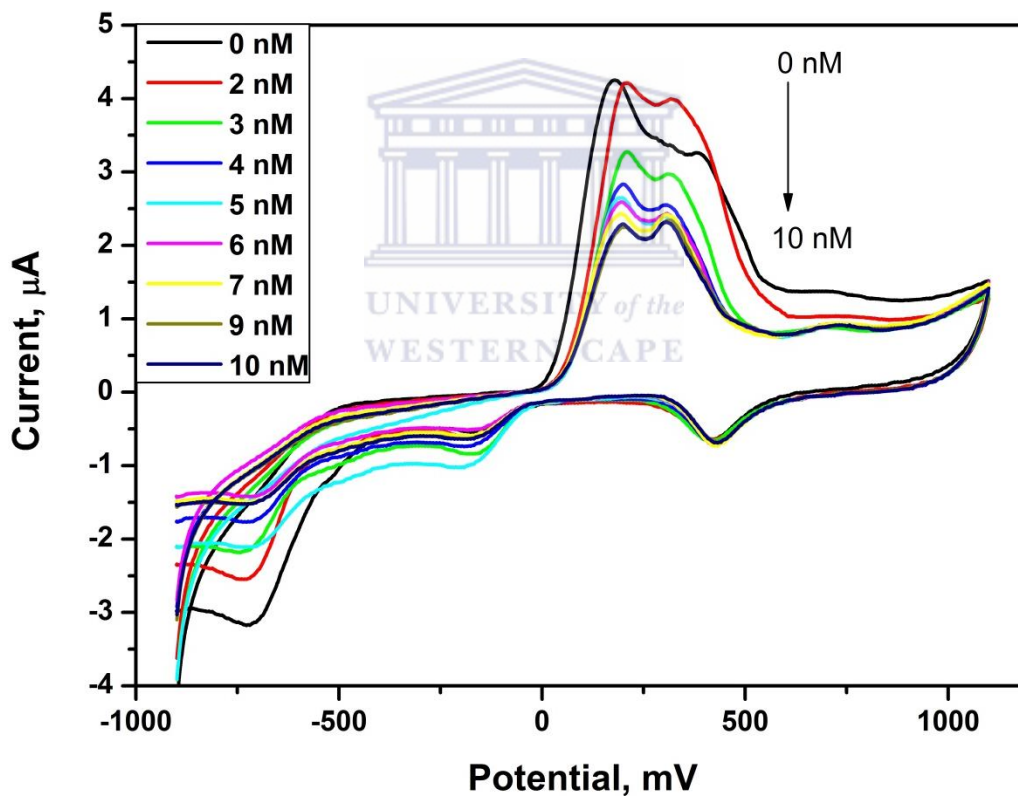


Figure 32: CV response of probe ssDNA/3MPA-In₂Te₃ QDs/AuE to different concentrations of complementary ssDNA (target) in 0.10 M TE buffer solution, pH 8.00 at 10mV/s.

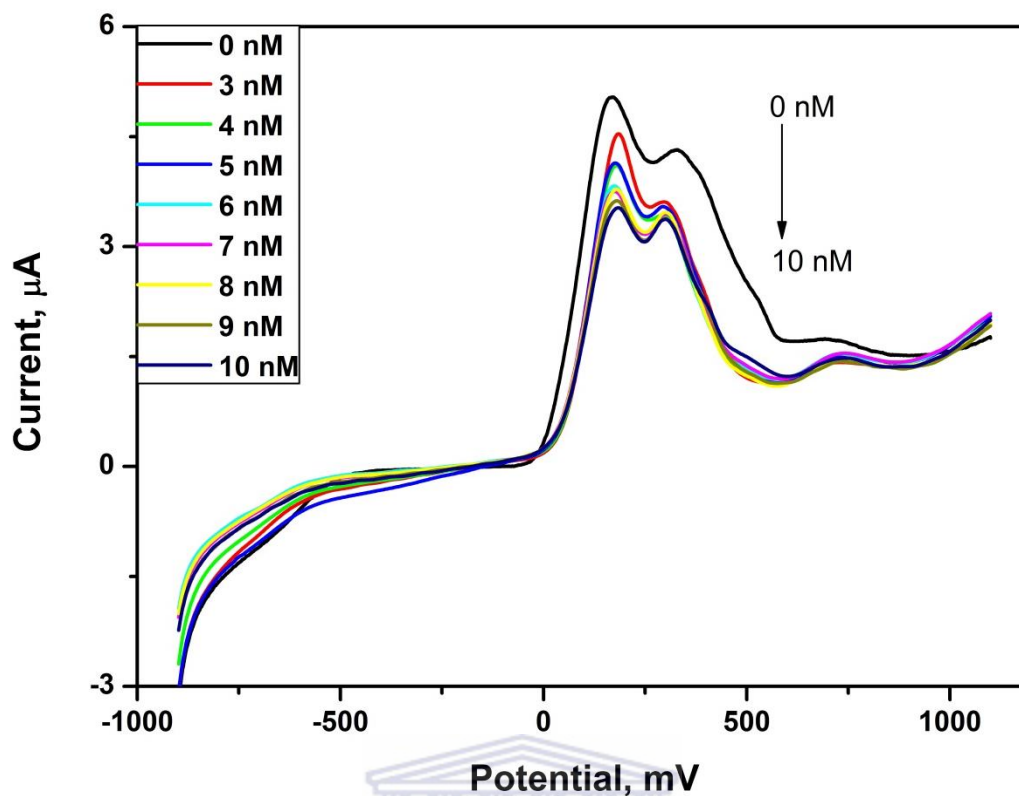


Figure 33: SWV response of probe ssDNA/3MPA-In₂Te₃ QDs/AuE to different concentrations of complementary ssDNA (target) in 0.10 M TE buffer solution, pH 8.00 at 10mV/s.

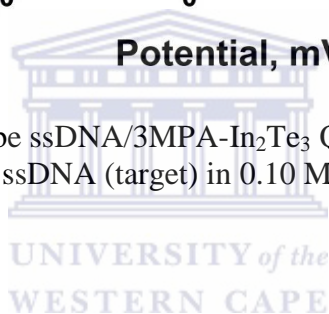


Figure 34 and **Figure 35** below show the calibration curves corresponding to the CV and SWV responses, respectively. Reader should bear in mind that only 5 concentrations was selected for both CV and SWV calibration curves since the dynamic linear range of the QDs based genosensor is within these 5 concentrations. Therefore the CV current was linearly dependent on the concentration of the complementary ssDNA in the range 4 nM to 9 nM with $R^2 = 0.994$. The sensitivity was derived from slope (0.115 $\mu\text{A}/\text{nM}$) of calibration curve, shown in **Figure 34**, and the limit of detection (LOD) was determined by using the equation below,

$$LOD = \frac{3 \times SD \text{ of blank}}{\text{Sensitivity}} \quad (4.5.1.1)$$

Where SD is equivalent to the standard deviation of the current response of the 3MPA-In₂Te₃ QDs based genosensor for eight measurements. Thus the LOD was calculated as 0.0075 ng/mL. The SWV response also showed a linear response with $R^2 = 0.989$ in the range 3 nM to 10 nM, shown in **Figure 35**. The corresponding sensitivity and LOD was 0.144 μ A/nM and 0.0062 ng/mL, respectively.

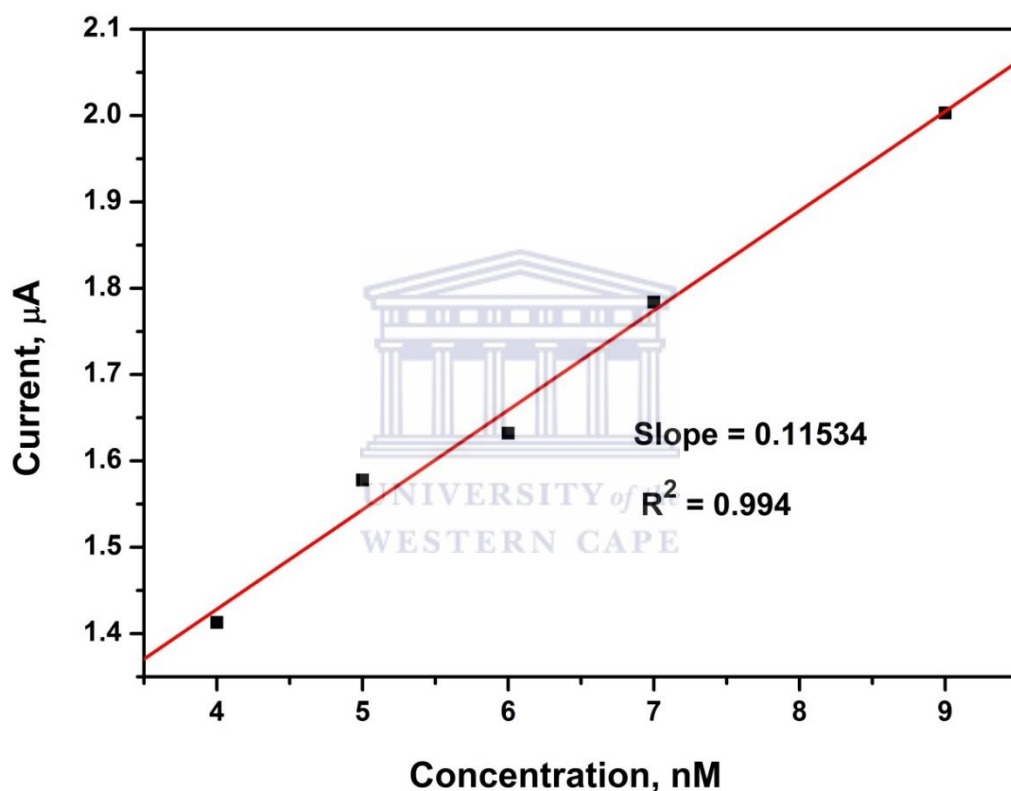


Figure 34: Calibration curve of 3MPA-In₂Te₃ QDs based genosensor showing CV responses to different concentration of complementary ssDNA (target).

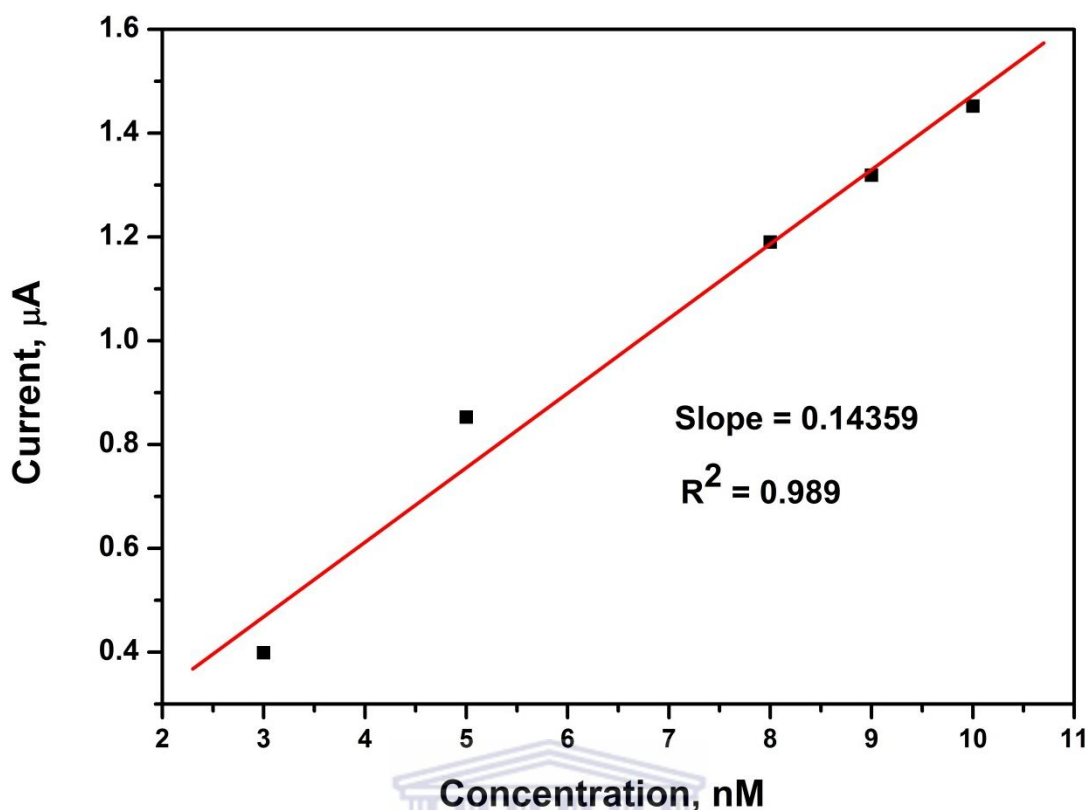


Figure 35: Calibration curve of 3MPA-In₂Te₃ QDs based genosensor showing SWV responses to different concentration of complementary ssDNA (target).

UNIVERSITY of the
WESTERN CAPE

4.5.2 Response dynamic of 3MPA-In₂Te₃ QDs based genosensor to complementary ssDNA (target) using EIS

The responses of the probe ssDNA/3MPA-In₂Te₃/AuE to different concentration of complementary ssDNA in 0.10 M TE buffer solution, pH 8.00 were performed with EIS. The conditions for performing these electrochemical processes were discussed in Chapter 3 section 3.5.1.3. The Nyquist plots were interpreted by the equivalent circuit model showed as an inset in **Figure 36**. It was observed that the charge transfer resistance increased with increasing analyte concentration. The increase in charge transfer resistance might be due to decrease in current caused by the insulating properties of dsDNA that was formed on the AuE during the hybridization process. The EIS results obtained is in accordance with the results

obtained for voltammetric studies of the probe ssDNA/3MPA-In₂Te₃/AuE response to different concentration of complementary ssDNA.

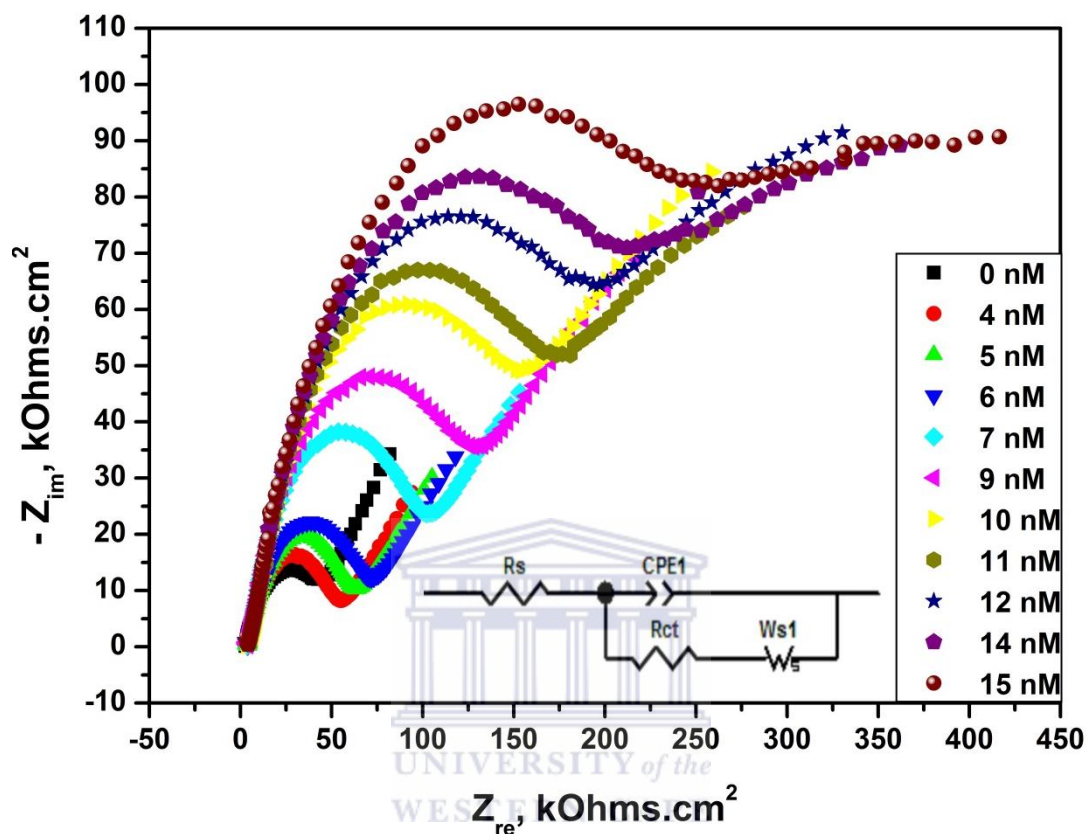


Figure 36: Impedimetric response of probe ssDNA/3MPA-In₂Te₃ QDs/AuE to different concentrations of the complementary ssDNA (target) in 0.10 M TE buffer solution, pH 8.00.

Figure 37 shows the calibration plot of charge transfer resistance versus concentration of complementary ssDNA. The curve showed a linear relationship with $R^2 = 0.997$ in the range 4 nM to 15 nM. The corresponding sensitivity and detection limits were 2.44 Ω/nM and 0.00014 ng/mL, respectively.

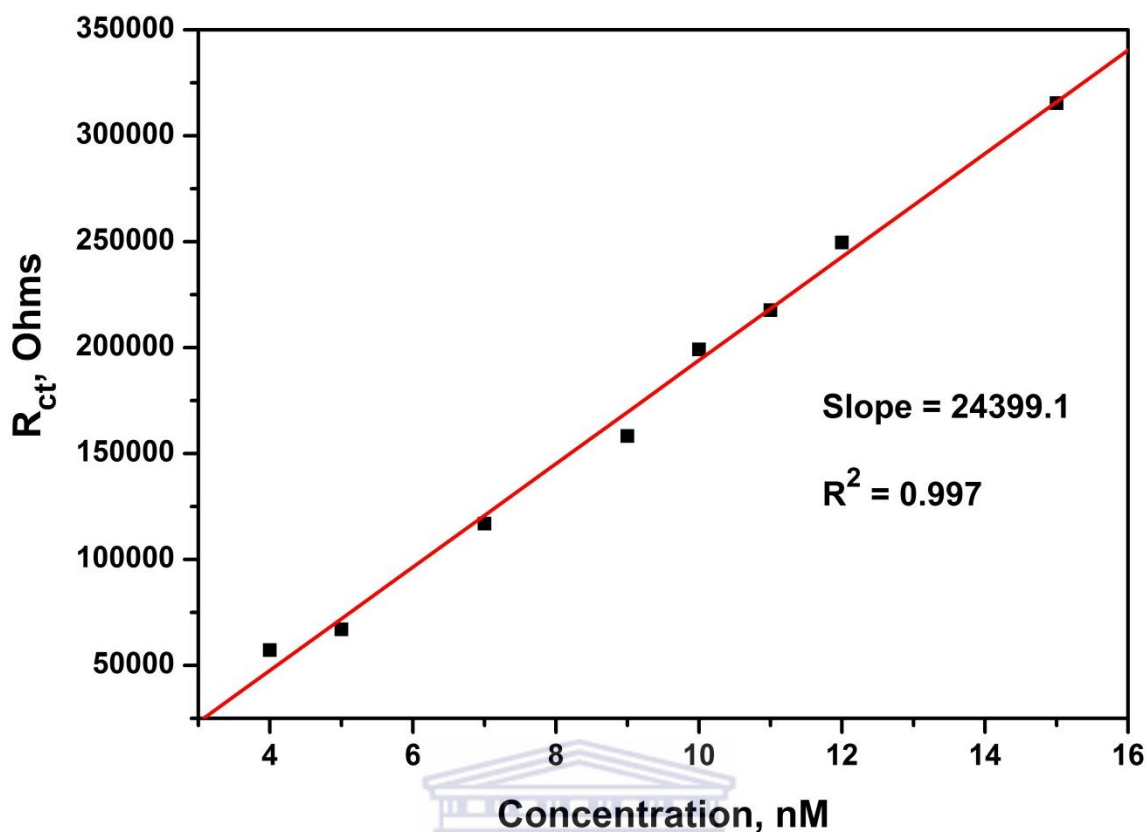


Figure 37: Calibration curve of 3MPA-In₂Te₃ QDs based genosensor showing EIS response to different concentration of complementary ssDNA (target).

UNIVERSITY of the
WESTERN CAPE

4.6 Comparison of the analytical performance of the QDs based genosensor using CV, SWV and EIS

CV, SWV and EIS were used to study the 3MPA-In₂Te₃ QDs based genosensor response to different concentrations of complementary ssDNA. The performance of the 3MPA-In₂Te₃ QDs based genosensor using these three techniques were based on linear range, sensitivity and LOD. These analytical parameters were compared for the different techniques (CV, SWV and EIS) used and are described in **Table 8** below.

Table 8: Analytical performance of the 3MPA-In₂Te₃ QDs based genosensor for CV, SWV and EIS techniques used.

Analytical technique	Linear range in (nM)	Sensitivity in ($\mu\text{A/nM}$) and (Ω/nM)	LOD in (nM)	LOD in (ng/mL)
CV	4-9	0.115	1.09	0.0075
SWV	3-10	0.144	0.91	0.0062
EIS	4-15	2.44	0.02	0.00014

It was observed that all three analytical techniques exhibited good linearity since their R^2 were 0.99. From the data in **Table 8** it can be seen that the EIS was the best technique for determining the performance of the 3MPA-In₂Te₃ QDs based genosensor to different concentrations of complementary ssDNA (target). By using EIS technique the 3MPA-In₂Te₃ QDs based genosensor showed a higher sensitivity (2.44 Ω/nM) towards detecting telomerase with a detection limit as low as 0.00014 ng/mL compared to both CV and SWV as shown in **Table 8**.

4.7 Sensor control experiments

4.7.1 Sensor control experiments using SWV

Control experiments were performed in order to investigate the selectivity of the QDs based genosensor towards complementary ssDNA (target analyte). **Figure 38** below shows the SWV response of the probe ssDNA/3MPA-In₂Te₃ QDs/AuE to 10 nM of complementary, 3-base mismatch and non-complementary ssDNA in 0.10 M TE buffer solution, pH 8.00, respectively. The results shown in **Figure 38** indicate that when comparing the anodic oxidation signal of non-complementary ssDNA with that of probe ssDNA/3MPA-In₂Te₃ QDs/AuE there was no significant change in the signal. This observation suggests that hybridization did not occur since the non-complementary ssDNA exhibited non-specific adsorption. However the anodic oxidation signal of 3-base mismatch ssDNA was lower compared to that of non-complementary ssDNA but higher than that of complementary ssDNA which indicate that some degree of hybridization occurred. This phenomenon was observed because the bases do not match absolutely; therefore hybridization cannot be carried out thoroughly (*Lan et al., 2010*). These experimental results indicate that the 3MPA-In₂Te₃ QDs based genosensor is highly selective to the complementary ssDNA.

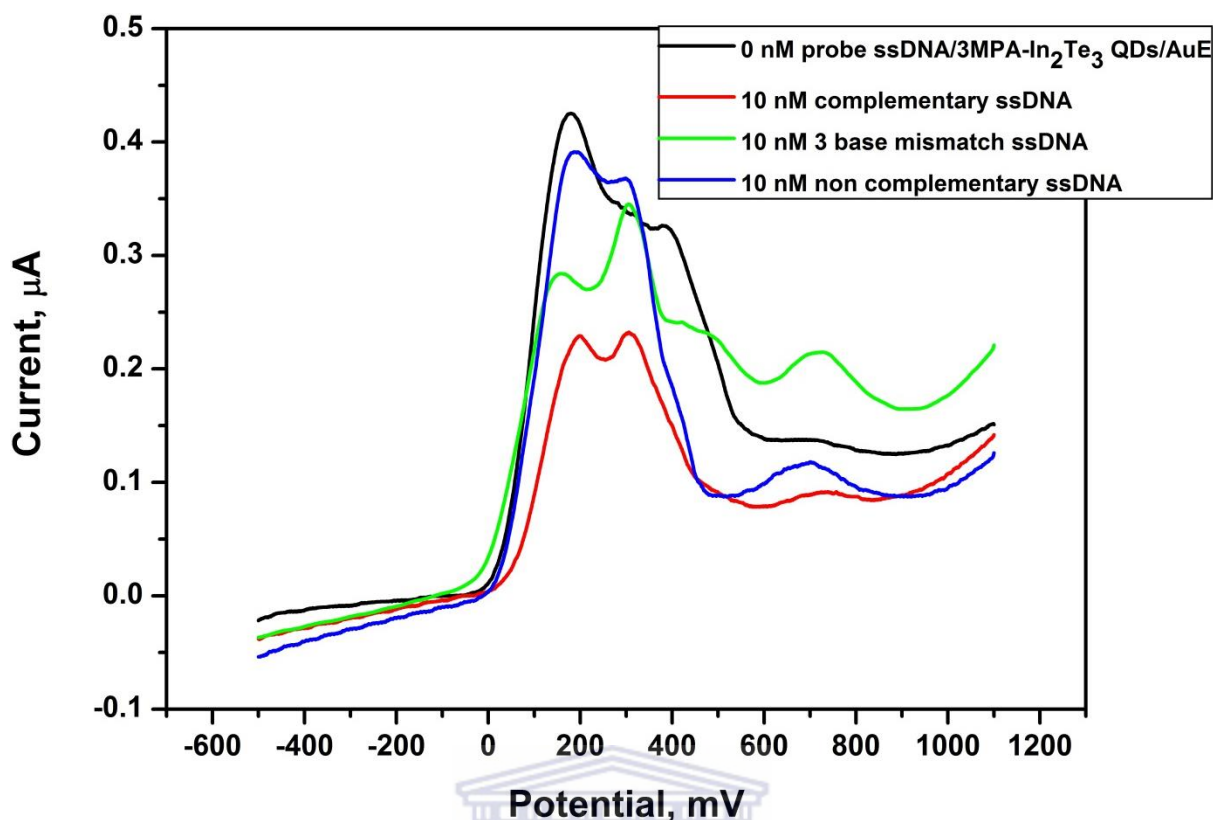


Figure 38: Anodic SWV response of the probe ssDNA/3MPA-In₂Te₃ QDs/AuE to 10 nM of complementary, 3 base mismatched and non-complementary ssDNA in 0.10 M TE buffer solution, pH 8.00 at 10mV/s, respectively.

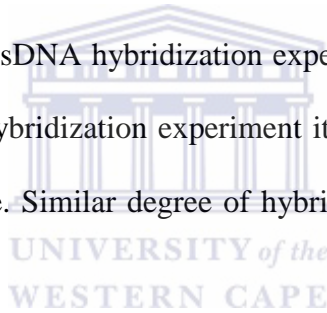
UNIVERSITY of the
WESTERN CAPE

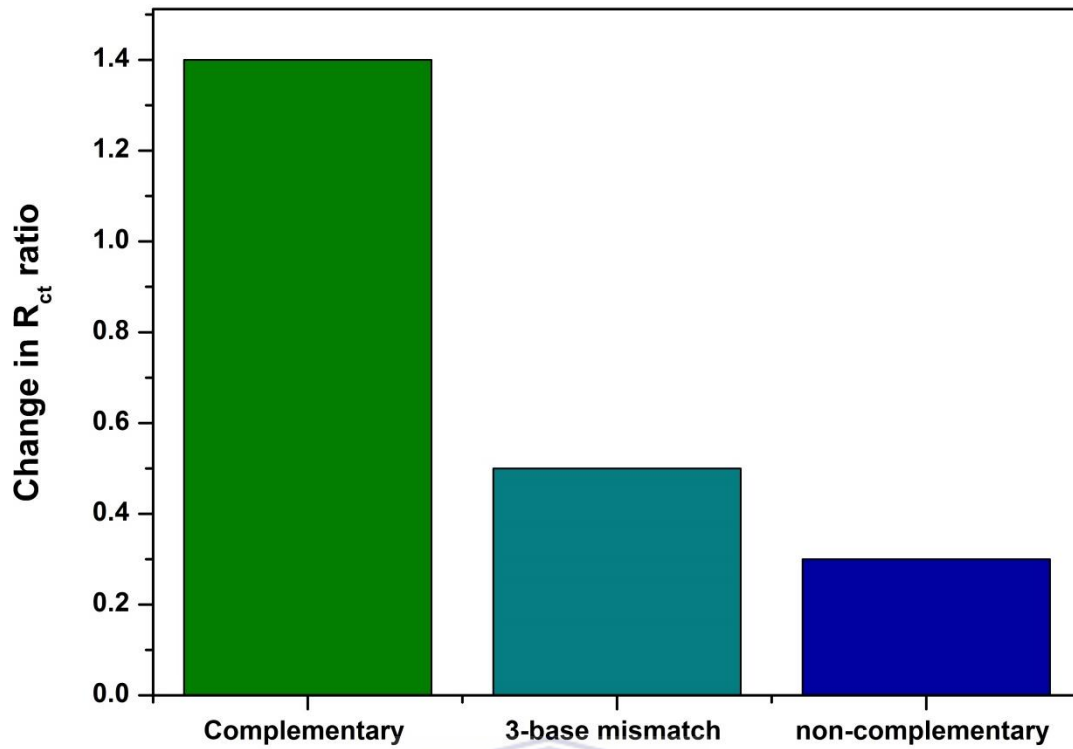
4.7.2 Sensor control experiments using EIS

The selectivity of 3MPA-In₂Te₃ QDs based genosensor was investigated by incubating it in 0.10 M TE buffer solution, pH 8.00 that contained 10 nM of complementary, 3-base mismatch and non-complementary ssDNA, respectively. EIS technique was used and the results were expressed as the relative R_{ct} variation between the values obtained for the different hybridization experiments (complementary, 3-base mismatch and non-complementary) and R_{ct} value due to the bare electrode (Bonanni *et al.*, 2009). These relative variations are represented as a ratio of delta increments and is given by the following equation below,

$$\Delta_{Ratio} = \frac{\Delta R_{ct}(Sample)}{\Delta R_{ct}(Probe)} \quad (4.7.2.1)$$

Where, $\Delta R_{ct}(Sample) = R_{ct}(Sample) - R_{ct}(Bare\ electrode)$ and $\Delta R_{ct}(Probe) = R_{ct}(Probe) - R_{ct}(Bare\ electrode)$, respectively. If the value of Δ_{Ratio} is greater than 1 it implies that hybridization process took place and if the value of Δ_{Ratio} is close to 1 it implies that no hybridization process occurred (Bonanni *et al.*, 2009). The results shown in **Figure 39** indicate that hybridization occurred between probe ssDNA/3MPA-In₂Te₃ QDs/AuE and complementary ssDNA since the Δ_{Ratio} value was greater than 1. The 3-base mismatch ssDNA hybridization experiment gave a much lower Δ_{Ratio} value than the complementary ssDNA hybridization experiment. This was attributed to the fact that the bases do not match absolutely; therefore hybridization cannot be carried out thoroughly. However, since the Δ_{Ratio} value of 3-base mismatch ssDNA hybridization experiment is slightly higher than that of non-complementary ssDNA hybridization experiment it indicates that a certain degree of affinity interaction did take place. Similar degree of hybridization was observed for control experiments done by SWV.





Experiment

Figure 39: Δ_{Ratio} values obtained after hybridization of probe ssDNA/3MPA- In_2Te_3 QDs/AuE with 10 nM complementary, 3-base mismatch and non-complementary ssDNA, respectively.

UNIVERSITY of the
WESTERN CAPE

CHAPTER 5

Chapter overview

This chapter gives a brief overview of the main objectives achieved and discusses the advantages of the 3MPA-In₂Te₃ QDs based genosensor. It also outlines future recommendations for optimizing the performance of the QDs based genosensor by focusing on improving the genosensor's design.

5.0 CONCLUSION AND RECOMMENDATIONS

5.1 Conclusion

In conclusion, we have reported for the first time the successful fabrication and implementation of highly sensitive 3MPA-In₂Te₃ QDs based genosensor for detection of telomerase biomarker. The proposed 3MPA-In₂Te₃ QDs based genosensor is a simple, inexpensive, easy to use genosensor that was highly sensitive and selective towards its target analyte. The colloidal poly-dispersed 3MPA-In₂Te₃ QDs introduced into the genosensor system were successfully synthesized by a simple, inexpensive and reproducible aqueous method. HR-TEM studies revealed formation of small sized QDs about 6 nm in diameter while UV-VIS studies of the QDs showed presence of absorption peaks in the ultraviolet region (100-400 nm) which confirmed the formation of these small sized QDs. The 3MPA-In₂Te₃ QDs showed interesting electro-catalytic properties which allowed them to act as a mediating platform between DNA and the AuE. The successful detection of telomerase was achieved by allowing hybridization process to occur between the probe ssDNA drop coated on the 3MPA-In₂Te₃ QDs/AuE surface and its complementary ssDNA in biological buffer solution (0.10 M TE buffer solution, pH 8.00). Three analytical techniques were used to study the performance of the 3MPA-In₂Te₃ QDs based genosensor towards different concentration

of complementary ssDNA. It was observed that all three analytical techniques exhibited good linearity since their R^2 corresponded to 0.99. However, it was observed that EIS was the best technique for the detection of telomerase compared to both CV and SWV since it showed a higher sensitivity ($2.44 \Omega/\text{nM}$) towards detecting telomerase with a detection limit as low as 0.00014 ng/mL . Control experiments were also carried out by monitoring the hybridization process in the presence and absence of complementary ssDNA and it was determined that the QDs based genosensor was highly selective towards complementary ssDNA. In view of the attractive analytical characteristics and advantages, the ultimate goal of the developed QDs based genosensor is to apply it in real clinical samples of cancer cells or bodily fluids of cancer patients for the detection of telomerase cancer biomarker.

5.2 Recommendations for future study

Further studies of the QDs based genosensor design and application is discussed below.

- It is proposed that the mediating platform must be stabilized to allow lower detection of telomerase at much lower concentrations.
- More in-depth research in novel nanomaterials must be done since it is the coupling of these nanomaterials to the genosensor that increases its sensitivity as well as specificity.
- It is suggested to make use of real sample (cancerous cells) from various tumours and body fluids of cancer patients instead of using standard telomerase solutions for the detection
- It is also suggested to focus on more than one cancer type (oral, prostate and bladder etc.) since 85% of more than 950 primary tumours express telomerase activity.

- Various detection methods (e.g. 12-multichannel robotic electrochemical analyser, electrochemiluminescence (ECL), electrochemical quartz crystal microbalance (EQCM), optical (UV-vis) and photoluminescence) must be studied in order to determine the best technique for telomerase detection.



REFERENCES

1. Kulla, E. and Katz, E., 'Biosensor Techniques Used for Determination of Telomerase Activity in Cancer Cells'. *Sensors* **2008**, 8, 347-369.
2. Anand, P.; Kunnnumakara, A.B.; Sundaram, C.; Harikumar, K.B.; Tharakan, S.T.; Lai, O.S.; Sung, B. and Aggarwal, B.B., 'Cancer is a Preventable Disease that Requires Major Lifestyle Changes'. *Pharmaceutical Research* **2008**, 25, 2097-2116.
3. Whelan, S.A.; Lu, M.; He, J.; Yan, W.; Saxton, R.E.; Faull, K.F.; Whitelegge, J.P. and Chang, H.R., 'Mass Spectrometry (LC-MS/MS) Site-Mapping of N-Glycosylated Membrane Proteins for Breast Cancer Biomarkers'. *Journal of Proteome Research* **2009**, 8, 4151-4160.
4. Schmidt, P.M.; Lehmann, C.; Matthes, E. and Bier, F.F., 'Detection of activity of telomerase in tumour cells using fiber optical biosensors'. *Biosensors and Bioelectronics* **2002**, 17, 1081-1087.
5. Belair, C.D.; Yeager, T.R.; Lopez, P.M. and Reznikoff, C.A., 'Telomerase activity: A biomarker of cell proliferation, not malignant transformation'. *Proceedings of the National Academy of Science of the United States of America* **1997**, 94, 13677-13682, Cell Biology.
6. Hess, J.L. and Highsmith, Jr, W.E., 'Telomerase Detection in Body Fluids'. *Clinical Chemistry* **2002**, 48, 18-24.
7. Jakupciak, J.P.; Wang, W.; Barker, P.E.; Srivastava, S. and Atha, D.H., 'Analytical Validation of Telomerase Activity for Cancer Early Detection'. *Journal of Molecular Diagnostics* **2004**, 6, 157-165.
8. Choi, Y.-E.; Kwak, J.-W. and Park, J., 'Nanotechnology for Early Cancer Detection'. *Sensors* **2010**, 10, 428-455.

9. Madani, S.Y.; Shabani, F.; Dwek, M.V. and Seifalian, A.M., 'Conjugation of quantum dots on carbon nanotubes for medical diagnosis and treatment'. *International Journal of Nanomedicine* **2013**, 8, 941–950.
10. Yun, Z.; Zhengtao, D.; Jiachang, Y.; Fangqiong, T. and Qun, W., 'Using cadmium telluride quantum dots as a proton flux sensor and applying to detect H9 avian influenza virus'. *Analytical Biochemistry* **2007**, 364, 122–127.
11. Sadik, O.A.; Aluoch, A.O. and Zhou, A., 'Status of biomolecular recognition using electrochemical techniques'. *Biosensors and Bioelectronics* **2009**, 24, 2749–2765.
12. Yang, M.; Javadi, A. and Gong, S., 'Sensitive electrochemical immunosensor for the detection of cancer biomarker using quantum dot functionalized graphene sheets as labels'. *Sensors and Actuators B* **2011**, 155, 357–360.
13. Peng, C.-W. and Li, Y., 'Application of Quantum Dots-Based Biotechnology in Cancer Diagnosis: Current Status and Future Perspectives'. *Journal of Nanomaterials* **2010**, 1-11.
14. Wagner, M.K.; Li, F.; Li, J.; Li, X.-F. and Le, X.C., 'Use of quantum dots in the development of assays for cancer biomarkers'. *Analytical and Bioanalytical Chemistry* **2010**, 397, 3213–3224.
15. Zhang, H.; Yee, D. and Wang, C., 'Quantum dots for cancer diagnosis and therapy: biological and clinical perspectives'. *Nanomedicine* **2008**, 3, 83-91.
16. Gao, X. and Dave, S.R., 'Quantum Dots for Cancer Molecular Imaging'. *Advances in Experimental Medicine and Biology* **2007**, 620, 57-73.
17. Frasco, M.F. and Chaniotakis, N., 'Semiconductor Quantum Dots in Chemical Sensors and Biosensors'. *Sensors* **2009**, 9, 7266-7286.

18. Ning, J.; Xiao, G.; Xiao, N.; Wang, L.; Liu, B. and Zou, B., 'Shape and crystal phase controlled synthesis of InSe nanocrystals via a simple and facile way'. *Journal of Crystal Growth* **2011**, 336, 1–5.
19. Michalet, X.; Pinaud, F.F.; Bentolila, L.A.; Tsay, J.M.; Doose, S.; Li, J.J.; Sundaresan, G.; Wu, A.M.; Gambhir, S.S. and Weiss, S., 'Quantum dots for live cells, in vivo imaging, and diagnostics'. *Science* **2005**, 307, 538-544.
20. Crouch, D.; Norager, S.; O'Brien, P.; Park, J.H.; Pickett, N. and Kelly, J.M., 'New synthetic routes for quantum dots'. *Philosophical Transactions of the Royal Society A: Mathematical, Physical and Engineering Sciences* **2003**, 361, 297-310.
21. Weng, J. and Ren, J., 'Luminescent quantum dots: a very attractive and promising tool in biomedicine'. *Current medicinal chemistry* **2006**, 13, 897-909.
22. Murray, C.B.; Norris, D.J. and Bawendi, M.G., 'Synthesis and characterization of nearly monodisperse CdE (E = S, Se, Te) semiconductor nanocrystallites'. *Journal of the American Chemical Society* **1993**, 115, 8706-15.
23. Quintanilla, A.; Butselaar-Orthlieb, V.C.L.; Kwakernaak, C.; Sloof, W.G.; Kreutzer, M.T. and Kapteijn, F., 'Weakly bound capping agents on gold nanoparticles in catalysis: Surface poison?' *Journal of Catalysis* **2010**, 271, 104–114.
24. Koç, K.; Tepehan, F.Z. and Tepehan, G.G., 'Growth kinetics of MPS-capped CdS quantum dots in self-assembled thin films'. *Nanoscale Research Letters* **2012**, 7, 610.
25. Wageh, S.; Higazy, A.A. and Hassouna, A.S., 'Optical properties and thermal degradation of CdSe capped with 3-mercaptopropionic acid'. *Journal of Materials Science: Materials in Electronics* **2013**, 24, 3049-3057.
26. Ndagili, P.M.; Jijana, A.M.; Baker, P.G.L. and Iwuoha, E.I., '3-Mercaptopropionic acid capped ZnSe quantum dot-cytochrome P450 3A4 enzyme biotransducer for 17 β -estradiol'. *Journal of Electroanalytical Chemistry* **2011**, 653, 67–74.

27. Guerra, C.F.; Bickelhaupt, F.M.; Snijders, G.J. and Baerends, E.J., 'The Nature of the Hydrogen Bond in DNA Base Pairs: The Role of Charge Transfer and Resonance Assistance'. *Chemistry: A European Journal* **1999**, 5, 3437-3697.
28. Watson, J.D. and Crick, F. H.C., 'A structure for deoxyribose nucleic acid'. *Nature* **1953**, 171, 737–738.
29. Arnott, S. and Hukins, D.W.L., 'Optimised parameters for A-DNA and B-DNA'. *Biochemical and Biophysical Research Communications* **1972**, 47, 1504–1509.
30. Rich, A. and Zhang, S., 'Z-DNA: The long road to biological function'. *Nature Reviews Genetics* **2003**, 4, 566–572.
31. Wang, J.; Rivas, G. and Cai, X., 'Adsorption and Detection of Peptide Nucleic Acids at Carbon Paste Electrodes'. *Electroanalysis* **1997**, 9, 120-124.
32. Brett, C.M.A.; Brett, A.M.O. and Serrano, S.H.P., 'An EIS study of DNA-modified electrodes'. *Electrochimica Acta* **1999**, 44, 4233-4239.
33. Li, Y.; Qi, H.; Yang, J. and Zhang, C., 'Detection of DNA immobilized on bare gold electrodes and gold nanoparticle-modified electrodes via electrogenerated chemiluminescence using a ruthenium complex as a tag'. *Microchimica Acta* **2009**, 164, 69 – 76.
34. Palecek, E.; Fojta, M.; Jelen, F. and Vetterl, V., 'in the Encyclopedia of Electrochemistry', *Bioelectrochemistry* (Eds.: A.J. BARD, M. STRATSMANN), Wiley-VCH, Weinheim **2002**, 9, 365–429.
35. Palecek, E., 'Past, present and future of nucleic acids electrochemistry'. *Talanta* **2002**, 56, 809–819.
36. Bohunicky, B. and Mousa, S.A., 'Biosensors: the new wave in cancer diagnoses'. *Dove Press Journal: Nanotechnology, Science and Applications* **2011**, 4, 1-10.

37. Manne, U.; Srivastava, R. and Srivastava, S., 'Keynote review: Recent advances in biomarkers for cancer diagnosis and treatment'. *Drug Discovery Today* **2005**, 10, 965–976.
38. Levenson, V.V., 'Biomarkers for early detection of breast cancer: What, when, and where?' *Biochimica et Biophysica Acta* **2007**, 1770, 847–856.
39. Kocevar, N.; Hudler, P. and Komel, R., 'The progress of proteomic approaches in searching for cancer biomarkers'. *New Biotechnology* **2013**, 30, 319–326.
40. Ohshima, K.; Karube, K.; Shimazaki, K.; Kamma, H.; Suzumiya, J.; Hamasaki, M. and Kikuchi, M., 'Imbalance between Apoptosis and Telomerase Activity in Myelodysplastic Syndromes: Possible Role in Ineffective Hemopoiesis'. *Leukemia and Lymphoma* **2003**, 44, 1339-1346.
41. Gouvea, C., (2011). Biosensors for health applications, *Biosensors for Health, Environment and Biosecurity*, Prof. Pier Andrea Serra (Ed.), ISBN: 978-953-307-443-6, InTech, Available from: <http://www.intechopen.com/books/biosensors-for-health-environment-and-biosecurity/biosensors-for-healthapplications>.
42. Sreenivasulu, K. and Lakshmi, M.V., 'Telomerase: Roles in aging, cancer and hereditary disease'. *Biotechnology and Molecular Biology Review* **2011**, 6, 118-125.
43. Meyerson, M., 'Role of Telomerase in Normal and Cancer Cells'. *Journal of Clinical Oncology* **2000**, 18, 2626-2634.
44. Blackburn, E.H., 'Telomeres and telomerase: their mechanisms of action and the effects of altering their functions'. *Federation of European Biochemical Societies Letters* **2005**, 579, 859–862.
45. Maesawa, C.; Inaba, T.; Sato, H.; Iijima, S.; Ishida, K.; Terashima, M.; Sato, R.; Suzuki, M.; Yashima, A.; Ogasawara, S.; Oikawa, H.; Sato, N.; Saito, K. and Masuda,

- T., 'A rapid biosensor chip assay for measuring of telomerase activity using surface plasmon resonance'. *Nucleic Acids Research* **2003**, 31, e4
46. Pavlov, V.; Willner, I.; Dishon, A. and Kotler, M., 'Amplified Detection of Telomerase Activity Using Electrochemical and Quartz Crystal Microbalance Measurements'. *Biosensors and Bioelectronics* **2004**, 20, 1011-1021.
47. Zhong, L.-P.; Chen, G.-F.; Xu, Z.-F.; Zhang, X.; Ping, F.-Y. and Zhao, S.-F., 'Detection of telomerase activity in saliva from oral squamous cell carcinoma patients'. *International Journal of Oral Maxillofacial Surgery* **2005**, 34, 566-570.
48. Skvortsov, D.A.; Zvereva, M.E.; Shpanchenko, O.V. and Dontsova, O.A., 'Assays for Detection of Telomerase Activity'. *ACTA NATURAE* **2011**, 3, 48-68
49. Kim, N.W.; Piatyszek, M.A.; Prowse, K.R.; Harley, C.B.; West, M.D; Ho, P.L.C.; Coviello, G.M.; Wright, W.E.; Weinrich, S.L. and Shay, J.W., 'Specific association of human telomerase activity with immortal cells and cancer'. *Science* **1994**, 266, 2011-2015.
50. Saldanha, S.N.; Andrews, L.G. and Tollefsbol, T.O., 'Analysis of telomerase activity and detection of its catalytic subunit, hTERT'. *Analytical Biochemistry* **2003**, 315, 1-21.
51. Kim, N.W., 'Clinical implications of telomerase in cancer'. *European Journal of Cancer* **1997**, 33, 781-6.
52. Holt, S.E.; Norton, J.C.; Wright, W.E. and Shay, J.W.; 'Comparison of the telomeric repeat amplification (TRAP) to the new TRAP-eze telomerase detection kit'. *Methods in Cell Science* **1996**, 18, 237-48.
53. Wu, Y-Y.; Hruszkewycz, A.M.; Delgado, R.M.; Yang, A.; Vortmeyer, A.O. and Moon Y-W., 'Limitations on the quantitative determination of telomerase activity by

- the electrophoretic and ELISA based TRAP assays'. *Clinica Chimica Acta* **2000**, 293, 199–212.
54. Clark, L.C. Jnr.; 'Monitor and control of blood and tissue O₂ tensions'. *Transactions - American Society for Artificial Internal Organs* **1956**, 2, 41-48.
55. Li, Y.; Liu, B.; Li, X. and Wei, O., 'Highly sensitive electrochemical detection of human telomerase activity based on bio-barcode method'. *Biosensors and Bioelectronics* **2010**, 25, 2543.
56. Su, L.; Zou, L.; Fong, C-C.; Wong, W-L.; Wei, F.; Wong, K-Y.; Wu, R.S.S. and Yang, M., 'Detection of cancer biomarkers by piezoelectric biosensor using PZT ceramic resonator as the transducer'. *Biosensors and Bioelectronics* **2013**, 46, 155–161.
57. Mascini, M. and Tombelli, S., 'Biosensors for biomarkers in medical diagnostics'. *Biomarkers* **2008**, 13, 637-657.
58. Pividori, M.I.; Merco, A. and Alegret, S., 'Electrochemical genosensor design: immobilisation of oligonucleotides onto transducer surfaces and detection methods'. *Biosensors and Bioelectronics* **2000**, 15, 291–303.
59. Wang, J., 'Electrochemical nucleic acid biosensors'. *Analytica Chimica Acta* **2002**, 469, 63–71.
60. Watterson, J.H.; Piunno, P.A.E.; Wust, C.C. and Krull, U.J., 'Effects of Oligonucleotide Immobilization Density on Selectivity of Quantitative Transduction of Hybridization of Immobilized DNA'. *Langmuir* **2000**, 16, 4984-4992.
61. Bonannia, A. and del Vallea, M., 'Use of nanomaterials for impedimetric DNA sensors: A review'. *Analytica Chimica Acta* **2010**, 678, 7–17.

62. Weizmann, Y.; Patolsky, F.; Katz, E. and Willner, I. 'Amplified Telomerase Analysis by Using Rotating Magnetic Particles: The Rapid and Sensitive Detection of Cancer Cells'. *A European journal of chemical biology* **2004**, 5, 943-948.
63. Bonanni, A.; Esplandiu, M.J.; Pividori, M.I.; Alegret, S. and del Valle, M., 'Impedimetric genosensors for the detection of DNA hybridization'. *Analytical and Bioanalytical Chemistry* **2006**, 385, 1195–1201.
64. Topkayaa, S.; Ozkan-Ariksoysala, D.; Kosovab, B.; Ozelb, B. and Ozsoza, M., 'Electrochemical DNA biosensor for detecting cancer biomarker related to glutathione S-transferase P1 (GSTP1) hypermethylation in real samples'. *Biosensors and Bioelectronics* **2012**, 31, 516– 522.
65. Tian, J.; Liu, R.; Zhao, Y.; Xu, Q. and Zhao, S., 'Controllable synthesis and cell-imaging studies on CdTe quantum dots together capped by glutathione and thioglycolic acid'. *Journal of Colloid and Interface Science* **2009**, 336, 504-509.
66. Swalec, L., 'Synthesis of CdTe Quantum Dots and Their Use in Environmental Monitoring', MSc. thesis, Worcester Polytechnic Institute, **2011**.
67. Hayyana, M.; Mjallib, F.S.; Hashima, M.A.; AlNashefc, I.M. and Meid, T.X., 'Investigating the electrochemical windows of ionic liquids'. *Journal of Industrial and Engineering Chemistry* **2013**, 19, 106–112.
68. Helfrick, Jr. J.C. and Bottomley, L.A., 'Cyclic Square Wave Voltammetry of Single and Consecutive Reversible Electron Transfer Reactions'. *Analytical Chemistry* **2009**, 81, 9041–9047.
69. Mirceski, V. and Gulaboski, R., 'Surface catalytic mechanism in squarewave voltammetry'. *Electroanalysis* **2001**, 13, 1326.

70. Dogan-Topal, B.; Ozkan S.A. and Uslu, B., 'The Analytical Applications of Square Wave Voltammetry on Pharmaceutical Analysis'. *The Open Chemical and Biomedical Methods Journal* **2010**, 3, 56-73.
71. Mohilner D.M., 'The Electrical Double Layer. In: *Electroanalytical Chemistry*, (Ed: A.J. Bard) Marcel Dekker, New York **1966**, 1, 241-409.
72. Smith D.E., In: *Electroanalytical Chemistry*, (Ed: A.J. Bard), Marcel Dekker, New York **1966**, 1, 1.
73. Hamdy, A.S.; El-Shenawy E. and El-Bitar, T., 'Electrochemical Impedance Spectroscopy Study of the Corrosion Behavior of Some Niobium Bearing Stainless Steels in 3.5% NaCl'. *International Journal of Electrochemical Science* **2006**, 1, 171-180.
74. Sluyters-Rehbach, M. and Sluyters, J.H., In: *Electroanalytical Chemistry* (Ed: A.J. Bard), Marcel Dekker, New York **1970**, 4, 1.
75. Lee, C.H.; Park, H.B.; Lee, Y.M. and Lee, R.D., 'Importance of Proton Conductivity Measurement in Polymer Electrolyte Membrane for Fuel Cell Application'. *Industrial and Engineering Chemistry Research* **2005**, 44, 7617-7626.
76. Macdonald, D.D., 'Reflections on the history of electrochemical impedance spectroscopy'. *Electrochimica Acta* **2006**, 51, 1376-1388.
77. Muda, R.; Lewis, E.; O'Keefe, S.; Dooly, G. and Clifford, J., 'A Compact Optical Fibre Based Mid- Infrared Sensor System for Detection of High Level Carbon Dioxide Emissions in Exhaust Automotive Applications'. *Procedia Chemistry* **2009**, 1, 593-596
78. Tadano, S. and Giri, B., 'X-ray diffraction as a promising tool to characterize bone nanocomposites'. *Science and Technology of Advanced Materials* **2011**, 12, 11.

79. Moram, M.A. and Vickers, M.E., 'X-ray diffraction of III-nitrides'. *Reports on Progress in Physics* **2009**, 72, 40.
80. Baker, M.J.; Gazi, E.; Brown, M.D.; Shanks, J.H.; Gardner P. and Clarke, N.W., 'FTIR-based spectroscopic analysis in the identification of clinically aggressive prostate cancer'. *British Journal of Cancer* **2008**, 99, 1859 – 1866
81. Wang, J.L., 'Transmission Electron Microscopy of Shape-Controlled Nanocrystals and Their Assemblies'. *The Journal of Physical chemistry B* **2000**, 104, 1153-1175.
82. Vernon-Parry, K.D., 'Scanning Electron Microscopy: an introduction'. *Ill-Vs Review* **2000**, 13, 40-44.
83. Gullapalli, S. and Barron, A., Characterization of Group 12-16 (II-VI) Semiconductor Nanoparticles by UV-visible Spectroscopy, Connexions Web site. <http://cnx.org/content/m34601/1.1/>, Jun 12, **2010**, Accessed on 25 August 2013.
84. Strehlow, W.H. and Cook, E.L., 'Compilation of energy band gaps in elemental and binary compound semiconductors and insulators'. *Journal of Physical and Chemical data* **1973**, 2, 163-199
85. Matheswaran, P.; Sathyamoorthy, R.; Saravanakumar, R. and Velumani, S., 'AC and dielectric properties of vacuum evaporated InTe bilayer thin films'. *Materials Science and Engineering B* **2010**, 174, 269–272.
86. Galian, R.E. and de la Guardia, M., 'The use of quantum dots in organic chemistry'. *Trends in Analytical Chemistry* **2009**, 28, 279–291.
87. Tai, G.; Miao, C.; Wang, Y.; Bai, Y.; Zhang, H. and Guo, W., 'Solvothermal synthesis and thermoelectric properties of indium telluride nanostring-cluster hierarchical structures'. *Nanoscale Research Letters* **2011**, 6, 329.

88. Li, H.; Shih, W.Y. and Shih, W-H., 'Synthesis and Characterization of Aqueous Carboxyl-Capped CdS Quantum Dots for Bioapplications'. *Industrial and Engineering Chemistry Research* **2007**, 46, 2013-2019.
89. Jone, M.R.; Macfarlane, R.J.; Lee, B.; Zhang, J.; Young, K.L.; Senesi A.J. and Mirkin, C.A., 'DNA-nanoparticle superlattices formed from anisotropic building blocks'. *Nature Materials* **2010**, 9, 913-917.
90. Chung, Y. and Lee, C-W., 'Electrochemical behaviors of Indium', *Journal of Electrochemical Science and Technology* **2012**, 3, 1-13.
91. Martin-Gonzalez, M.S.; Prieto, A.L.; Gronsky, R.; Sands, T. and Stacy, A.M., 'Insights into the Electrodeposition of Bi_2Te_3 '. *Journal of The Electrochemical Society* **2002**, 149, C546-C554.
92. Khene, S.; Moeno, S. and Nyokong, T., 'Voltammetry and electrochemical impedance spectroscopy of gold electrodes modified with CdTe quantum dots and their conjugates with nickel tetraamino phthalocyanine'. *Polyhedron* **2011**, 30, 2162–2170.
93. Poznyak, S.; Osipovich, N.; Shavel, A.; Talapin, D.; Gao, M.; Eychmuller, A. and Gaponik, N., 'Size-dependent electrochemical behavior of thiol-capped CdTe nanocrystals in aqueous solution'. *Journal of Physical Chemistry B* **2005**, 109, 1094-1100.
94. Bard, A.L. and Faulkner, L.R., 'Electrochemical Methods: Fundamentals and Applications'. John Wiley & Sons, Inc.: 605 Third Avenue, New York, NY 10158-0012, (2012) 850-6011, USA **2001**, 1-736.
95. Naik, T.R.R. and Naik, H.S.B., 'Electrochemical Investigation of DNA Binding on Carbaldehyde Oxime by Cyclic Voltammetry'. *International Journal of Electrochemical Science* **2008**, 3, 409 – 415.

96. Arjmand, F.; Aziz, M. and Tabassum, S., 'Cyclic Voltammetry-An Electrochemical Approach to Study Metal-based Potential Antitumor Drug-DNA Interaction'. *Current Analytical Chemistry* **2011**, 7, 71-79.
97. Cagnin, S.; Caraballo, M.; Guiducci, C.; Martini, P.; Ross, M.; SantaAna, M.; Danley, D.; West T. and Lanfranchi, G., 'Overview of Electrochemical DNA Biosensors: New Approaches to Detect the Expression of Life'. *Sensors* **2009**, 9, 3122-3148.
98. Kratochvílová, I.; Král, K.; Bunček, M.; Víšková, A.; Nešpůrek, S.; Kochalska, A.; Todorciuc, T.; Weiter, M. and Schneider, B., 'Conductivity of natural and modified DNA measured by scanning tunneling microscopy. The effect of sequence, charge and stacking'. *Biophysical Chemistry* **2008**, 138, 3-10.
99. Lan, M.; Chen, C.; Zhou, Q.; Teng, Y.; Zhao, H. and Niu, X., 'Voltammetric detection of microcystis genus specific-sequence with disposable screenprinted electrode modified with gold nanoparticles'. *Advanced Materials Letters* **2010**, 3, 217-224.
100. Bonanni, A.; Esplandiu, M.J. and del Valle, M., 'Impedimetric genosensors employing COOH-modified carbon nanotube screen-printed electrodes'. *Biosensors and Bioelectronics* **2009**, 24, 2885-2891.